MODIFICATIONS ON THE EXISTING DESIGN PARAMETERS TO IMPROVE THE PERFORMANCE OF INFILTRATION TREATMENT BMPS IN COLD CLIMATES

By

ZAIN MOHAMMED AL-HOURI

A dissertation submitted in partial fulfillment of
the requirements for the degree of

DOCTOR OF PHILOSOPHY

WASHINGTON STATE UNIVERSITY
Department of Civil and Environmental Engineering

August 2008

To the Faculty of Washington State University:

The members of the Committee appointed to examine the dissertation of ZAIN MOHAMMED AL-HOURI find it satisfactory and recommend that it be accepted.

_____
Chair

_____

_____

_____

ACKNOWLEDGMENT

I would like to express my sincere appreciation to my advisor, Dr. Michael Barber, for providing professional and personal guidance and support throughout my academic program. I would also like to thank Dr. Muhunthan Balasingam, Dr. Marc Beutel, and Dr. Jeffrey Ullman for serving on my committee and guiding me through the dissertation process. Thanks are also extended to Dr. David Yonge for providing constructive comments and useful suggestions for this research.

Deepest gratitude is also due to my friend Aleisa Barber who stood by me through the hard times, and shared with me and my kids all the good times. I will always be grateful to her for all the assistant and encouragement she offered me during my stay in the U.S.

Additionally, I wish to express my love and gratitude to my family; my parents who taught me to believe in myself, and my brothers and sisters who have supported me during the period of my study and at all times. And even though they were far away, their thoughts and prayers reached me and kept me going during the past years. Special thanks also to my husband, Abbas, who inspired me toward the completion of the PhD study, strengthen me, and consistently encouraged me. All my love goes to my kids; Diana and Yazeed, for their patience and help during the past three years. With you all I share my success.

I am also grateful to all the professors who have taught me during the periods of my graduate study especially Dr. John Wu for her invaluable encouragement and support. The assistance of the staff of the Civil and Environmental Engineering Department as well as Albrook Hydraulic Lab is gratefully acknowledged. Finally, sincere thanks for all the friends and colleagues who have offered me personal help, support and encouragement over the past three years; everything you offered me even the little is truly appreciated.

MODIFICATIONS ON THE EXISTING DESIGN PARAMETERS TO IMPROVE THE PERFORMANCE OF INFILTRATION TREATMENT BMPS IN COLD CLIMATES

Abstract

by Zain Mohammed Al-Houri, Ph.D.
Washington State University
August 2008

Chair: Michael E. Barber

Many newly developed areas rely on infiltration treatment best management practices (BMPs) for managing excess stormwater runoff volumes. Semi-arid, cold climates pose unique challenges to designers of infiltration treatment BMPs. This study addresses two of the cold climate challenges and proposes modified design parameters to improve the performance of infiltration treatment facilities in these regions. The proposed modifications account for both: 1) reduced soil infiltration caused by frozen soils, and 2) increased runoff volumes during snowmelt and rain-on-snow events.

To study the impacts of frozen conditions on the conductivity of soils, a laboratory-scale experiment was carried out on frozen soil columns collected from two BMPs sites located in the cities of Spokane and Richland, Washington. Hydraulic conductivity measurements were conducted on 16 frozen soil columns using a developed air permeameter flow test. The time allowed for soil-water redistribution prior to freezing was varied among the soil columns (t = 2, 4, 8, and 24 hr) to investigate its significance on the reduction of conductivity of frozen soils. Results showed that conductivity of frozen soils depends greatly on the time available for soil-water redistribution prior to freezing. Based on the results of

this experiment, two regression equations were proposed to assist in the selection of appropriate hydraulic conductivity reduction factors for loam and sandy loam soils when designing infiltration treatment facilities subject to freezing conditions.

Increases in runoff volumes caused by snowmelt and rain-on-snow events were investigated by the assessment of the initial abstraction ratio I_a/S in the SCS curve number (SCS-CN) equation. This was accomplished by designing, constructing and testing a 1.22 m wide x 2.44 m long rainfall simulator system to mimic design storm rainfall distributions on snow covering an impervious plot. By comparing calculated versus measured runoff hydrographs obtained from 19 rain-on-snow simulated under different snow conditions (snow depths and densities) and plot slopes, an alternative methodology for assigning I_a/S ratios during rain-on-snow events was developed.

These new design parameters will result in more effective BMP designs in terms of runoff treatment. Nevertheless, the final designs will ultimately require larger and more costly stormwater facilities.

TABLE OF CONTENTS

Page

LIST OF TABLES

LIST OF FIGURES

Dedication

This dissertation is dedicated to my mother and father

for their unconditional love and support

CHAPTER ONE

INTRODUCTION AND OVERVIEW

1.1 INTRODUCTION

As urban development increases, the percentage of impervious surfaces increases, thereby reducing infiltration quantities and increasing runoff volumes. Reduced infiltration and increased runoff can cause many adverse impacts including increased flooding and erosion of stream banks as well as the increased likelihood that the runoff will become contaminated with pollutants that may threaten the aquatic ecosystem (Urbonas and Stahre, 1993; Booth and Jackson, 1997; NRDC, 1999). To mitigate these impacts, stormwater runoff treatment Best Management Practices (BMPs) are often used (Young et al., 1996; USEPA, 1999; MPCA, 2000; ASCE, 2000, 2001). Runoff treatment is achieved in these facilities by physical, biological and chemical removal mechanisms. The design of treatment BMPs is usually based on either the water quality design flow rate (Flow Control facilities) or the water quality design runoff volume (Volume facilities) (WDOT, 1993, 2004; FHWA, 2005). Types of treatment BMPs include ponds, wetlands, infiltration systems, filtering systems and open channel systems (Yu et al., 1994; Strecker et al., 2002, 2004; NCHRP, 2006).

Appropriate BMP selection involves several site-specific factors including impact area, soil type, available highway right-of-away area, community and environmental factors, expected pollutant concentration, precipitation characteristics, and nature of the receiving waters (USEPA, 2004). Once these factors have been evaluated, the preferred BMP type will be chosen based on overall cost effectiveness. Designing BMPs properly is essential to achieve the required levels of treatment with minimum construction costs, few maintenance requirements, and effective design lives.

In semi-arid regions, many new developments rely on infiltration treatment BMPs for managing excess stormwater runoff volumes. Infiltration treatment BMPs are impoundments, typically basins, trenches, or porous pavements that serve the dual purpose of removing pollutants from stormwater and recharging the groundwater (USEPA, 1999). These facilities are usually designed to handle the entire runoff volume generated from the contributing drainage area (WSDOT, 2004). Design runoff volumes are computed from design storms (e.g., the 24-hour SCS Type 1A storm) and appropriate return frequencies (e.g., 6-month return period) using a single event hydrograph method (WDOE, 2004; WSDOT, 2004). These outflow hydrographs are combined with estimated infiltration rates to determine the sizes and geometries of infiltration facilities such that the BMPs fully dewater the design volumes within a specified time (e.g. 24 hours) after storm events cease. Although many single event models are available, most of the parameters used in these models were developed for warm-weather climates subject to summertime rainfall events. For example, the Santa Barbara Urban Hydrograph (SBUH) methodology is a popular single event runoff model that was originally developed for warm or moderate climates but is nevertheless used almost exclusively for modeling stormwater facilities in many areas where cold climates prevail such as Eastern Washington, Minnesota, and Oregon (MPCA, 2000; Taylor and Gangnes, 2004; WDOE, 2004). The SBUH model applies the U.S. Soil Conservation Service Curve Number (SCS-CN) equations to an approach that determines the runoff hydrograph (SFWMD, 1994; Tsihrintzis and Hamid, 1997; WSDOT, 2004). Applying this method using the standard parameters (e.g. the initial abstraction ratio, I_a/S) developed in the original SCS-CN equation for surface runoff volume does not account for the effect of storms likely to occur in cold climate regions.

Cold climate regions are identified as those that have average daily maximum temperature of 35^{o}F or less during January, a growing season of less than 120 days, and mean annual snowfall greater than 3 feet (Caraco and Claytor, 1997). Cold climate conditions introduce new challenges to the selection, design and maintenance of stormwater treatment BMPs (WDOE, 2004). Among these challenges are: reduced soil infiltration due to the presence of soil frost, frozen pipes due to cold temperatures, and high runoff volumes during snowmelt and rain-on-snow events. These challenges can cause significant impacts on the performance of stormwater BMPs that use infiltration as a mitigation strategy and thus it is important to adjust traditional design criteria to make them effective in cold regions (Caraco and Claytor, 1997).

In response to these concerns, this research explores the impact of cold climates on the performance of infiltration treatment BMP facilities. This research work addresses two design challenges associated with cold climates and how they affect the water quantity sizing requirements for infiltration facilities:

1) Reduced soil infiltration due to the presence of soil frost, and

2) High runoff volumes during snowmelt and rain-on-snow events.

Modifications to the design parameters currently used in the analytical approaches for estimating surface runoff and infiltration rates are proposed to account for the unique conditions in cold climates and to improve the performance of the infiltration facilities during the cold periods.

1.2 PROBLEM STATEMENT

The size of existing infiltration facilities currently in use in many areas vulnerable to cold weather are selected based on a design runoff volume and infiltration rate estimate that are often determined from model predictions developed for warm weather climates. However, two of inevitable consequences for cold weather are frozen ground and precipitation in the form of snow. The presence of frozen ground can inhibit the infiltration capacity of the soil thus causing increased runoff volumes and decreased infiltration and deep percolation rates. In addition, the presence of snow on the BMP catchment area at the onset of a rainfall event can produce increased runoff volumes from snow melting. When combined with frozen soil conditions, snow melting will fill or saturate the stormwater BMP prior to an actual design event (WDOE, 2004) thus preventing the stormwater BMP facility from satisfying the flow control and runoff quality requirements. To account for such cold conditions, there is a need to improve existing design parameters in the current analytical approaches used to estimate runoff volumes and infiltration rates to ensure efficient BMP performance during cold periods. Ultimately, this will require larger, more costly facilities to achieve the same level of treatment.

1.3 OBJECTIVES

The overall goal of this research is to develop and verify a methodology for improving the performance of the stormwater infiltration facilities in areas throughout the world that are vulnerable to cold weather conditions by modifying the existing design parameters used by engineers for predicting runoff treatment volumes and infiltration rates to

account for the conditions associated with cold climates. This will be accomplished by achieving two main objectives:

1. Develop an approach for determining correction factors for infiltration rates to account for reduced infiltration due to frozen soil conditions, and
2. Modify the SCS-CN initial storage abstraction ratio to account for increased runoff volumes caused by snowmelt or rain-on-snow events.

1.4 RESEARCH APPROACH

The following investigational approaches have been used to achieve the objectives of this project:

1. Laboratory column experiments were conducted to study the effect soil-water redistribution time prior to freezing on the hydraulic conductivity reduction of frozen soils using a constructed air permeameter flow test apparatus.
2. A rainfall simulator system was designed, constructed and tested to obtain runoff data from controlled design storm rainfall distributions on snow covering an impervious plot.
3. SBUH Model calibration and validation were performed using the measured rainfall runoff data to determine an alternative λ (or I_a/S) value(s) that would be more applicable for use during rain-on-snow events.

The format of this dissertation presents each of the major research objectives in separate chapters. This chapter (Chapter 1) presents an overview of the work. Chapter two presents the background, rationale, procedure and results related to the laboratory

experiments performed to investigate the impact of frozen soil conditions on reducing soil hydraulic conductivity. The experiment included development of an air permeameter flow apparatus to measure hydraulic conductivity of 16 frozen soil columns constructed using soils from two BMPs sites in Spokane and Richland, Washington. The water content and the allowable redistribution time prior to freezing varied between each of the soil columns to evaluate the significance of these parameters on permeability reduction. The results obtained from this experiment were used to develop criteria to guide the selection of an appropriate correction factor for hydraulic conductivity to incorporate in the design of infiltration facilities to account for freezing ground conditions in cold regions.

Chapter three presents the background, rationale, procedure and results related to the construction of a mobile rainfall simulator. The rainfall simulator was used to allow the application of controlled long-duration design storm rainfall events (in terms of intensity and duration) on a test plot under different snow depths and plot slopes in order to investigate the effects of snowmelt and rain-on-snow events on the generated runoff volumes. The experiment was designed to explore alternatives and modifications to the traditional design parameters used for estimating the snowmelt runoff volumes and single event hydrographs.

The modeling component involved using the SBUH single event hydrograph method to calibrate design method parameters. Using measured rainfall/runoff data, the calibration and verification tasks allowed for modification of the initial abstraction storage ratio to account for rain-on-snow conditions.

The approaches described were aimed at improving the estimation of runoff volumes and infiltration rates at which these runoff volumes seep into the subsurface during cold weather conditions, and not on the water quality aspects. The approaches were proven using

information collected in Eastern Washington. The methodologies developed can be implemented in any cold climate area to provide better local criteria for BMPs. The specific results generated by this study provided complementary information to the existing design criteria described in the Washington Department of Ecology Stormwater Management Manual for Eastern Washington (WDOE, 2004) and the Washington State Department of Transportation Highway Runoff Manual (WSDOT, 2004).

Chapter four summarizes the approaches used in this study, the objectives and results obtained from each of the approaches as well as the conclusion of this research. Because Chapter two and three are written in journal format, details of the literature review and calculation procedures are provided in Appendices.

1.5 REFERENCES

American Society of Civil Engineers, ASCE (2000). "National Stormwater Best Management Practices (BMP) Database." Urban Water Resources Research Council of ASCE for the EPA, Office of Science and Technology, Washington, DC, (http://www.bmpdatabase.org/).

American Society of Civil Engineers, ASCE (2001). "A Guide for Best Management Practice (BMP) Selection in Urban Developed Areas." Reston, VA.

Booth, D.B., and Jackson, C.R. (1997). "Urbanization of Aquatic Systems–Degradation Thresholds, Stormwater Detention, and the Limits of Mitigation." *Journal of the American Water Resources Association*, 2 (5), 1077-1090.

Caraco, D., and Claytor, R. (1997). "Stormwater BMP Design Supplement for Cold Climates." Prepared by Center for Watershed Protection, Ellicott City, MD, for U.S. EPA Office of Wetlands, Oceans, and Watersheds, Washington, DC.

Federal Highway Administration, FHWA (2005). "Stormwater Best Management Practices in An Ultra-Urban Setting: Selection And Monitoring." U.S. Department of Transportation Federal Highway Administration, www document, http://www.fhwa.dot.gov/environment/ultraurb/5mcs9.htm

Minnesota Pollution Control Agency, MPCA (2000). "Protecting Water Quality in Urban Areas Best Management Practices for Dealing with Storm Water Runoff from Urban, Suburban And Developing Areas In Minnesota." Saint Paul, MN.

National Cooperative Highway Research Program, NCHRP (2006). "Evaluation of Best Management Practices for Highway Runoff Control." Report No 565, Transportation Research Board of the National Academy, Washington, DC.

Natural Resources Defense Council, NRDC (1999). "Stormwater Strategies: Community Responses to Stormwater Pollution." www document, http://www.nrdc.org/water/pollution/storm/stoinx.asp

South Florida Water Management District, SFWMD (1994) "Management And Storage of Surface Waters, Permit Information Manual.", Volume IV, Regulation Department, South Florida Water Management District, West Palm Beach, FL, USA.

Strecker, E., Quigley, M., Urbonas, B., Howell, J., and Hesse, T. (2002). "Urban Stormwater BMP Performance Monitoring A Guidance Manual for Meeting the National Stormwater BMP Database Requirements". EPA-821-B-02-001, Office of Water, Washington, DC.

Strecker, E., Quigley, M., Urbonas B., and Jones, J. (2004). "Analyses of the Expanded EPA/ASCE International BMP Database and Potential Implications for BMP Design." Proceedings of the World Water and Environmental Congress, Salt Lake City, UT.

Taylor, B., and Gangnes, D. (2004). "Methods for Quantifying Runoff Reduction of Green Roofs." Prepared for the Green Roof for Healthy Cities Conference, Portland, OR.

Tsihrintzis, V.A. and Hamid, R. (1997). "Urban Stormwater Quantity/Quality Modeling Using the SCS Method and Empirical Equations." *Journal of American Water Resources Association*, 33(1), 163–176.

Urbonas, B., and Stahre, P. (1993). " Stormwater Best Management Practices and Detention for Water Quality, Drainage and CSO Management.", PTR Prentice Hall, NJ

U.S. Environmental Protection Agency, USEPA (1999). "Preliminary Data Summary of Urban Storm Water Best Management Practice." EPA-821-R-99-012, Office of Water Environmental Protection, Washington, DC.

U.S. Environmental Protection Agency, USEPA (2004). "Stormwater Best Management Practice Design Guide." EPA-600-R-04-121, Office of Water Environmental Protection, Washington, DC.

Washington State Department of Ecology, WDOE (1993). "Selecting Best Management Practices For Stormwater Management" Publication Number 04-10-076, Olympia, WA.

Washington State Department of Ecology, WDOE (2004). "Stormwater Management Manual for Eastern Washington." Publication Number 04-10-076, Olympia, WA.

Washington State Department of Transportation, WSDOT (2004). "Highway Runoff Manual." Publication Number M 31-16, Olympia, WA.

Young, G.K., Stein, S., Cole, P., Kammer, T., Graziano, F., and Bank, F. (1996). "Evaluation and Management of Highway Runoff Water Quality." FHWA-PD-96-032. Federal Highway Administration, Office of Environment and Planning.

Yu, S.L., R.J. Kaighn, and S.L. Liao (1994). "Testing of Best Management Practices for Controlling Highway Runoff, Phase II." Virginia Department of Transportation, Report No. FHWA/VA-94-R21, Richmond, VA.

CHAPTER TWO

IMPACTS OF FROZEN SOILS ON THE PERFORMANCE OF INFILTRATION TREATMENT FACILITIES

2.1 ABSTRACT

Infiltration treatment best management practices (BMPs) mitigate stormwater runoff from impervious surfaces, taking advantage of water percolation through soil to remove pollutants and recharge groundwater. However, in cold regions, frozen soil moisture negatively impacts infiltration facility performance by reducing available pore spaces for infiltrating water, causing a significant increase in runoff volumes. To understand the impacts of frozen soils on hydraulic conductivity rates and to improve infiltration treatment BMP designs for cold climates, laboratory experiments examined two soil types (loam and sandy loam) from infiltration treatment facility sites located in the cities of Spokane and Richland, Washington. Hydraulic conductivity measurements for unfrozen and frozen soil columns were performed using a developed air permeameter flow test. The time allowed for soil-water redistribution prior to freezing was varied among the soil columns (t = 2, 4, 8, and 24 hr) to determine reduction of hydraulic conductivity in frozen soils. Depending on the time allowed for soil-water redistribution prior to freezing, hydraulic conductivity decreased by 0 to 2 orders of magnitude with depth in the frozen loam soil columns, while it decreased by 1 to 3 orders of magnitude for frozen sandy loam soil columns. For both soils, the minimum reduction in soil hydraulic conductivity was observed when the soil columns were drained for a 24-hour prior to the onset of freezing. However, while a 24-hour draining period was sufficient for the hydraulic conductivity of the loam soil to return to the same order of magnitude before freezing (10^{-3} cm/s), this draining period was insufficient for the frozen

sandy loam soil to regain a hydraulic conductivity similar to the unfrozen soil. Two regression equations were derived from the results to provide appropriate hydraulic conductivity correction factors for loam and sandy loam soils to improve BMP design in cold regions.

Key words: infiltration, frozen soils, stormwater BMPs, hydraulic conductivity

2.2 INTRODUCTION

In cold climate regions, the presence of frozen soils can dramatically influence water flow processes such as runoff, infiltration and deep percolation. The freezing process blocks void spaces with ice crystals, which reduce infiltration and storage capacity and correspondingly increases surface water runoff. This significantly impacts the performance of stormwater best management practices (BMPs) that use infiltration as a mitigation strategy and requires appropriate design modifications to increase effectiveness in cold climates (Caraco and Claytor, 1997).

Numerous studies have investigated the impacts of soil frost and frozen soil on hydraulic conductivity and infiltration rates using different procedures and techniques (Takeshi et al., 1985; Seyfried and Murdock, 1997; Zhao and Gray, 1999; Stadler et al., 2000; Stähli et al., 2004; Iwata et al. 2008). Although infiltration capacity and hydraulic conductivity in frozen soils has been shown to be closely linked to soil water content at the time of freezing (Orlando et al., 1996; Wiggert et al., 1997; McCauley et al., 2000 and 2002; Bayard et al., 2005), using average values to predict frozen soil infiltration rates can lead to errors since internal water distribution may interact with the freezing process and influence

the hydraulic conductivity (Pikul et al., 1996; Seyfried and Murdock, 1997). Limited research has investigated the importance of soil-water redistribution and the temporal effects of this process prior to freezing on changes in frozen soil hydraulic conductivity (Butler et al., 1996; Stähli et al., 1999).

The internal pore water distribution indicates that water infiltrating through soil preferentially resides in the largest pores since these regions are under the least amount of surface tension (Miller, 1973). However, following the infiltration process, this water usually undergoes a redistribution process that causes water to drain from the soil via gravity and pressure forces. Water drains more rapidly from the larger pores than the smaller ones, causing them to become mostly filled with air. Hence, the longer the time available for soil-water redistribution after infiltration ceases and before the onset of freezing, the more air-filled pore space will be available for infiltrating water during the next rainfall event. The information on the available soil-water redistribution time prior to freezing can be used as a key factor to estimate the reduction in hydraulic conductivity during freezing conditions. This data is of critical important for selecting the appropriate design infiltration rate when designing and sizing the required infiltration facility in cold regions.

2.3 OBJECTIVES

The objectives of this study are to:

1) Evaluate the significance of antecedent water content and the differences in time available for soil-water redistribution prior to freezing on frozen soil conductivity.

2) Develop criteria to guide the selection of correction factors for the hydraulic conductivity values when designing the infiltration facilities to account for freezing conditions in cold regions.

The first hypothesis is that the time available for water redistribution after infiltration ceases and before the onset of freezing is the control factor to the soil-water distribution, and availability of air-filled pore space for infiltrating water during the next rainfall event. The second hypothesis is that weather conditions are expected to negatively impact the performance of infiltration treatment BMPs during the cold season. To guarantee effective performance of these facilities during the cold season, a correction factor should be applied to the design value of hydraulic conductivity. Local conditions from Eastern Washington were used to test the proposed hypotheses.

2.4 MATERIALS AND METHODS

2.4.1 Soil Properties

Laboratory studies were conducted using re-compacted soils from two highway BMP field locations in eastern Washington near the cities of Richland and Spokane. The grain size distributions of the two soils were determined using sieve analysis technique (Figure 2.1). The Spokane and Richland soils were classified according to the Soil Taxonomy (USDA, 1975) as loam and sandy loam, respectively. Infiltration is considered the primary function of both facilities. The physical properties of the two soils are summarized in Table 2.1.

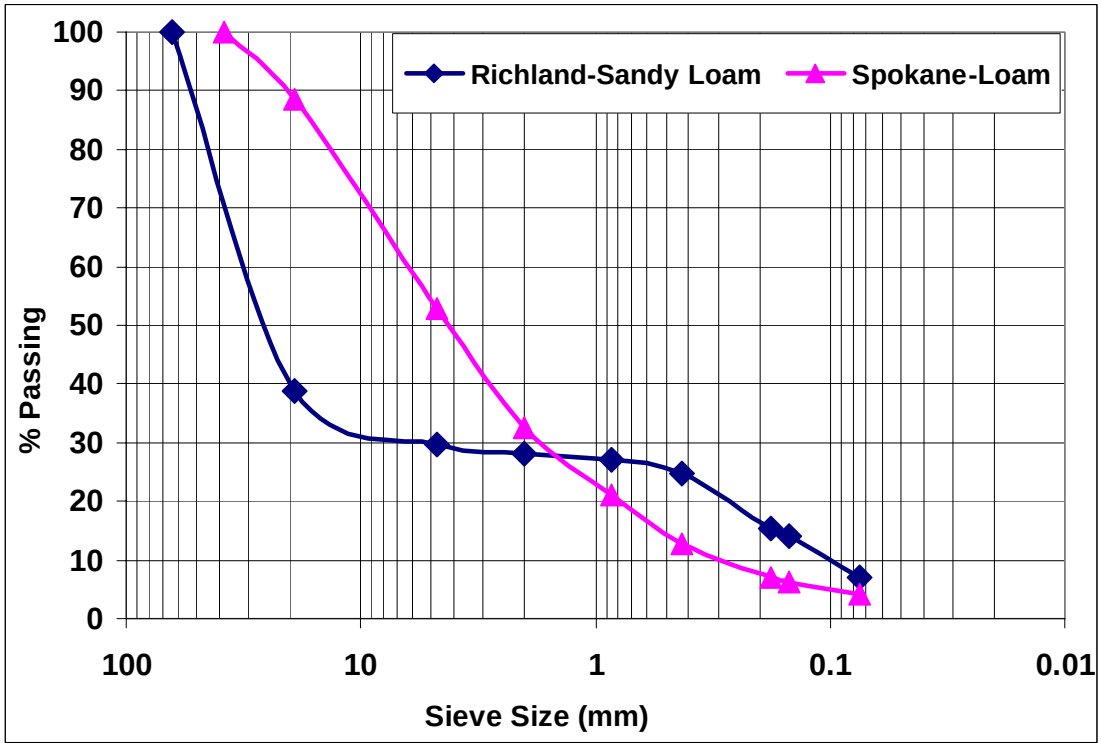

Figure 2.1. Grain size distribution for soils collected from two highway BMPs in Spokane and Richland, WA.

Table 2.1. Physical characteristics of soils from Spokane, and Richland sites.

Site Location	Soil Type	Sand Content (%)	Silt Content (%)	Clay Content (%)	Bulk Density, ρ_b (g/cm^3)	Particle Density, ρ_s (g/cm^3)	Porosity, n *(%)*
Spokane	Loam	47.50	33.8	18.8	1.63	2.67	0.43
Richland	Sandy loam	67.5	20	12.5	1.69	2.65	0.36

2.4.2 Soil Columns Preparation

The soil was dried in an oven at 105^{o}C (221 ^{o}F) until it reached a constant weight and subsequently cooled to room temperature in preparation for the column experiments. The soils were packed into a polyvinylchloride (PVC) cylinder with a 10.2 cm (4 in) inner diameter and 45 cm (18 in) length. Based on the cross-sectional area of the soil column and the bulk density of each soil (listed in Table 2.1), the weights of oven-dried soil necessary to fill 5 cm (2 in) segments of the column were calculated. The weighed soils were then placed into the soil column and packed to depth of 5 cm (2 in) to maintain constant bulk density along the soil column. Four soil columns were constructed for each soil type. In order to assess the significance of the time available for soil-water redistribution prior to freezing on the hydraulic conductivity reduction at different depths along the soil column, each soil column was built in three sections (each 15 cm in length) with a very thin mesh separating each consecutive section, and a steel mesh with larger thickness glued to the bottom of the lower section to hold the soil. The impact of the separating mesh on infiltration was examined and determined to be insignificant. For each soil type, the tops of the columns were irrigated with equal volumes of water at room temperature and then drained for different period of time (t = 2, 4, 8, and 24 hr) to obtain different profiles of water content prior to freezing conditions. The volume of water drained from the bottom of each soil column at the end of each time was measured and the final water content of each soil column was calculated. The volumetric moisture contents of the soil columns of each soil type are listed in Table 2.2. Each soil column was then placed in a Styrofoam insulation case that was 5-cm thick on the sides and bottom and then stored in a freezer for 4 to 6 days at a temperature below the freezing temperature (Figure 2.2). This was done to ensure that freezing initiated at

the top surface of the soil column and freezing front propagated downward through each soil column as would be the case in the field. After complete freezing, the conductivity of each soil column was measured by conducting an air permeameter flow test. Detailed description of the air flow experiment is presented in the next section. In addition to the air permeameter flow test for hydraulic conductivity measurement of each of the soil columns, an attempt was made to visualize the air void distributions in these sections using x-ray computed tomography (CT) and image analysis techniques. Details descriptions of the x-ray CT procedure and the outcomes of this part of the study are provided in Appendix B.

To assure the quality of results and assess potential inherent variations, duplicates were performed for each of the primary soil columns. Thus, eight soil columns were constructed for each of the two soils for a total of 16 columns.

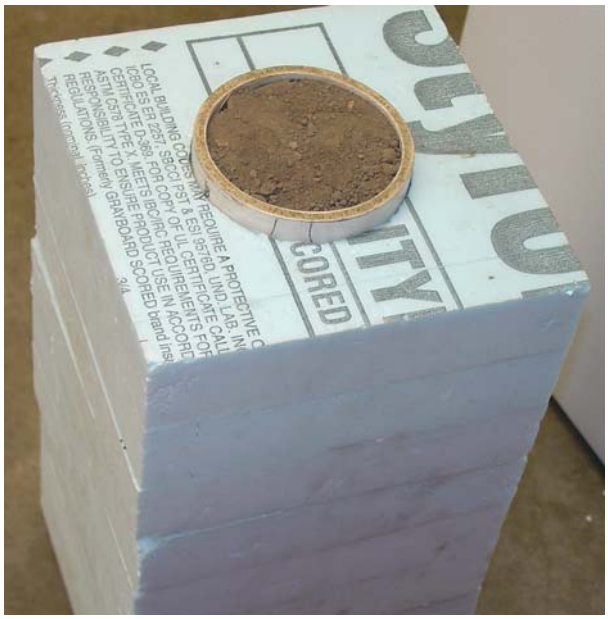

Figure 2.2. Soil column placed in an insulation case.

Table 2.2. Volumetric moisture contents for sandy loam and loam soil.

Column Label	Soil-water redistribution time, T (hr)	Volume of water-applied, V_{wa} (ml)	Volume of water-drained, V_{wd} (ml)	Volumetric moisture content, θ (%)
Sandy loam soil				
2A	2	1343	500	23
2B	2	1343	500	23
4A	4	1343	380	26
4B	4	1343	360	27
8A	8	1343	340	27
8b	8	1343	293	28
24A	24	1343	420	25
24B	24	1343	440	24
Loam soil				
2A	2	1611	670	25
2B	2	1611	680	25
4A	4	1611	780	22
4B	4	1611	800	22
8A	8	1611	650	26
8B	8	1611	710	24
24A	24	1611	670	25
24B	24	1611	670	25

2.4.3 Air Permeability Flow Test

This experiment used a stand-alone air permeameter similar to that developed by Massmann and Johnson (2001) (Figure 2.3). This test was selected because of its suitability for frozen soils since the permeability of air can be measured without phase changes occurring inside the media (Seyfried and Murdock, 1997).

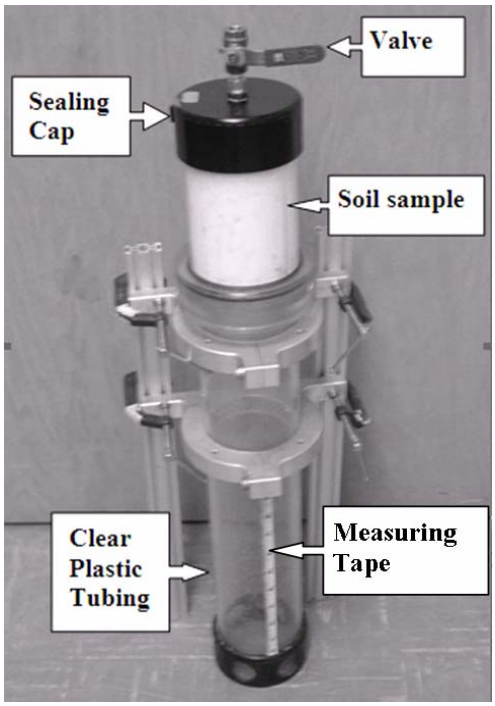

Figure 2.3. Air permeability flow test setup for measuring soil hydraulic conductivity.

To estimate the hydraulic conductivity of each soil column before and after freezing, the air permeability flow tests were conducted in a cold chamber. The tests were performed on the top, center and bottom sections of each soil column. For unfrozen soil, the measurements were performed on each dry-soil column before adding the water. Each section of the soil column was connecting to clear rigid plastic tubing that was 10.2 cm (4 in) in diameter and 50.8 cm (20 in) long using a plastic fitting. This lower clear tubing serves as a pressurized air reservoir. During each test, the top of the soil column section was sealed using a 10.2 cm (4 in) tubing cap, and the lower tubing section was submerged in a container of water at 4^{o}C (39.2 ^{o}F). When the valve in the sealing cap was opened, air flowed upward through the soils in the upper section as water rose and displaced the trapped air in the lower section. The head of the air in the lower tubing (H_0) was measured before the valve was opened using a measuring tape. The time for water to rise inside the lower tubing was

recorded using a stop watch. H_1 was measured when the timer was stopped. The head of the air changed from H_0 to H_1 as a function of time (t) in the clear plastic tubing. The air conductivity was computed using the following relationship (Massmann and Johnson, 2001):

$$K_{air} = \left(\frac{\rho_{air}}{\rho_w} \right) \frac{L}{(t_1 - t_0)} \ln(H_0 - H_1) \quad (1)$$

where L is the soil column length [L], H_o-H_1 [L] is the head fall during the time t_1-t_o, and ρ_{air} and ρ_w are densities of air and water [M/L^3], respectively.

The conductivity of air was then used in the following equation to determine the saturated water conductivity (Massmann et al., 2003):

$$K_w = \frac{\mu_{air} \rho_w}{\mu_w \rho_{air}} K_{air} \quad (2)$$

where K_w is the hydraulic conductivity [L/T], μ_w is the dynamic viscosity of the water at the test temperature [M/T·L], and ρ_w is the water density [M/L^3].

For each section of the unfrozen and frozen soil columns, the air conductivity test was repeated until a minimum of five consistent measurements were obtained.

2.5 RESULTS AND DISCUSSION

Air permeability flow tests were performed on the top, center and bottom sections of each soil column before and after freezing. Different times were allowed for soil-water redistribution prior to freezing to provide a variety of scenarios that may be encountered in the field. The soil columns were considered completely frozen after being in the freezer for 4 to 6 days, hence the frost depth was considered equal to 45 cm (18 in) for each of the soil columns.

For unfrozen soils, results indicate that average hydraulic conductivities varied minimally between the sections of each soil column as well as between the primary and duplicate unfrozen soil columns of each soil type. For the loam soil, measured hydraulic conductivity values for unfrozen soil columns and their duplicates varied from 1.9E-03 cm/s (7.5E-04 in/s) to 6.71E-03 cm/s (2.6E-03 in/s) with a geometric mean of 3.56E-03 cm/s (1.4E-03 in/s). For the sandy loam soil, measured hydraulic conductivity values for unfrozen soil columns and their duplicates varied from 2.27E-03 cm/s (8.9E-04 in/s) to 7.37E-03 cm/s (2.9E-03) with a geometric mean of 4.55E-03 cm/s (1.8E-03 in/s).

The hydraulic conductivity measurements for unfrozen soils were compared to hydraulic conductivity estimated by other empirical approaches. Details of the empirical approaches are presented in Appendix A. Results of the comparison are listed in Table 2.3. This table shows that the different approaches resulted in rather different ranges of soil hydraulic conductivity that are orders of magnitude different. This variation in hydraulic conductivity values can be explained by the different assumptions associated with each of these empirical approaches as well as the differences in the input data used for predicting the hydraulic conductivity in each equation.

Table 2.3. Unfrozen soil hydraulic conductivity obtained by air permeameter flow tests compared to estimates by other empirical approaches.

Equation	Hydraulic Conductivity *K* (cm/s) *Loam*	Hydraulic Conductivity *K* (cm/s) *Sandy loam*
Equation 3.A[a]	9.00E-02	1.00E-02
Equation 5.A[b]	2.01E-05	2.45E-05
Equation 7.A[c]	5.55E-02	1.74E-02
Equation 8.A[d]	7.24E-03	2.14E-03
Equation 13.A[e]	3.56E-03	4.55E-03

[a] Hazen (1911), [b] Rawls and Brakensiek (1985), [c] Massmann et al., (2003), [d] Kozeny-Carman (in Bear 1990), [e] Air Permeameter flow Test.

The effect of the time allowed for soil-water redistribution prior to freezing on the hydraulic conductivity of the frozen loam and sandy loam soils is illustrated by data presented in Table 2.4 and Table 2.5, respectively. Results of the tests for the primary loam soil columns and their duplicates are provided in Table 2.4. Results of the tests for the primary sandy loam soils and their duplicates are presented in Table 2.5. These tables illustrate variability exists for hydraulic conductivity values among the primary and duplicate soil columns of same redistribution time. This variability can be attributed to inherent differences in tourtuosity and connectivity of pores in the individual soil columns. However, the overall response and hypothesis with respect to redistribution time was verified in the duplicates.

The effect of the available time for soil-water redistribution prior to freezing on the conductivity of frozen soil was also demonstrated with Figures 2.4 and 2.5. Figure 2.4

compares the primary and duplicate test results for loamy soils, and illustrates the range of hydraulic conductivities measured for those columns before and after freezing. Similarly, Figure 2.5 compares the primary and duplicate test results for sandy loam soil columns, and illustrates the range of hydraulic conductivities measured for those columns before and after freezing. The results reveal that the time allowed for soil-water redistribution has a strong influence on hydraulic conductivity values in frozen soils. Short soil-water redistribution times resulted in considerable decreases in hydraulic conductivity for all sections in each soil column. For example, the hydraulic conductivities of the loam soil columns that were drained for only two hours prior to freezing decreased one to two orders of magnitude. On the other hand, increasing the allowable time for soil-water redistribution before the onset of freezing resulted in less reduction in the hydraulic conductivity of the frozen soil column across depths especially in the top section (0-15 cm depth). Moreover, as sufficient time passed between infiltration and the onset of subzero temperature, the frozen soil columns started to exhibit the same behavior as the unfrozen soil columns with respect to hydraulic conductivity in all sections. However, while a 24-hour period appeared to be sufficient for the hydraulic conductivity of the frozen loam soil to return to the same order of magnitude as its value before freezing, the sandy loam soil appeared to require more than 24-hour of draining prior to freezing in order to behave the same as unfrozen soil (Figure 2.5).

Table 2.4. Hydraulic conductivities determined by air permeameter flow tests for unfrozen and frozen loam soil columns.

Column Label	Drainage Time (hr)	Section Label	Average hydraulic conductivity, K±σ K (cm/s) *Unfrozen soil*	Average hydraulic conductivity, K±σ K (cm/s) *Frozen soil*
Loam soils				
2A	2	B	2.14E-03±6.98E-04	4.35E-05±1.49E-05
		C	3.77E-03±1.06E-03	3.66E-04±2.22E-05
		T	4.04E-03±1.72E-03	4.74E-04±9.32E-05
2B	2	B	2.13E-03±6.86E-04	1.76E-05±1.35E-05
		C	3.76E-03±1.75E-03	5.72E-05±5.14E-06
		T	4.25E-03±1.58E-03	1.36E-04±2.98E-05
4A	4	B	2.62E-03±1.03E-03	8.26E-05±8.19E-06
		C	2.73E-03±1.10E-03	1.40E-03±4.61E-04
		T	2.79E-03±1.08E-03	2.20E-03±4.71E-04
4B	4	B	4.63E-03±2.16E-03	1.62E-04±5.46E-05
		C	4.15E-03±1.84E-03	1.15E-04±3.55E-05
		T	4.82E-03±1.34E-03	7.44E-04±1.77E-04
8A	8	B	3.25E-03±6.99E-04	1.50E-04±4.05E-05
		C	1.90E-03±2.65E-04	1.45E-03±1.16E-04
		T	2.95E-03±4.19E-04	2.41E-03±1.81E-04
8B	8	B	2.67E-03±3.83E-04	1.34E-04±2.44E-05
		C	4.38E-03±1.66E-03	1.51E-03±2.31E-04
		T	6.71E-03±6.34E-04	2.82E-04±6.17E-05
24A	24	B	2.79E-03±1.34E-03	1.74E-04±2.28E-05
		C	3.90E-03±2.07E-03	1.41E-03±4.15E-04
		T	5.93E-03±1.76E-03	1.09E-03±2.47E-04
24B	24	B	3.31E-03±1.22E-03	1.29E-03±1.70E-04
		C	3.16E-03±1.10 E-03	1.32E-03±1.48E-04
		T	2.78E-03±2.70E-03	1.13E-03±1.06E-04

A stands for the primary soil columns

B stands for the replicates soil columns

Table 2.5. Hydraulic conductivities determined by air permeameter flow tests for unfrozen and frozen sandy loam soil columns.

Column Label	Drainage Time (hr)	Section Label	Average hydraulic conductivity, K±σ K (cm/s) *Unfrozen soil*	Average hydraulic conductivity, K±σ K (cm/s) *Frozen soil*
Sandy Loam soils				
2A	2	B	5.86E-03±5.73E-04	1.70E-04±9.35E-06
		C	4.67E-03±4.90E-04	1.24E-04±1.61E-05
		T	5.04E-03±3.58E-04	1.98E-05±1.98E-05
2B	2	B	2.64E-03±1.25E-04	2.22E-05±1.16E-06
		C	2.55E-03±1.59E-04	3.50E-05±1.59E-06
		T	2.57E-03±3.82E-04	7.60E-05±1.98E-06
4A	4	B	5.74E-03±8.73E-04	7.74E-05±1.16E-05
		C	6.89E-03±1.02E-03	8.67E-05±1.27E-05
		T	7.37E-03±2.82E-03	3.51E-06±7.79E-08
4B	4	B	4.49E-03±1.04E-03	2.44E-05±6.76E-06
		C	5.15E-03±1.66E-03	5.66E-05±3.58E-05
		T	4.75E-03±1.74E-03	3.67E-06±1.32E-07
8A	8	B	4.70E-03±1.48E-03	3.30E-05±1.05E-05
		C	5.36E-03±1.67E-03	4.26E-06±1.66E-06
		T	7.03E-03±1.62E-03	2.81E-06±5.00E-07
8B	8	B	5.60E-03±2.83E-03	5.95E-05±2.63E-05
		C	4.43E-03±1.50E-03	2.38E-05±4.43E-06
		T	4.72E-03±1.14E-03	3.79E-05±1.10E-05
24A	24	B	3.35E-03±2.76E-04	1.56E-04±3.42E-05
		C	3.59E-03±1.18E-04	2.23E-04±1.53E-04
		T	4.62E-03±5.11E-04	1.39E-05±6.33E-07
24B	24	B	2.98E-03±2.06E-04	1.49E-04±2.51E-05
		C	2.89E-03±3.50E-04	1.34E-04±2.68E-05
		T	2.27E-03±7.60E-05	1.63E-05±7.11E-07

A stands for the primary soil columns

B stands for the replicates soil columns

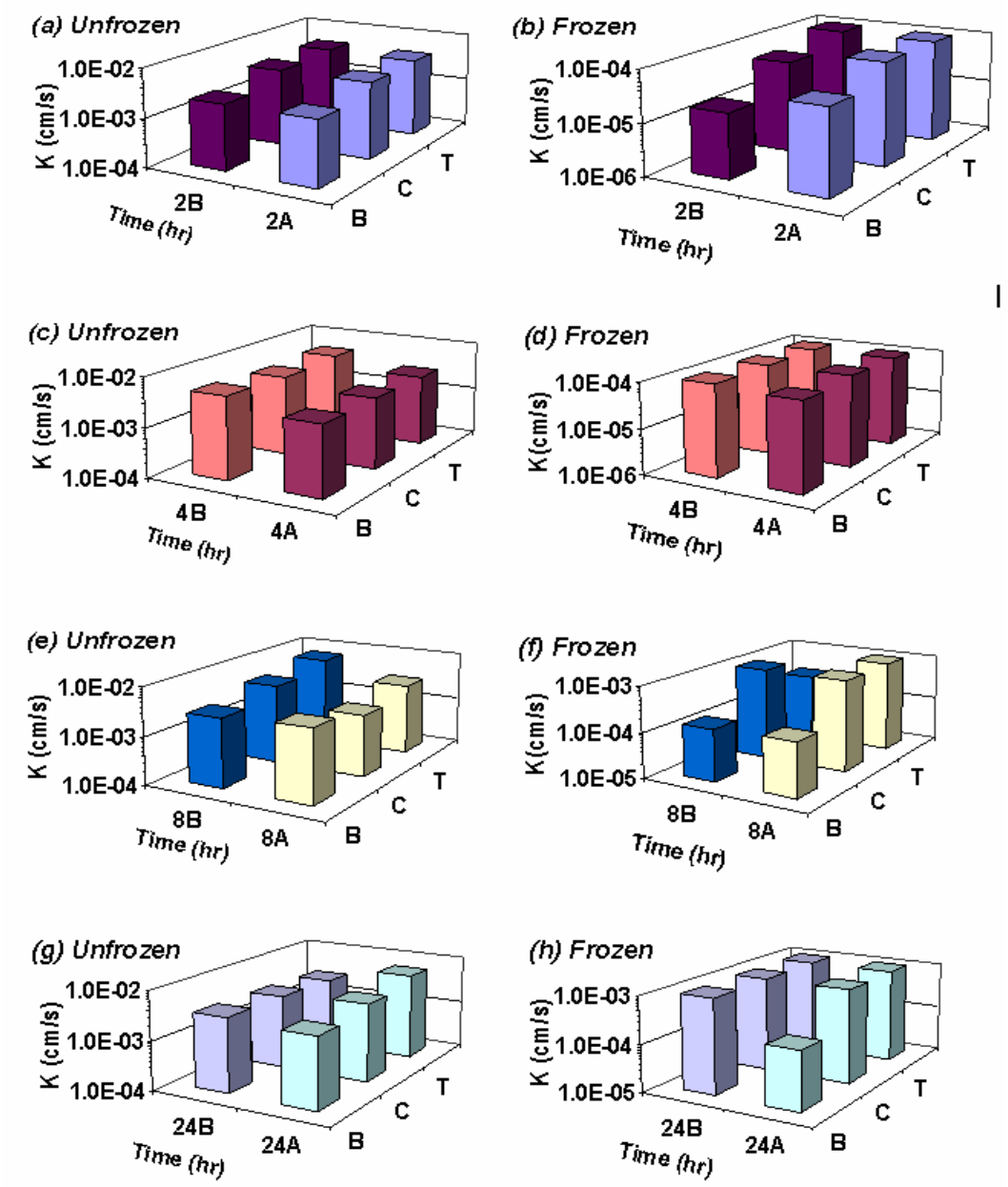

Figure 2.4. Average hydraulic conductivity for the unfrozen and frozen loam soil columns, Spokane site.

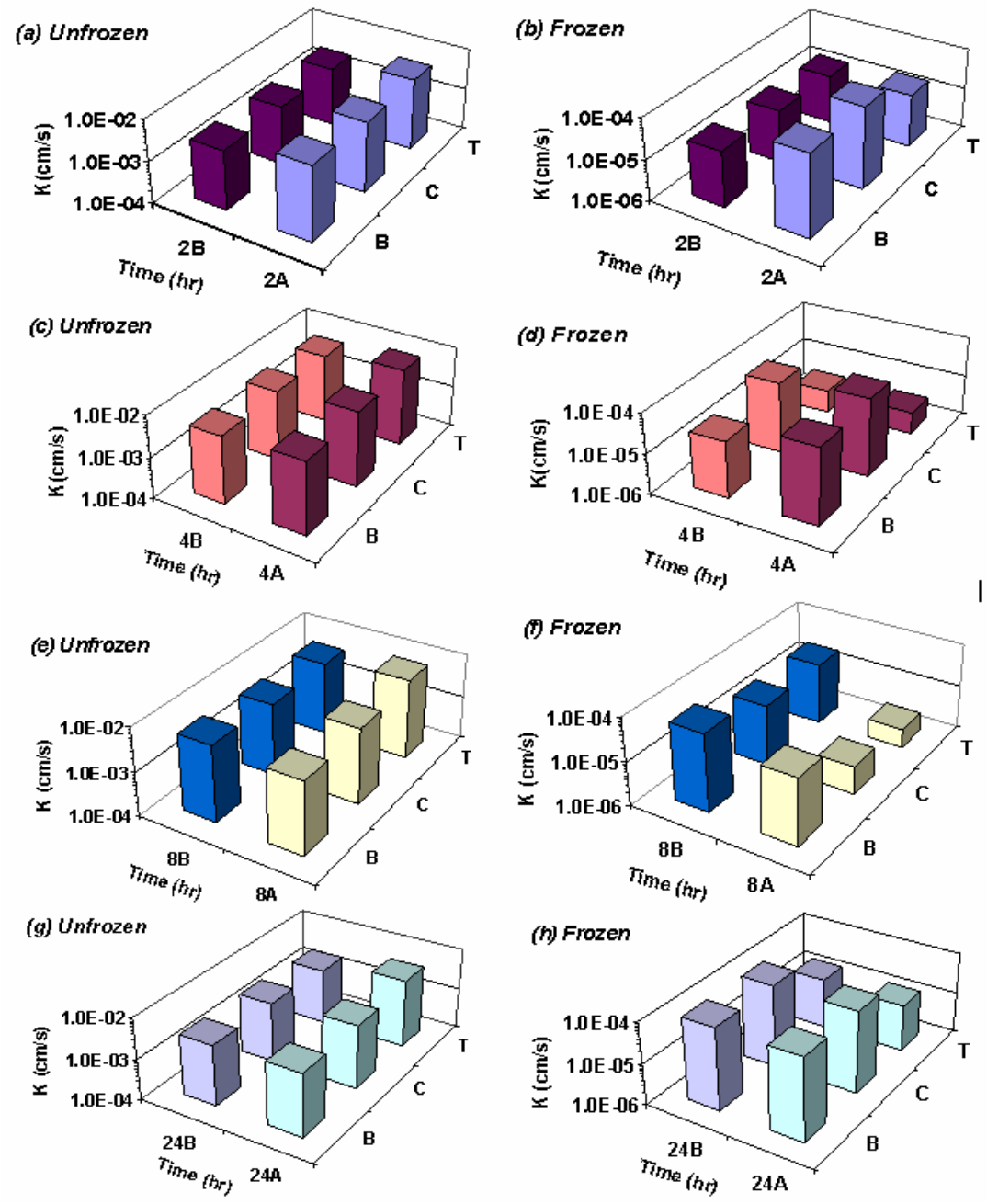

Figure 2.5. Average hydraulic conductivity for the unfrozen and frozen sandy loam soil columns, Richland site.

Variations in hydraulic conductivity rates for frozen loam and sandy loam soils were attributed to the interference of freezing-induced redistribution phenomenon during prefreezing and freezing periods (Dirksen and Miller, 1966). Since the freezing initiated at the top surface of the soil column and freezing front propagated downward towards the bottom of the soil column, the soil temperature gradient forces the soil water to move from the warm end (lower sections of the soil column) towards the cold end (upper section of the soil column). This upward water movement presumably retards vertical soil-water distribution, which in turn would retain water in the top sections of the sandy loam soil. The effect of soil temperature gradient was more significant in the sandy loam than in loam soil, because the courser soil contains a high percentage of large pores that hold water weekly bound to the soil by capillary forces (Stephens, 1996). Butler et al. (1996) also observed the phenomenon of freezing-induced upward water movement in a field lysimeter experiment and provided a detailed illustration of the phenomena.

The experimental data was used to establish a correlation between the soil-water redistribution time and the expected reduction in soil hydraulic conductivity after freezing. Hydraulic conductivity measurements from the three sections of each soil column were combined using the harmonic mean to obtain one representative value of hydraulic conductivity (K_{equiv}) for each soil column:

$$K_{equiv} = \frac{d}{\sum (d_i / K_i)} \tag{3}$$

The correction factor (*CF*) for each soil column was then computed as the ratio of the frozen soil hydraulic conductivity to the unfrozen soil hydraulic conductivity. For each soil type, the correction factors (*CF*) were plotted versus the allowed soil-water

redistribution times (t) as shown in Figures 2.6 and 2.7 to obtain two linear relationships for loam (Eq.15) and sandy loam (Eq. 16) soils using regression analysis:

$$CF = 0.0101t + 0.0161 \quad (4)$$

$$CF = 0.0003t + 0.0033 \quad (5)$$

The proposed equations can provide appropriate correction factors for loam and sandy loam soils to improve infiltration facility design in cold regions.

Based on these results, it is critical to consider the time available for soil-water redistribution after rainfall ceases and before the occurrence of sub-zero conditions to select appropriate design infiltration rates when sizing highway BMPs in cold regions. If historic information on the seasonality of storms indicates that precipitation primarily occurs at or near the end of winter, then consideration may be less important. However, the inland Pacific Northwestern U.S. historically experiences rain-on-snow events during the middle of winter (Ferguson, 2000; Marks et al., 2001), which suggests the necessity of factoring frozen soil conditions when selecting treatment BMP design parameters.

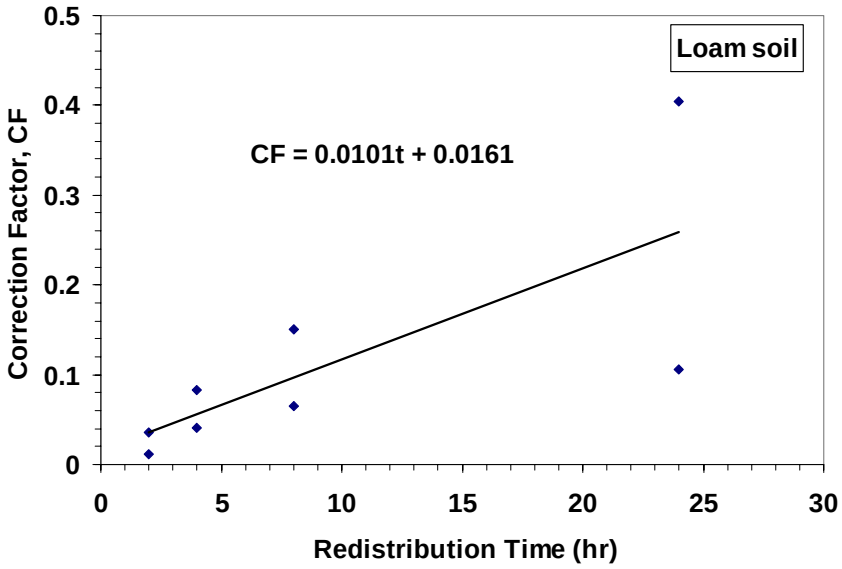

Figure 2.6. Correction factors relationship with soil-water redistribution times for the loam soil.

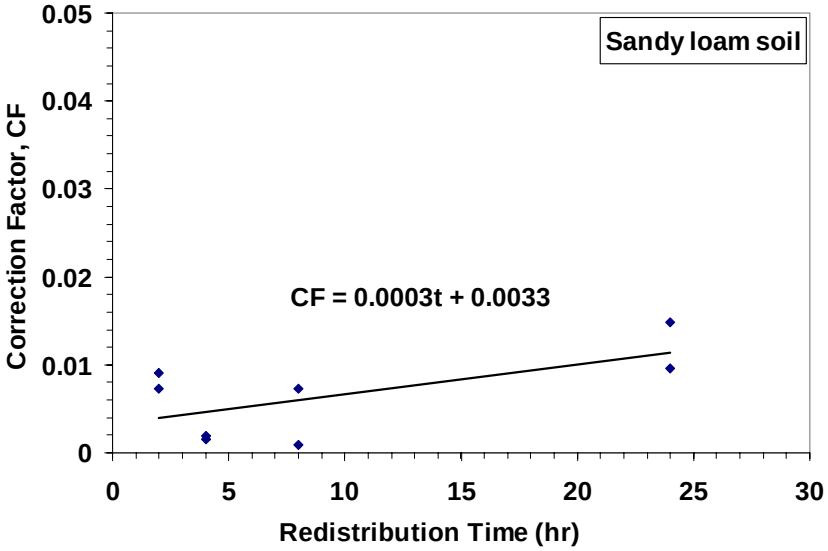

Figure 2.7. Correction factors relationship with soil-water redistribution times for the sandy loam soil.

2.6 CONCLUSIONS

Air permeameter flow tests were used in this research to obtain hydraulic conductivity measurements for unfrozen and frozen soils. For the loam soil, measured hydraulic conductivities ranged from 1.90E-03 cm/s (7.4E-04 in/s) to 6.71E-03 cm/s (2.64E-03 in/s) prior to freezing, and from 1.76E-05 cm/s (6.9E-06 in/s) to 1.09E-03 cm/s (4.29E-04 in/s) after freezing. On the other hand, measured hydraulic conductivities for sandy loam soil columns ranged from 2.27E-03 cm/s (8.94E-04 in/s) to 7.37E-03 cm/s (2.90E0-03 in/s) prior to freezing, and from 4.26E-06 cm/s (1.68E-06 in/s) to 1.24E-04 cm/s (4.88E-05 in/s) after freezing. The research findings revealed that the reduction in hydraulic conductivity of frozen soil depends greatly on the time allowed for soil-water redistribution prior to the onset freezing. The laboratory experiment suggested that allowing long periods for soil-water redistribution prior to freezing result in less reduction in soil hydraulic conductivity after freezing.

In addition, results showed that if a 24-hour period is allowed for soil-water redistribution before the onset of freezing, frozen loamy soils will behave the same as unfrozen soil in respect to hydraulic conductivity. Examining draining times longer than 24-hour would allow more accurate estimation of the threshold soil-water redistribution time after which the frozen sandy loam soil would start to behave as when unfrozen with respect to hydraulic conductivity. On the other hand, this study revealed that the soil texture has a significant effect on soil-water redistribution behavior during the freezing process due to differences in pore size distribution, and therefore it should be considered when estimating the hydraulic conductivity of frozen soils.

The regression equations developed for the loam and sandy loam soil allow designers to estimate an appropriate correction factor for soil hydraulic conductivity for frozen ground conditions if historic climate data indicates a need when sizing treatment infiltration facilities.

2.7 ACKNOWLEDGMENTS

The authors would like to acknowledge the Federal Highway Administration (FHWA) for financial support of this research. Gary Held's assistance with the air permeameter apparatus design and machining is greatly appreciated. In addition, Isak Andrews's help in conducting the laboratory air permeameter flow tests is appreciated.

2.8 REFERENCES

Bayard, D., Stähli, M., Parriaux, A., and Hannes, F. (2005). "The Influence of Seasonally Frozen Soil on the Snowmelt Runoff at Two Alpine Sites in Southern Switzerland." *Journal of Hydrology*, 309, 66-84.

Bear, J. (1990). "Dynamics of Fluids in Porous Media." New York, American Elsevier.

Butler, A., Burne, S., and Wheater, H. (1996). "Observations of Freezing-Induced Redistribution in Soil Lysimeters." *Hydrological Processes*, 10, 471-474.

Caraco, D., and Claytor, R. (1997). "Stormwater BMP Design Supplement for Cold Climates." Prepared by Center for Watershed Protection, Ellicott City, MD, for U.S. EPA Office of Wetlands, Oceans, and Watersheds, Washington, DC.

Dirksen,C., and Miller, R.D. (1966). "Closed-System Freezing of Unsaturated Soil." Soil *Science Society of America Journal*, 30, 168-173.

Ferguson, Sue A. (2000). "The Spatial and Temporal Variability of Rain-On-Snow." In Proceedings of the International Snow Science Workshop, 1-6 October 2000, Big Sky, Montana, American Avalanche Association, 178-183.

Hazen, A. (1911). "Discussion: Dams on Sand Foundation." *Transactions, American Society of Civil Engineers*, 73, 199.

Iwata, Y., Hayashi, M., Hirota, T. (2008). "Comparison of Snowmelt Infiltration under Different Soil-Freezing Conditions Influences by Snow Cover." *Vadose Zone Journal,* 7(1), 79-86.

Marks, D., Link, T., Winstral, A., and Garen, D. (2001). "Simulating Snowmelt Processes during Rain-On-Snow over a Semi-Arid Mountain Basin." *Annals of Glaciology*, 32(1), 195-202.

Massmann, J.W., and Johnson, L. (2001). "A Set of Exercises Illustrating Flow in Porous Media." *Ground Water*, 39(4), 499-503.

Massmann, J.W., and Allen, T. (2003). "A Design Manual for Sizing Infiltration Ponds." Final Research Report, Research Project Agreement No Y8265, Implementation of Infiltration Ponds Research.

McCauley, C.A., White, D.M., Lilley, M.R., and Nyman, D.M. (2000). "Fuel Penetration Rates in Frozen Soils: Bethel, Alaska." *Proceedings of the American Water Resources Association (AWRA) Spring Specialty Conference.*

McCauley, C.A., White, D.M., Lilley, M.R., and Nyman, D.M. (2002). "A Comparison of Hydraulic Conductivities, Permeabilities and Infiltration Rates in Frozen and Unfrozen soils." *Cold Regions Science and Technology,* 34, 117-125.

Miller, R.D. (1973). "Soil Freezing in Relation to Pore Water Pressure and Temperature." *Permafrost, 2nd International Conference Proceedings National Academy of Sciences Washington, DC,* 334-352.

Orlando B.A., Wiggert, D.C., and Davies, S.H. (1996). "Hydraulic Conductivity of Frozen Granular Soils." *Journal of Environmental Engineering*, 122(3), 212-216.

Pikul, J.L., Wilkins, D.E., Aase, J.K., Zuzel, J.F. (1996). "Contour Ripping: A Tillage Strategy to Improve Water Infiltration into Frozen Soil." *Journal of Soil and Water Conservation.* 51(1), 76-86.

Rawls, W.J., Brakensiek, D.L. (1985). "Prediction of Soil Water Properties for Hydrologic Modeling." *Proceeding of Symposium on Watershed Management, ASCE*, 293-299.

Seyfried, M.S., Murdock, M.D. (1997). "Use of Air Permeability to Estimate Infiltrability of Frozen Soil." *Journal of Hydrology*, 202, 95-107.

Stadler, D., Stähli, M., Aeby, P., and Flühler, H. (2000). "Dye Tracing and Image Analysis for Quantifying Water Infiltration into Frozen Soils." *Soil Science Society American Journal*. 64, 505-526.

Stähli, M., Jansson, P.E. and Lundin, L.C. (1999). "Soil Moisture Redistribution and Infiltration in Frozen Sandy Soils." *Water Resources Research*, 35(1), 95-104.

Stähli, M., Bayard, D., Wydler, H., and Flühler, H. (2004). "Snowmelt Infiltration into Alpine Soils Visualized by Dye Tracer Technique." *Artic, Antarctic, and Alpine Research*, 36 (1), 128-135.

Stephens, Daniel B. (1996). "Vadose Zone Hydrology." CRC Press Inc, Boca Raton, Florida.

Takeshi I., Yoneyama, K., and Nishio, N. (1985). "X-ray Technique for Observation of Ice Lens Growth in Partially Frozen Saturated Soil." *Cold Regions Science and Technology Journal*, 11(3), 213-221.

U.S. Department of Agriculture, USDA (1975). "Soil Taxonomy Handbook." 436, Washington, USA.

Wiggert, D. C., Andersland, O.B., and Davies, S.H., (1997). "Movement of Liquid Contaminants in Partially Saturated Frozen Granular Soils." *Cold Regions Science and Technology*, 25, 111-117.

Zhao, L.T. and Gray, D.M., (1999). "Estimating Snowmelt Infiltration into Frozen Soils." *Hydrological Processes*, 13, 1827-1842.

CHAPTER THREE

Assessment of the SCS-CN Initial Abstraction Ratio for Predicting Runoff Treatment Volumes during Rain-on-Snow Events

3.1 ABSTRACT

The initial abstraction ratio (I_a/S) in the SCS-CN equation for surface runoff volume is generally assumed to be 0.20. However, mounting evidence indicates that the I_a/S ratio is typically less than 0.20 and is not constant but rather varies from storm to storm and from watershed to watershed. The impacts on runoff prediction are considerable particularly in semi-arid climates where typical 6-month design storms are less than 1 inch of total effective precipitation. Furthermore, in cold climates, the presence of snow cover at the onset of rainfall influences the abstraction ratio and increases runoff volumes due to the rapid snow melting. In addition, frozen soil conditions can significantly impact this ratio by limiting the near surface pore-volume available for initial abstractions. In this study, we investigated the validity of the currently used 0.20 initial abstraction ratio in semi-arid cold climate regions where most design storm runoff events are generated as a result of rain-on-snow events with frozen ground conditions. To accomplish this, a rainfall simulator system was developed to simulate rainfall on a 1.22 m wide x 2.44 m long plot. The programmable rainfall simulator produced rain intensities and durations according to the design hyetographs encountered in semi-arid cold regions. The artificial rainfall intensities were less than 3.5 mm/hr and were simulated under different snow depths (2.0–10.0 cm) and plot slopes (1-5%). An alternative methodology for assigning I_a/S ratios for use in semi-arid climates has been developed. An example case study for application in Eastern Washington regions subjected to cold weather conditions was used to demonstrate the utility of the methodology. The new methodology

provides an easy way to improve the designer estimate of the initial losses during rain-on-snow events and more accurately determine runoff design volumes.

Keywords: stormwater management, curve number, SBUH method, rainfall simulator.

3.2 INTRODUCTION

Increased stormwater runoff as a result of urbanization generates both quantity and quality concerns. Studies have concluded that increased stormwater runoff causes eroded stream banks, channel instability, increased turbidity and pollution, and increased downstream flooding (Booth and Jackson, 1997; NRDC, 1999). These effects can have adverse impacts on fish and other organisms living in the stream and the receiving waters (NYSDEC, 1992; USEPA, 1995; USGS, 1995). Infiltration treatment best management practices (BMPs) are designed to reduce these impacts by retaining surface runoff volumes and allowing them to infiltrate into the ground thereby reducing both pollutant loading and peak stream discharges.

Designs of infiltration treatment BMPs are generally based on runoff volume computed from a prescribed precipitation event (e.g., the 24-hour SCS Type 1A storm) with a return frequency (e.g., 6-month) using a single event hydrograph model (WDOE, 2004; WSDOT, 2004). Many single event hydrograph models are available for computing the design runoff volumes. One widely used single event model is the Santa Barbara Urban Hydrograph (SBUH) model (Stubchaer, 1975). This model applies the U.S. Soil Conservation Service Curve Number (SCS-CN) equations to an approach that determines the runoff hydrograph (SFWMD, 1994; Tsihrintzis and Hamid, 1997; WSDOT, 2004). Based on

the computed design runoff volume, the size of the infiltration facility is selected so that it captures and treats a target percentage (e.g., at least 90 %) of the annual runoff volume (WDOE, 2004).

The abstraction ratio (I_a/S), defined as the ratio of the initial losses (I_a) to the maximum possible losses (S), in the original SCS-CN equation was developed based on actual watershed data from 24-hour duration storms and was fixed at a nation-wide average value of 0.20 (Plummer and Woodward, 1998). This approach does not allow for regionalized values based on geologic and climatic settings (Ponce and Hawkins, 1996). In addition, more recent research on the SCS-CN method has shown that the I_a/S ratio is not constant and that the assumption of I_a/S = 0.20 is usually high (Hawkins et al., 2003; Schneider and McCuen, 2005). Furthermore, the applicability of I_a/S = 0.20 to storm durations other than 24-hours is uncertain.

In this work, we examined the applicability of the originally developed abstraction ratio of 0.20 for long storm durations likely to occur in semi-arid cold climates where a considerable amount of annual precipitation falls in the form of snow. Snowfalls represents an important source of water in these regions since runoff generated from snow melting and rain-on-snow events play a major role in recharging ground water and replenishing surface water storage (USACE, 1998). However, such events can cause problems because of the increased runoff volumes generated from snow melt which can in turn fill or saturate the stormwater BMP prior to an actual design event (WDOE, 2004). If soils are frozen, runoff quantities associated with such events may cause significant flooding, erosion, and sedimentation in reservoirs. In addition, the presence of snow on the ground at the onset of rainfall does not account for the additional losses likely to occur and may therefore

underestimate the runoff hydrograph response time and the size of the required treatment facility. Based on these facts, the critical runoff event may be caused by these unique conditions, and therefore it may be more appropriate to use snowmelt events for the design of BMPs rather than the design rainfall events (USDA, 2004).

In many cold regions, under designed facilities may fail to achieve required treatment targets. Thus there is a need for reexamining the initial abstraction term during long duration, cold climate storms. To achieve this goal, an application case study using data collected in Eastern Washington was used to modify the existing design variables in the model, specifically the initial abstraction ratio (I_a/S) to account for cold weather conditions related to frozen ground and snow considerations including rain-on-snow and snowmelt events.

3.3 OBJECTIVES

The overall objectives of this work are to:

1) Assess the prediction errors resulting from using the traditional initial abstraction ratio in the SCS-CN equation to determine runoff volume for BMPs design in semi-arid cold climates,
2) Develop a new initial abstraction relationship for use in semi-arid cold climates by performing SBUH model calibration using measured rainfall runoff data from simulated rain-on-snow events.
3) Create an example case study for Eastern Washington to demonstrate the design impacts of more accurate runoff volume estimates generated from the long duration storms.

3.4 BACKGROUND THEORY

The SCS-CN method was derived analytically in the late 1950's by the former Soil Conservation Service (USDA-SCS, 1985), now the Natural Resources Conservation Service (NRCS). The derived equation takes the following form:

$$Q = \frac{(P - I_a)^2}{P - I_a + S} \tag{1}$$

where Q is the direct runoff depth [in], P is the event rainfall depth [in], I_a is the initial abstraction that occurs before the start of runoff including evaporation, evapotranspiration, interception, surface depression, and initial infiltration losses [in], and S is the potential maximum storage [in] defined as the maximum possible difference between P and Q that can occur for the given storm and watershed conditions (Woodward et al., 2002). When multiplied by the contributing drainage area, a runoff volume is generated.

For convenience in practical application, the parameter S was mapped into a dimensionless parameter CN, the curve number, which varies according to land use/cover, soil type, and antecedent moisture condition from 0 (no runoff) to 100 (all rainfall becomes runoff). The chosen relationship is:

$$S = \frac{1000}{CN} - 10 \tag{2}$$

The I_a was defined as the event rainfall required for the initiation of runoff and was assumed to be equal to some fraction of the maximum potential storage:

$$I_a = \lambda S \tag{3}$$

Substituting Equation 3 into Equation 1, rearranging the terms, and setting the initial abstraction value equal to 20% of the storage (*i.e.*, λ=0.20) , yields the well known form of the SCS-CN equation:

$$Q = \frac{(P - 0.2S)^2}{(P + 0.8S)} \quad \text{for } P \geq 0.2S,\ Q = 0 \text{ otherwise} \tag{4}$$

In 1966, the Santa Barbara County Flood Control and Water Conservation District used the SCS-CN equation to develop the Santa Barbara Urban Hydrograph (SBUH) method to compute runoff hydrographs for urbanized areas directly without applying the SCS unit hydrograph method. Since its inception, the method has been widely applied in several single event models, and it is currently recommended by Washington State Department of Transportation (WSDOT) for calculating the runoff treatment design volumes or flow rates of project sites in Eastern Washington. Inputs for the SBUH method include the pervious and impervious areas of the watershed, time of concentration, runoff curve numbers, soil characteristics, design storm precipitation and design storm hyetograph for a specific 24-hour event. Detailed description of computation steps for the SBUH methods can be found in Appendix C.

Numerous articles have been published concerning the SCS-CN method and several modifications have been proposed over the years on both the method and its parameters for more accurate computation of surface runoff volume (Mockus, 1964; Hawkins, 1975, 1978, 1979, 1993, 1998; Linsley et al., 1975; Gray et al., 1982; Hawkins et al., 2005, Perrone and Madramootoo, 1998; Schneider and McCuen, 2005; Mishra and Singh, 1999, 2003; Mishra et al., 2003, 2006). However, very few studies have investigated the applicability of the SCS-CN parameters in cold regions. Among these parameters is the initial abstraction storage ratio (I_a/S). The (I_a/S) ratio in the SCS-CN equation is generally assumed to be 0.20. However, indications are this parameter is not constant but rather varies from storm to storm and from watershed to watershed. Moreover, the value may be considerably less than 0.20. The

impacts on runoff prediction are considerable particularly in semi-arid climates where typical 6-month design storms are less than 1 inch of total effective precipitation. Furthermore, in cold climates, the presence of snow cover at the onset of rainfall influences the abstraction ratio and increases runoff volumes due to the rapid snow melting. In addition, frozen soil conditions can significantly impact this ratio by limiting the near surface pore-volume available for initial abstractions. In this work, rain-on-snow based hydrograph analysis was used as a tool to assess the SCS-CN initial abstraction ratio for predicting runoff treatment volumes in semi-arid cold climate regions where most design storm runoff events are generated as a result of rain-on-snow events with frozen ground conditions.

3.5 MATERIALS AND METHODS

The research goals were achieved through the following efforts: (1) an artificial rainfall simulator system was designed and constructed to mimic the natural long duration rainfall events applicable to cold regions (2) rainfall/runoff data were collected from several simulated rain-on-snow events, and (3) SBUH model calibration was performed to modify the existing initial abstraction parameter.

3.5.1 Rainfall simulator design

Previous researchers studying runoff, infiltration, and erosion processes have recognized the benefits of using rainfall simulators in their investigations (Bubenzer and Meyer, 1965; Meyer and Harmon, 1979; Miller, 1987; Frasier et al., 1998; Williams et al., 1998; Battany and Grismer, 2000; Humphry et al., 2002; Paige et al., 2003). In this work, an artificial rainfall simulator system was developed to apply a controlled amount and rate of

rainfall on a test plot. The rainfall simulator created rainfall characteristics typical of low energy natural storms encountered in the inland Pacific Northwest U.S. (Williams et al., 1998). The simulated storms had maximum intensities of less than 3.5 mm/hr over durations lasting 30 hours.

The rainfall simulator system consisted of a spray nozzles system, water tank, piping system, flow meter/controller, impervious snow table, air compressor, and a collection gutter on the down-gradient end draining to a tipping bucket recorder (Figure 3.1).

Figure 3.1. Rainfall simulator and plot frame set up.

The spray nozzle system comprised of two 2.44 m long x 5.1 cm thick (8.0 ft long x 2.0 in thick) frames made of wood, 14 KES white nozzles, and 9.5 mm (3/8 in) diameter

rigid PVC tubing. Seven nozzles were mounted 30.48 cm (1.0 ft) apart along both of the overhead members. After testing their performance and the coverage area across the plot at different heights, the nozzles' tips were located at 1.22 m (4.0 ft) above the plot surface. A 16-bit precision water flow meter and water flow controller (L-10LPM-D) with a solenoid control valve mounted to downstream of the controller was installed in line to regulate water flow to the spray nozzles during the application of the rainfall hyetographs. The solenoid valve operation, and thus the various rain intensities, was controlled by providing the flow meter with a set point that corresponded to a specific water flow rate and a defined time interval. The amount of water required for a simulating run was supplied to the nozzles by a 151.4 L (40 gallon) insulted steel vertical water tank placed near the simulator. An electric powered 2-hp, 45.42 L (12 gallon) air compressor was used to pressurize the water in the tank to approximately 413.7 KPa (60 psi) through a 9.5 mm (3/8 in) diameter hose connected to the water tank. A pressure regulator in the compressor was used to adjust the water tank pressure to ensure constant pressure within the tank during the simulated run. The simulated rainfall was applied over a 1.22 m wide x 2.44 m long (4.0 ft wide x 8.0 ft long) surface area made of wood. The plot was enclosed on three sides by 15.2 cm (6.0 in) height wood sheets nailed to each side edge in order to define the rainfall/snow catchment area and to prevent the loss of direct surface runoff. A steel mesh was fastened to the forth side of the plot to allow runoff to drain into a gutter installed at this edge and to prevent sliding of the snow while simulating different plot slopes.

3.5.2 Rainfall/Runoff Data Collection

The applied rainfall distribution for Spokane city as an example case study for application in Eastern Washington regions subjected to cold weather conditions was selected for performing the different rain-on-snow simulations. The long duration hyetograph was computed using the 24-hour, 6-month design storm of Spokane city after adjusting the design storm value using the associated regional conversion factor. Graphical representation of the long duration design storm hyetograph of Spokane city is shown in Figure 3.2. Tabular values of the regional long duration hyetographs and the methods used for computation are presented in Appendix D.

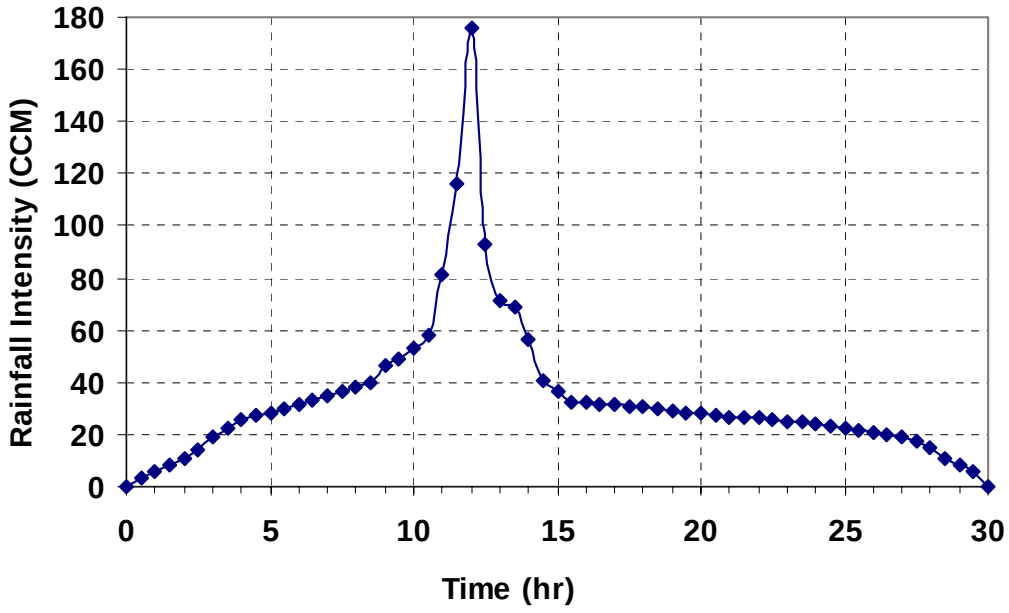

Figure 3.2. The long duration rainfall hyetograph for the city of Spokane, Washington and surrounding area.

During each simulated event, the continuously variable rainfall intensity and intervals were controlled by writing a script that defined the set point that corresponded to each of the rainfall intensities at the defined interval. Appendix E provides information on the method used for obtaining the set points and data that were sent to the flow meter device. The script was sent to the inline flow meter and controller device through serial communication with a laptop using a digital RS-232 signal and Hyperterminal® program (Figure 3.3).

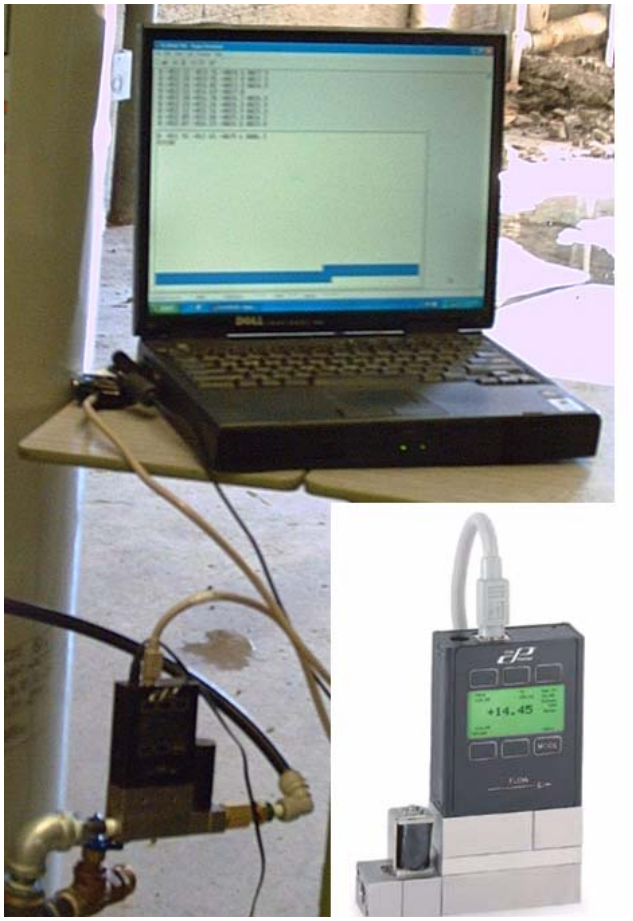

Figure 3.3. Flow meter and controller in connection with a laptop computer for applying controlled rainfall intensity on the test plot.

Runoff rates were monitored by collecting the runoff in the gutter installed at the down slope edge of the plot and passing it into a standard tipping bucket rain gauge equipped with Onset Hobo data logger that counted and recorded the time of each tip (Figure 3.4). Data stored by the Onset Hobo data logger was then used to determine the runoff rates for each event.

Figure 3.4. Tipping Bucket equipped with Onset Hobo data logger for runoff measurement.

The simulated rainfall/runoff events were designed to examine the impacts of different average snow depths (2.5 cm, 5 cm, 7.5 cm, and 10 cm) as well as various plot slopes (0.0159, 0.031 and 0.047 m/m) on runoff rates. For each test run, the snow water equivalent, defined as the amount of water contained within the snow pack, was determined by weighing the snow and then spreading it evenly across the test plot area to obtain the desired depth. The snow water equivalent (SWE) for each case was calculated as:

$$SWE = D_S \frac{\rho_s}{\rho_w} \quad (5)$$

where D_s is the snow depth [in], and ρ_s and ρ_w are the density of water and snow [Lb/in^3], respectively (Bedient and Huber, 2002).

Finally it is important to point out that these simulations were conducted inside but near a large sliding door that allowed exposure to near natural, but uncontrollable, air temperatures. Measurements of the average air temperature during the duration of each simulated events was obtained by averaging the values of the air temperatures that were captured and recorded by the flow meter during each of the defined rainfall interval.

3.6 RESULTS AND DISCUSSIONS

3.6.1 Runoff Hydrographs Analyses

The measured plot runoff from 19 rain-on-snow events simulated under various snow conditions and plot slopes was monitored and recorded. Table 3.1 presents a summary of the snow depths, densities, and plot conditions for each of the simulated events. The simulated events in Table 3.1 represent different characteristics of a snow layer in terms of the snow density for each case and the associated snow water equivalent for that layer. Some events were simulated using a fresh dry low density snow (new, just falling) and some were simulated using an old wet dense snow. Snow density variation between the same depth snow layers is the reason for the differences in the snow water equivalent computed for each simulated event.

Table 3.1. Details of input measured parameters for each of the simulated events

	Measured Parameters				*Calculated Parameters*	
Event #	Air Temperature, T_a (^oC)	Plot slope, S (%)	Snow weight, Wt (kg)	Snow depth, D_s (cm)	Snow density, ρ_s (g/cm^3)	Snow water equivalent, SWE (cm)
1	14.2	1.56	15.0	2.5	0.20	0.50
2	5.8	1.56	17.2	2.5	0.23	0.58
3	6.2	1.56	38.8	5.1	0.26	1.30
4	6.0	1.56	35.8	2.5	0.47	1.20
5	5.7	3.13	24.0	2.5	0.32	0.81
6	5.2	3.13	42.6	5.1	0.28	1.43
7	5.3	3.13	29.9	5.1	0.20	1.01
8	2.2	4.69	31.3	2.5	0.41	1.05
9	4.8	4.69	72.6	5.1	0.48	2.44
10	2.5	4.69	38.1	5.1	0.25	1.28
11	2.9	1.56	43.5	5.1	0.29	1.46
12	13.6	4.69	82.1	7.6	0.36	2.76
13	13.4	4.69	136.1	10.2	0.45	4.58
14	11.4	3.13	43.5	10.2	0.55	5.58
15	14.3	1.56	125.6	7.6	0.55	4.22
16	14.5	3.13	135.6	7.6	0.60	4.56
17	10.5	1.56	42.2	10.2	0.14	1.42
18	9.3	3.13	73.5	10.2	0.24	2.47
19	11.6	4.69	51.3	10.2	0.17	1.72

Measured runoffs generated from each of the simulated events listed in Table 3.1 were plotted to examine the hydrographs. Figures 3.5 through 3.23 compare the calculated runoff hydrograph with the observed runoff hydrograph obtained from each of the simulated events.

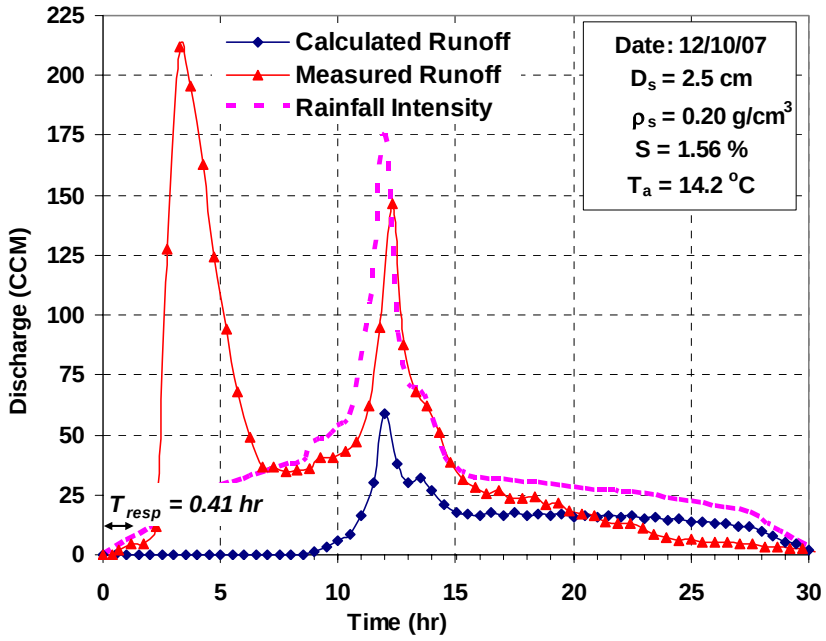

Figure 3.5. The pattern of rainfall input during event 1 and the calculated versus measured runoff hydrographs from this event.

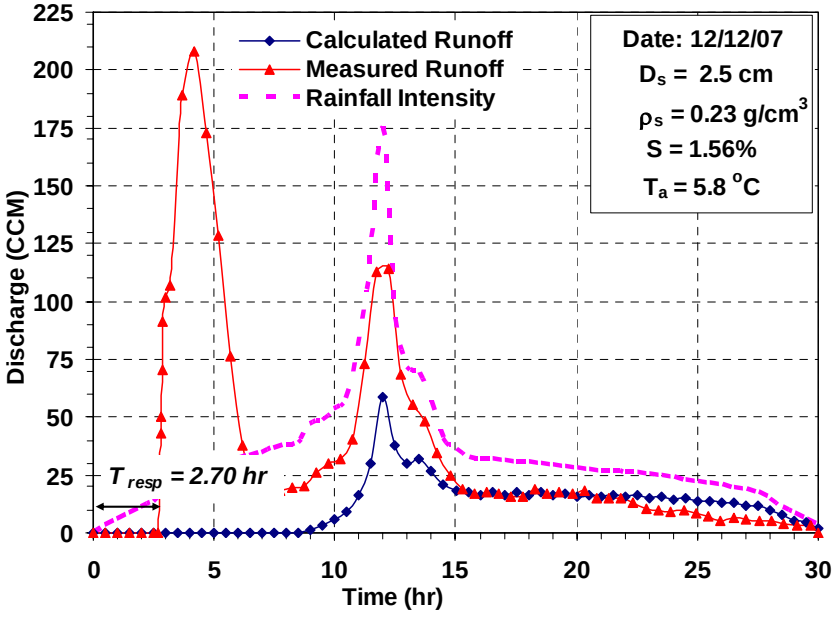

Figure 3.6. The pattern of rainfall input during event 2 and the calculated versus measured runoff hydrographs from this event.

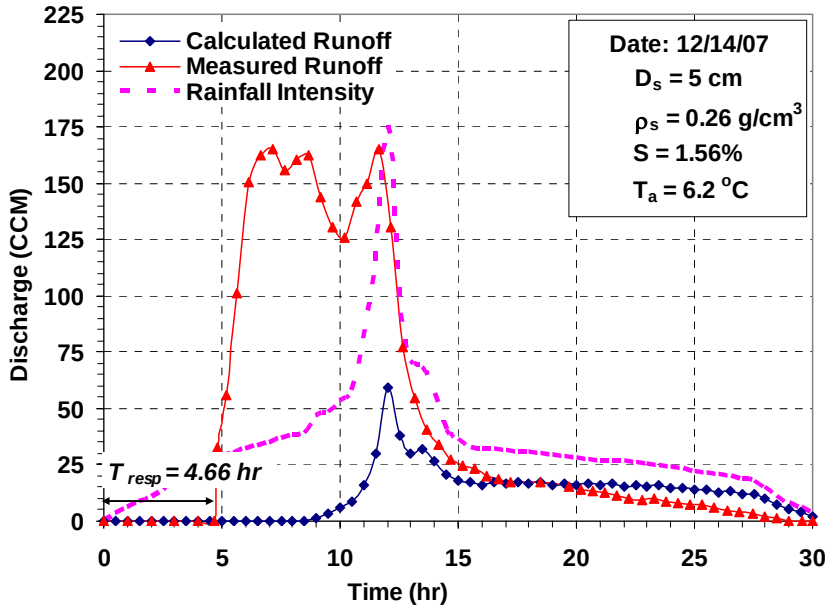

Figure 3.7. The pattern of rainfall input during event 3, and the calculated and measured runoff hydrographs from this event.

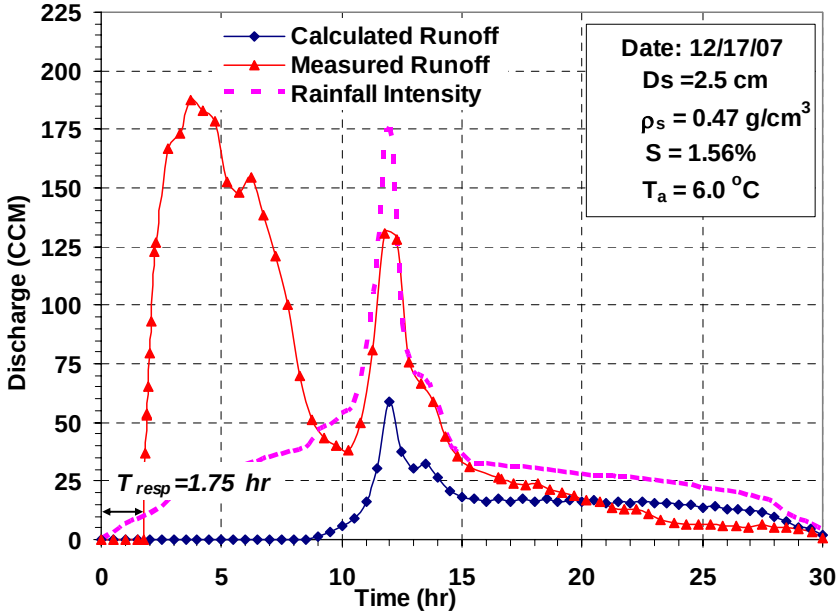

Figure 3.8. The pattern of rainfall input during event 4, and the calculated and measured runoff hydrographs from this event.

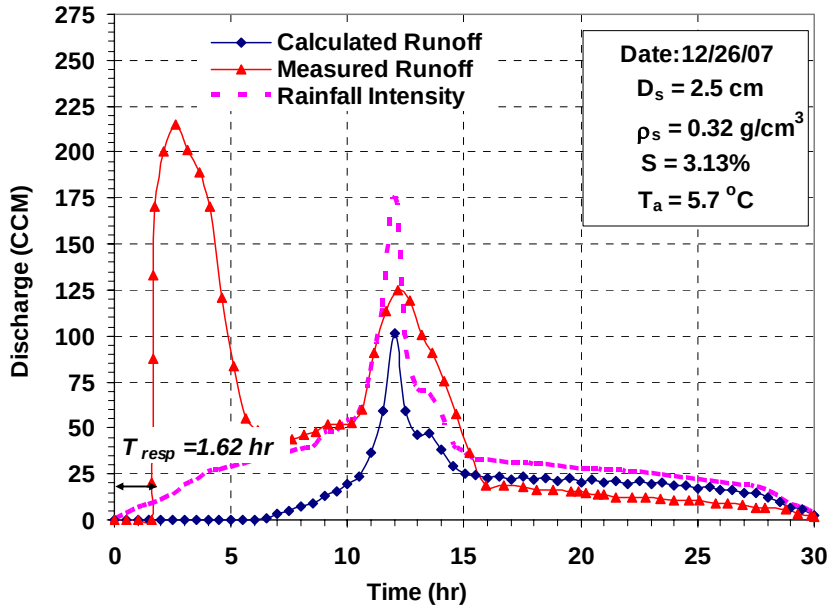

Figure 3.9. The pattern of rainfall input during event 5 and the calculated and measured runoff hydrographs from this event.

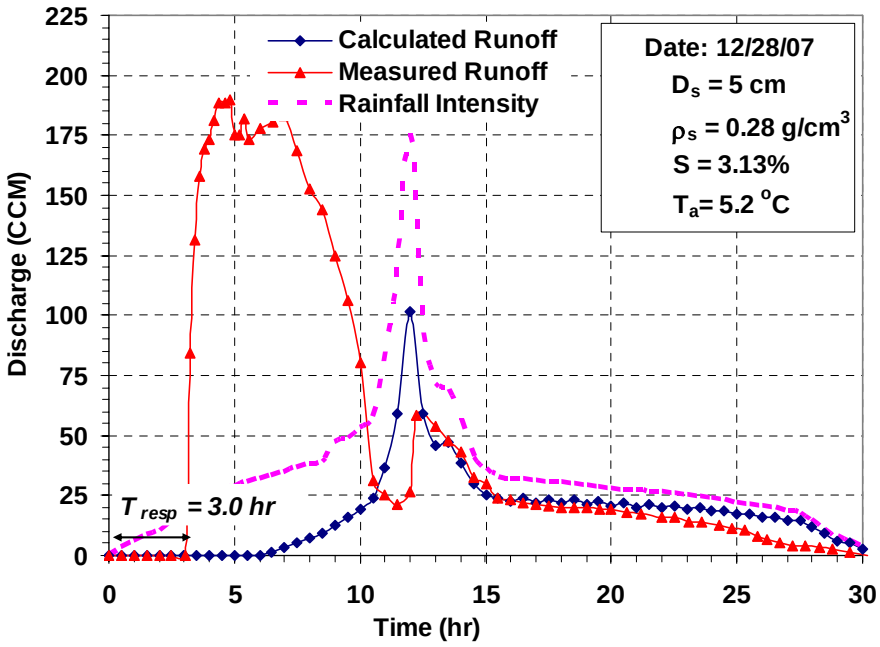

Figure 3.10. The pattern of rainfall input during event 6 and the calculated and measured runoff hydrographs from this event.

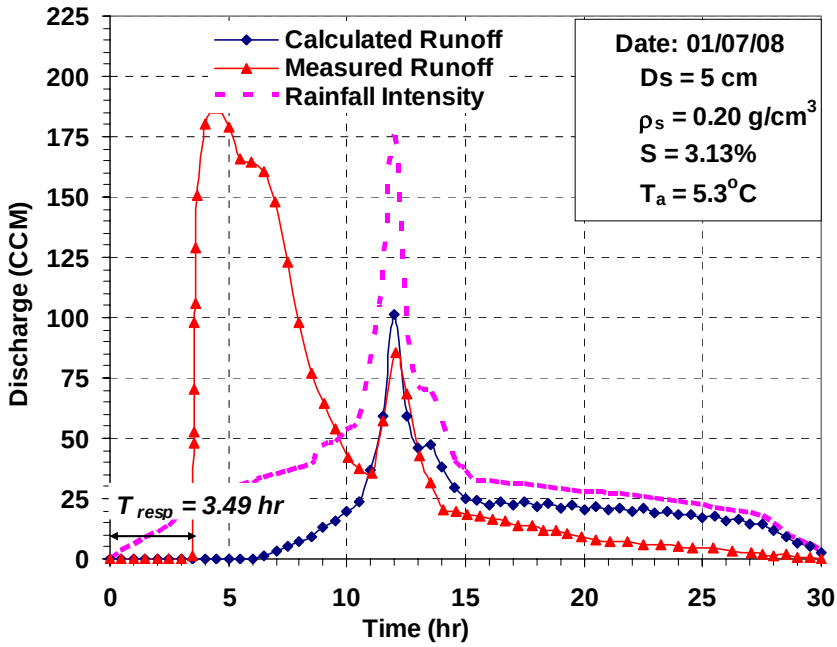

Figure 3.11. The pattern of rainfall input during event 7 and the calculated and measured runoff hydrographs from this event.

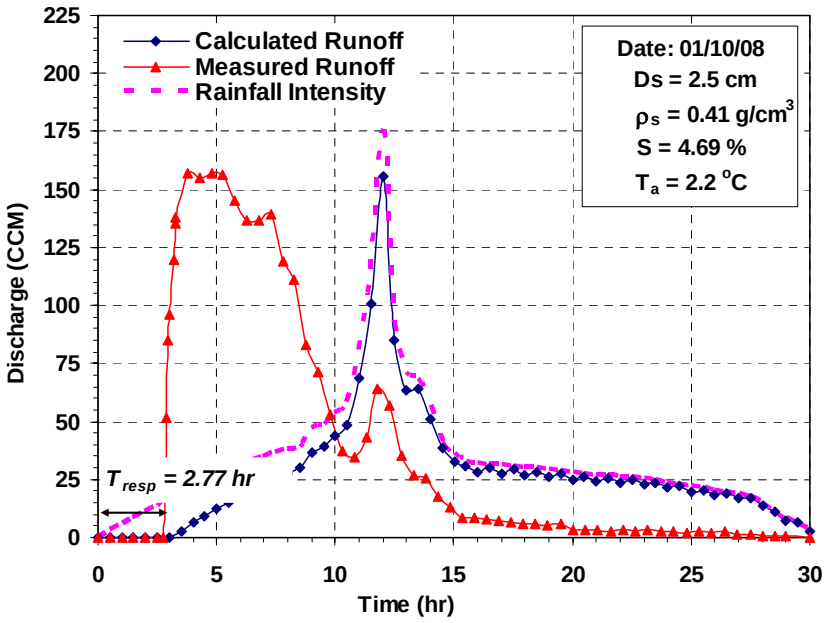

Figure 3.12. The pattern of rainfall input during event 8 and the calculated and measured runoff hydrographs from this event.

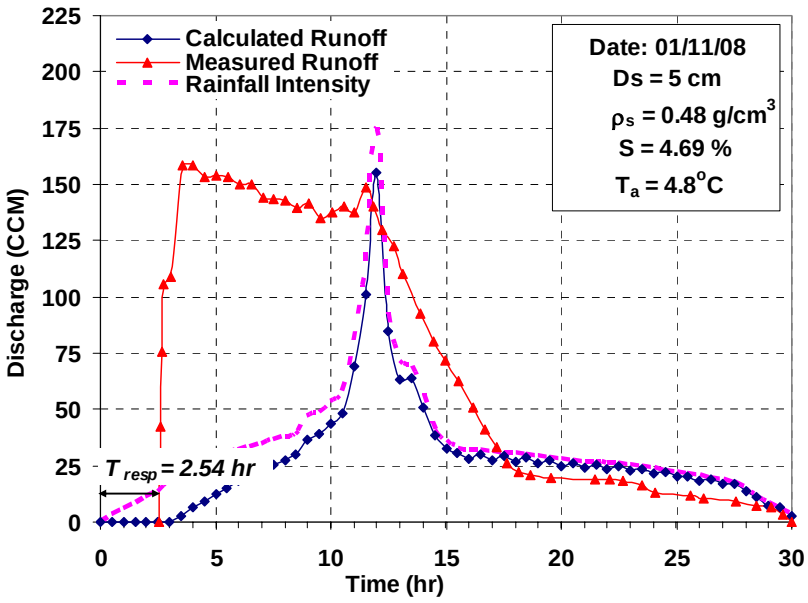

Figure 3.13. The pattern of rainfall input during event 9 and the calculated and measured runoff hydrographs from this event.

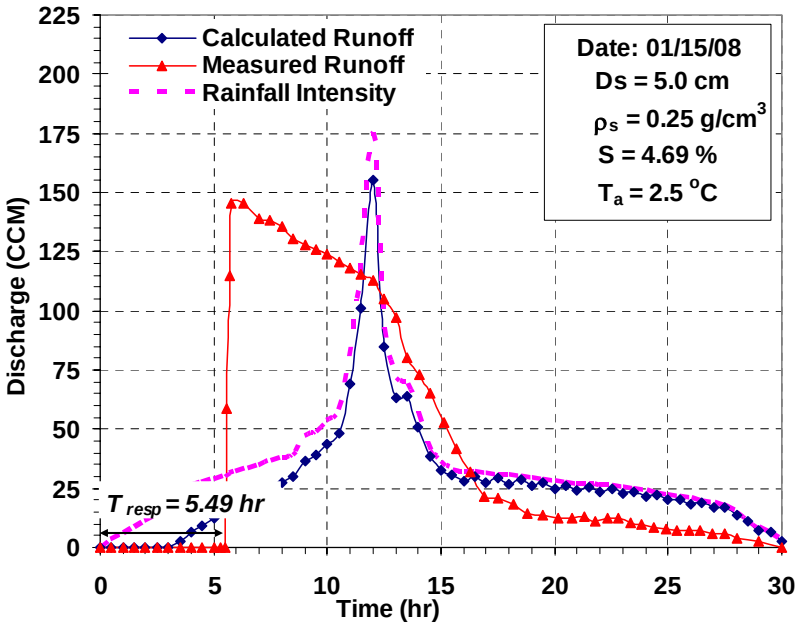

Figure 3.14. The pattern of rainfall input during event 10 and the calculated and measured runoff hydrographs from this event.

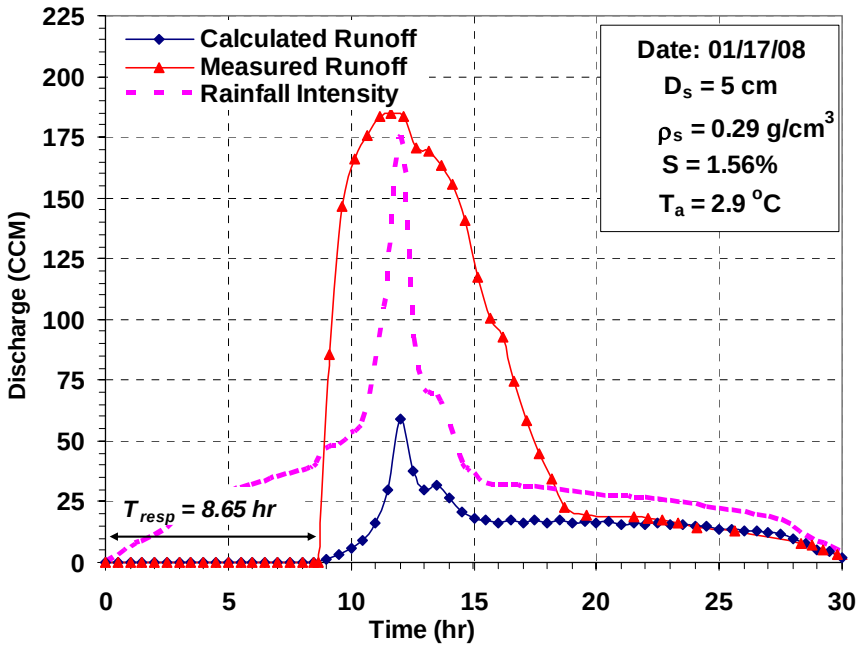

Figure 3.15. The pattern of rainfall input during event 11 and the calculated and measured runoff hydrographs from this event.

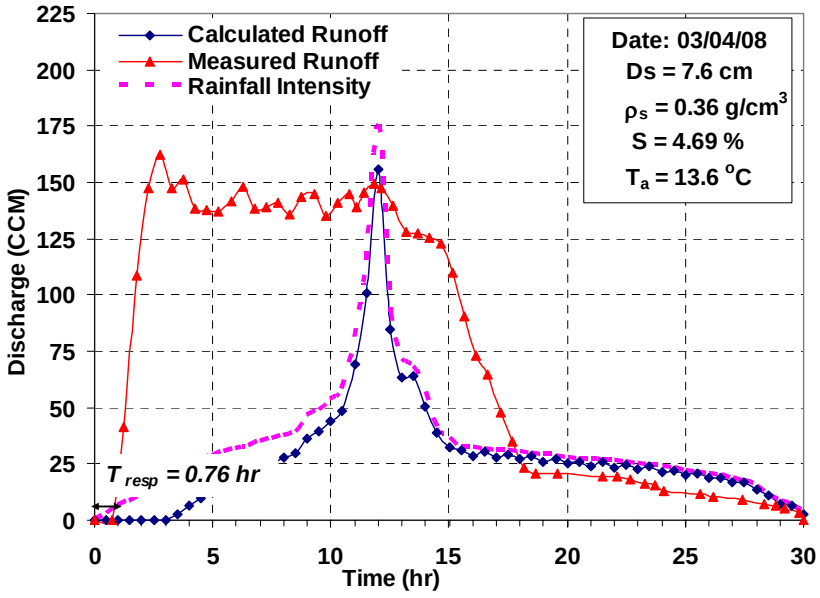

Figure 3.16. The pattern of rainfall input during event 12, and the calculated and measured runoff hydrographs from this event.

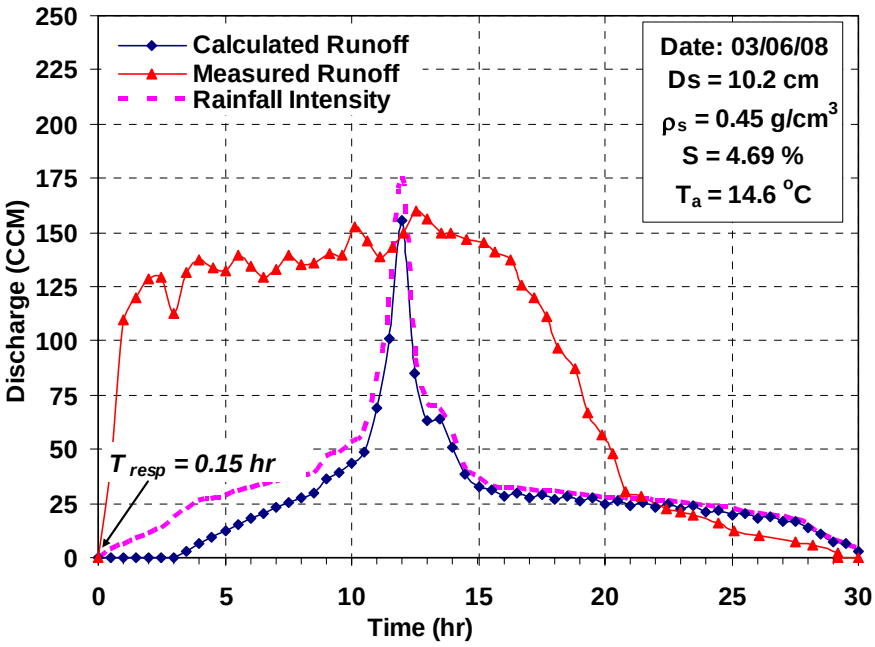

Figure 3.17. The pattern of rainfall input during event 13, and the calculated and measured runoff hydrographs from this event.

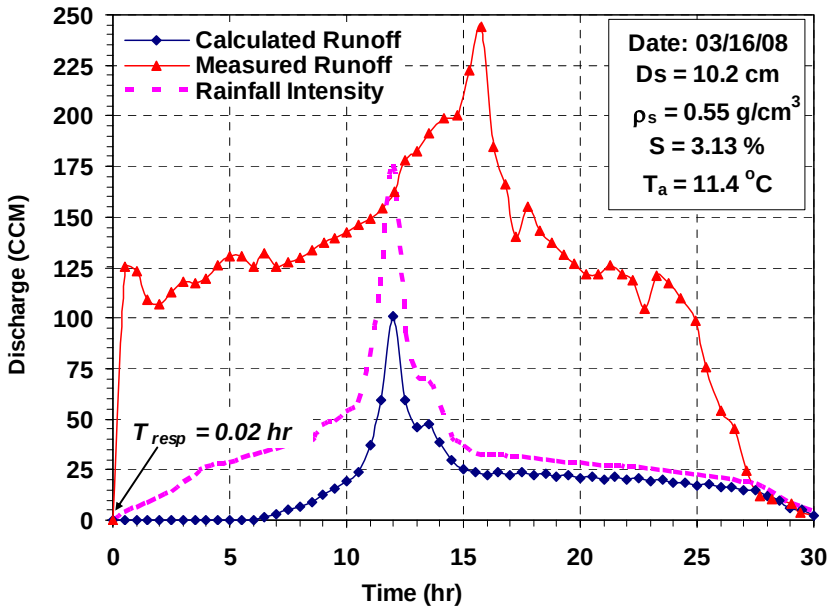

Figure 3.18. The pattern of rainfall input during event 14, and the calculated and measured runoff hydrographs from this event.

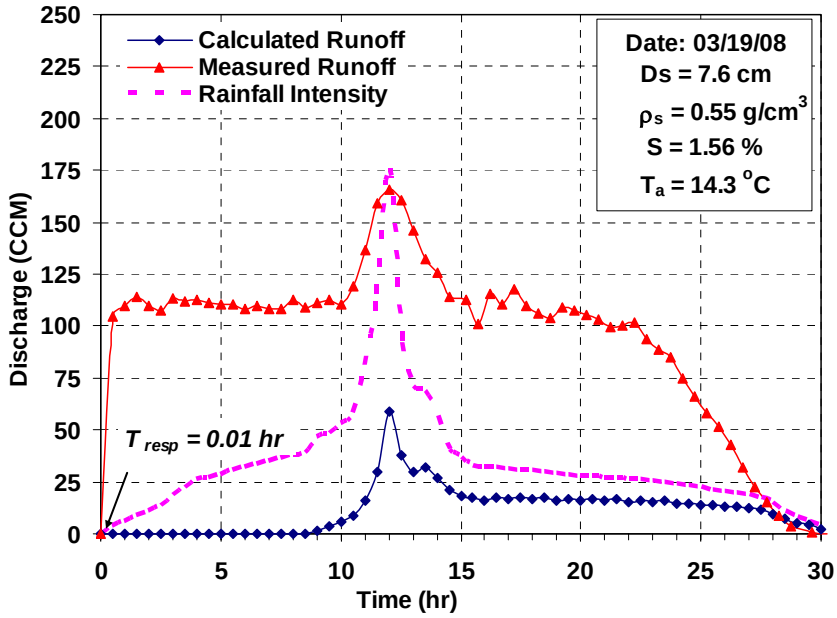

Figure 3.19. The pattern of rainfall input during event 15, and the simulated and measured runoff hydrographs from this event.

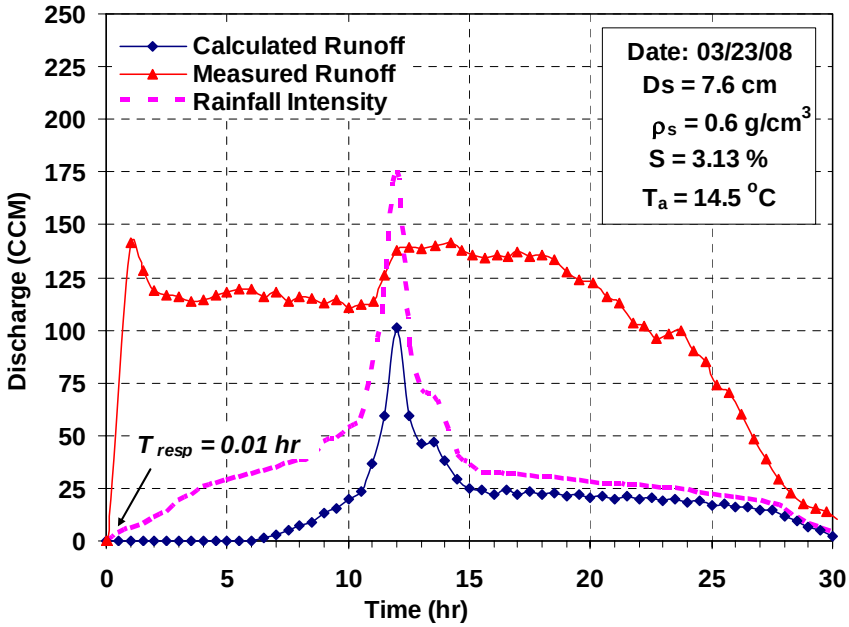

Figure 3.20. The pattern of rainfall input during event 16, and the calculated and measured runoff hydrographs from this event.

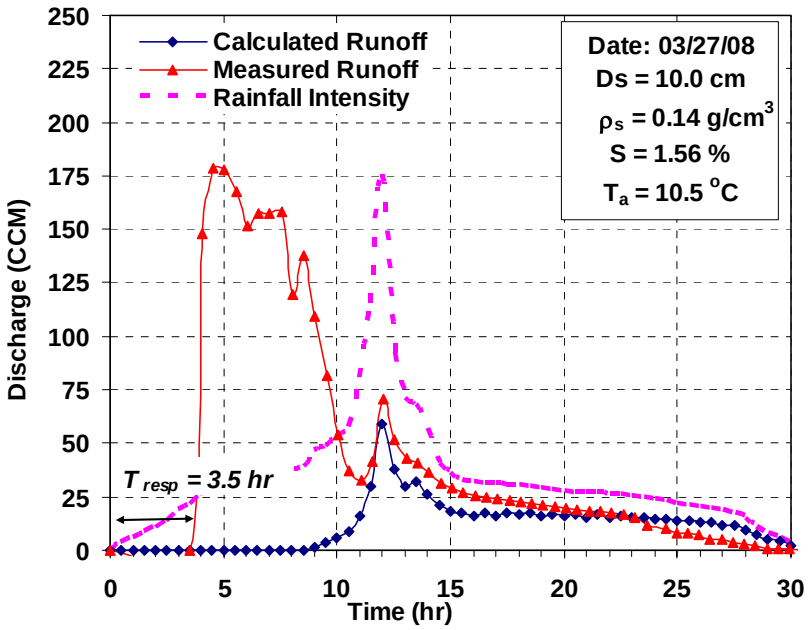

Figure 3.21. The pattern of rainfall input during event 17, and the calculated and measured runoff hydrographs from this event.

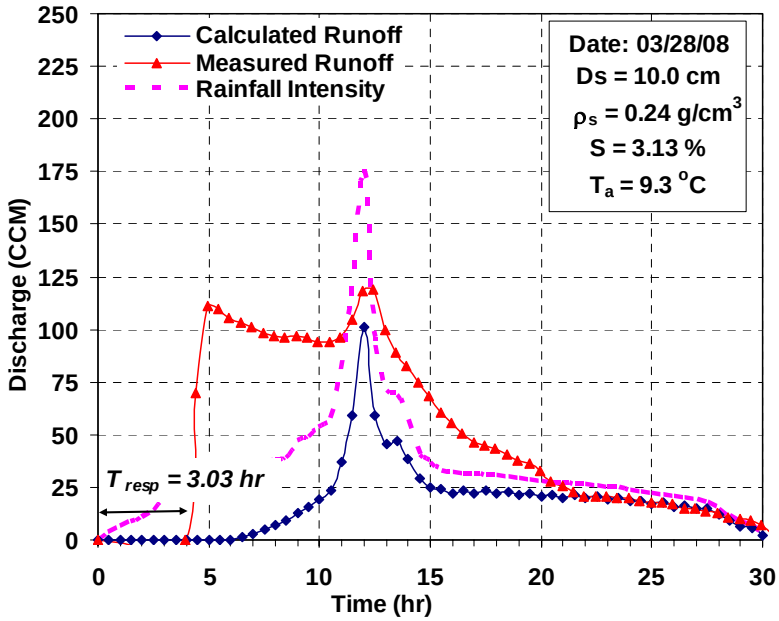

Figure 3.22. The pattern of rainfall input during event 18, and the calculated and measured runoff hydrographs from this event.

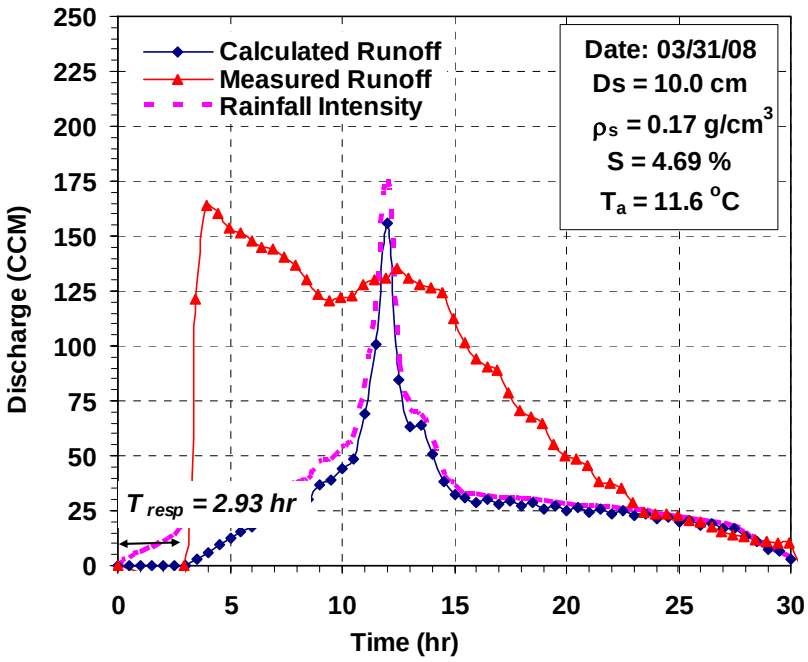

Figure 3.23. The pattern of rainfall input during event 19 and the calculated and measured runoff hydrographs from this event.

The SBUH method was used in this study to calculate the runoff hydrograph for each of the simulated rainfall events due to its historic application in Eastern Washington. To facilitate the calculation process, a spreadsheet (Microsoft Excel) model of the SBUH procedure was created. An example of the spreadsheet layout is presented in Figure 3.24. However, instead of using the customary used form of SCS-CN equation which fixes the λ parameter at 0.20, the general following form of the SCS-CN method was used. The total runoff depth for each time increment was computed as follow:

$$Q(t) = \frac{(P(t) - \lambda S)^2}{P(t) - S(\lambda + 1)} \qquad (6)$$

For all of the simulated rain-on-snow events, snow covers were assumed to occur on a frozen, saturated ground (no infiltration).

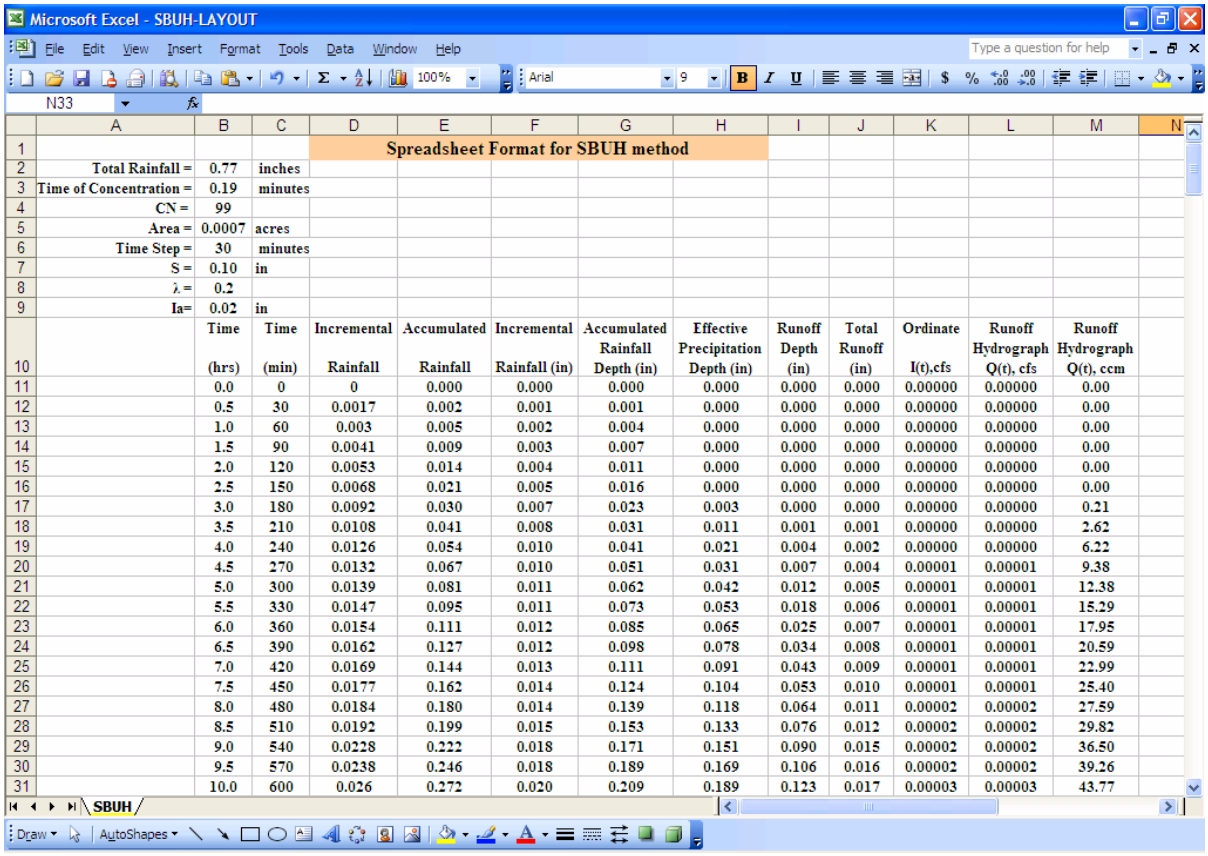

Microsoft Excel - SBUH-LAYOUT

Spreadsheet Format for SBUH method

Total Rainfall =	0.77	inches											
Time of Concentration =	0.19	minutes											
CN =	99												
Area =	0.0007	acres											
Time Step =	30	minutes											
S =	0.10	in											
λ =	0.2												
Ia=	0.02	in											
	Time (hrs)	Time (min)	Incremental Rainfall	Accumulated Rainfall	Incremental Rainfall (in)	Accumulated Rainfall Depth (in)	Effective Precipitation Depth (in)	Runoff Depth (in)	Total Runoff (in)	Ordinate I(t),cfs	Runoff Hydrograph Q(t), cfs	Runoff Hydrograph Q(t), ccm
	0.0	0	0	0.000	0.000	0.000	0.000	0.000	0.000	0.00000	0.00000	0.00
	0.5	30	0.0017	0.002	0.001	0.001	0.000	0.000	0.000	0.00000	0.00000	0.00
	1.0	60	0.003	0.005	0.002	0.004	0.000	0.000	0.000	0.00000	0.00000	0.00
	1.5	90	0.0041	0.009	0.003	0.007	0.000	0.000	0.000	0.00000	0.00000	0.00
	2.0	120	0.0053	0.014	0.004	0.011	0.000	0.000	0.000	0.00000	0.00000	0.00
	2.5	150	0.0068	0.021	0.005	0.016	0.000	0.000	0.000	0.00000	0.00000	0.00
	3.0	180	0.0092	0.030	0.007	0.023	0.003	0.000	0.000	0.00000	0.00000	0.21
	3.5	210	0.0108	0.041	0.008	0.031	0.011	0.001	0.001	0.00000	0.00000	2.62
	4.0	240	0.0126	0.054	0.010	0.041	0.021	0.004	0.002	0.00000	0.00000	6.22
	4.5	270	0.0132	0.067	0.010	0.051	0.031	0.007	0.004	0.00001	0.00001	9.38
	5.0	300	0.0139	0.081	0.011	0.062	0.042	0.012	0.005	0.00001	0.00001	12.38
	5.5	330	0.0147	0.095	0.011	0.073	0.053	0.018	0.006	0.00001	0.00001	15.29
	6.0	360	0.0154	0.111	0.012	0.085	0.065	0.025	0.007	0.00001	0.00001	17.95
	6.5	390	0.0162	0.127	0.012	0.098	0.078	0.034	0.008	0.00001	0.00001	20.59
	7.0	420	0.0169	0.144	0.013	0.111	0.091	0.043	0.009	0.00001	0.00001	22.99
	7.5	450	0.0177	0.162	0.014	0.124	0.104	0.053	0.010	0.00001	0.00001	25.40
	8.0	480	0.0184	0.180	0.014	0.139	0.118	0.064	0.011	0.00002	0.00002	27.59
	8.5	510	0.0192	0.199	0.015	0.153	0.133	0.076	0.012	0.00002	0.00002	29.82
	9.0	540	0.0228	0.222	0.018	0.171	0.151	0.090	0.015	0.00002	0.00002	36.50
	9.5	570	0.0238	0.246	0.018	0.189	0.169	0.106	0.016	0.00002	0.00002	39.26
	10.0	600	0.026	0.272	0.020	0.209	0.189	0.123	0.017	0.00003	0.00003	43.77

Figure 3.24. Spreadsheet layout used to obtain the calculated runoff hydrograph.

The actual measured runoff volumes and the peak discharges exceeded the simulated runoff volumes and peak discharges in all of the simulations. This was expected and could easily be attributed to the contribution of water from snow during melting to runoff volumes. On the other hand, the response time, defined as the time between the beginning of water input and the beginning of measurable response (Carey and Woo, 2001), reflected the integrated influences of: 1) snow cover conditions, 2) plot slope, and 3) average air temperature during the simulated events. Warmer temperatures (e.g. T_{air} > 10 ^{o}C) during simulated rain-on-snow events caused more rapid snow melting and earlier responses in the observed runoff hydrographs. Higher temperatures combined with an old dense snow pack

(e.g. events 12 to16) during the month of March caused runoff hydrographs to rise dramatically and much earlier than what was observed in the runoff hydrographs obtained early in the winter season (December and January). Additionally, plot slope had a significant effect on runoff onset; increased slopes caused faster observed runoff whereas decreased slopes caused later onsets of runoff.

Another aspect worth noting was that depending on these three variables, the shape of the output hydrograph produced from each simulated rain-on-snow event varied considerably. Some events produced a single extended runoff peak hydrograph while some events produced two runoff peaks hydrograph. The two-peak runoff output hydrographs were due to the snow melting process accelerated by the rain events which caused the first measured peak discharge to occur at much sooner than the simulated peak discharge. Following the snow melting period, runoff volume decreased and, as the rainfall event continued, a second peak occurred due only to the rainfall event. The single extended peak hydrographs with long response times appeared to be associated with cold, deep snow cover (e.g. Events 10 and 11), while the single extended peak hydrographs with rapid response times were observed in the springtime hydrographs (e.g. Events 13 and 14). Additionally, time to peak values observed in the simulated rain-on-snow events did not agree with those estimated by other available methods, for example, the SCS method for time to peak estimate.

This work proposed that knowledge of the response time of the output hydrographs could be used to predict initial losses during rain-on-snow events. Hence, the next step was to develop a SBUH model using the observed response times as the calibration parameter to predict the initial losses in each test run.

3.6.2 SBUH method calibration

Calibration was performed to determine an alternative λ (or I_a/S) value(s) that would be more applicable for use with the long duration storms occurring in Eastern Washington regions. For each simulated rain-on snow event, calibration was accomplished using a trial and error adjustment process for the initial abstraction ratio, λ, in the SBUH spreadsheet until the response time of the calculated runoff hydrograph matched the response time of the observed runoff hydrograph from the rain-on-snow event. The values of λ derived by the calibration of SBUH method, and the associated I_a values, for all of the rain-on-snow events are presented in Table 3.2.

Table 3.2. Values of the parameters derived from SBUH method calibration

Event #	Response time, T_{resp} (hr)	Initial abstraction ratio, λ	Initial abstraction, I_a (mm)
1	0.41	0.001	0.019
2	2.7	0.02	0.382
3	4.66	0.08	1.529
4	1.75	0.009	0.172
5	1.6	0.01	0.106
6	3.03	0.05	0.529
7	3.49	0.07	0.741
8	2.77	0.18	0.462
9	2.53	0.15	0.385
10	5.49	0.30	0.770
11	8.65	0.20	3.824
12	0.76	0.001	0.003
13	0.15	0.001	0.003
14	0.5	0.001	0.011
15	0.5	0.001	0.019
16	0.5	0.001	0.011
17	3.54	0.04	0.765
18	3.03	0.05	0.529
19	2.93	0.19	0.487

3.6.3 Regression equation for estimating the initial losses

To determine how the snow conditions, plot slopes and average air temperatures affected the initial abstraction storage ratio λ (or I_a/S), a multiple regression technique was used. A mathematical model that describes the behavior of λ from these variables was developed using Minitab15® statistical software. This model predicted λ in terms of snow depth (D_s), snow water equivalent (SWE), air temperature (T_a), and plot slope (S). The *p*-value at the 5 percent level (α = 0.05) was used to test the model. The first proposed model took the following form:

$$\lambda = A \cdot T_a^B \cdot S^C \cdot SWE^D \cdot D_s^E \tag{7}$$

where A, B, C, D, and E are regression constants.

Multiple regression analysis was performed to find the five regression constants (A, B, C, D and E) in Equation (7) as: A = 0.0872, B = –3.21 C = 0.17, D = –2.1, and E = 3.34. Substituting these values into Equation 7 yields the following equation:

$$\lambda = 0.08716 \cdot T_a^{-3.21} \cdot S^{0.17} \cdot SWE^{-2.1} \cdot D_s^{3.34} \tag{8}$$

where λ is the initial abstraction storage ratio [dimensionless], the T_a is the air temperature [^{o}C], S is the plot slope [%], *SWE* is the snow water equivalent [cm], and D_s is the snow depth [cm]. Based on *p*-value of < 0.001, and a coefficient of multiple determination (R^2) of 0.853, the proposed model is considered significant.

The *p*-values for the estimated coefficients of the average air temperature (T_a), the snow depth (D_s), and the SWE are less than 0.002, indicating that they are significantly related to the initial abstraction storage ratio at the 0.05 level. However, for the slope (S) coefficient the *p*-value is 0.756 thus indicating that the slope explained the least significant proportion of the variation in the initial abstraction storage ratio. This finding can be

explained by the fact that the slope effect was accounted for while calibrating the curve numbers (Appendix F). This suggests that a model with only T_a, D_s and SWE would be more appropriate for estimating the initial abstraction storage ratio.

The second proposed model was represented by the following equation:

$$\lambda = 0.10753 \cdot T_a^{-3.26} \cdot SWE^{-2.06} \cdot D_s^{3.36} \quad (9)$$

The *p*-value for the second model is less than 0.001 and the coefficient of determination (R^2) is 0.852. The *p*-values for the estimated coefficients of the average air temperature (T_a), the snow depth (D_s), and SWE are less than 0.001.

Based on the *p*-value and the R^2 of the new model, considering the snow conditions (D_s, and SWE), and the average air temperature during the cold season (T_a), was believed to be adequate for assigning a λ value during rain-on-snow events. Therefore Equation 9 was proposed in this study for assigning the initial abstraction storage ratio (λ) for predicting runoff treatment volumes during rain-on-snow events.

3.6.4 Verification

For verification of the proposed equation, λ was computed using the proposed regression equation (Equation 9) and compared to the observed initial abstraction storage ratio of the simulated rain-on-snow events. A plot of the best fit relationship between observed and modeled initial abstraction storage ratios is shown in Figure 3.25. As illustrated in the figure, the slope of the straight line is 1.69 and the y-intercept is 0.0361. In addition, the coefficient of determination is 0.84. However, while the regression line appeared to fit most of the data points, there were a few points which lie far away from regression line

(events 8, 9 and 10). These points (outliers) are found to be associated with the events that performed during cold air temperatures.

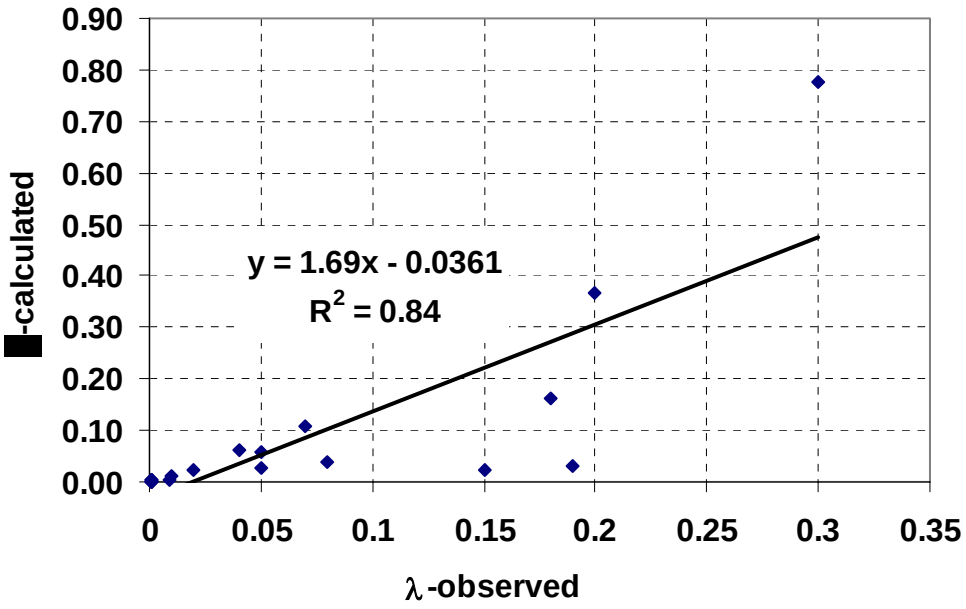

Figure 3.25. Calculated versus observed initial abstraction storage ratio, λ.

To demonstrate the validity of the calibration results, computation of the runoff hydrographs were re-carried out using the snow adjustment procedure (described in Appendix B) and the calibrated I_a/S values (Listed in Table 3.2). For each simulated event, the runoff hydrograph computed using the calibrated I_a/S values were compared to the measured runoff hydrograph. The calculated runoff hydrographs compared to the measured runoff hydrographs for the simulated event were plotted in Figures G.1 through G.19 in Appendix G. By comparing the runoff volume before and after calibration to the measured runoff volume, we found that using the calibrated I_a/S values improves the estimate of the predicted runoff volumes for most of the simulated events. However, while the proposed

regression equation for I_a/S estimate improves the design runoff volume estimate, it is at the same time increased the required BMP facility size. Figure 3.26 illustrates the percent change in the required facility area based on the assigned I_a/S value in deign runoff volume computation. Appendix H presents an example calculation to demonstrate the % increase in the required facility size near Spokane area.

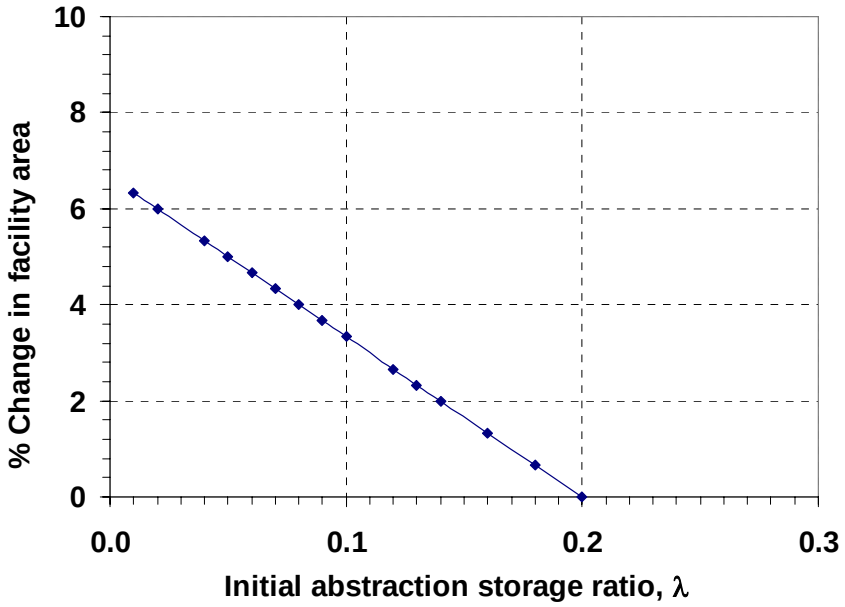

Figure 3.26. Percent change in required treatment facility area based on the assigned λ used in design runoff volume computation.

3.7 CONCLUSIONS

Deficiencies in the SCS initial abstraction estimate during cold weather conditions and, in particular, during rain-on-snow events was investigated in this study. A rainfall simulator was constructed to produce variable, low intensity rainfall of less than 3.5 mm/hr over a duration of 30 hours. The artificial rainfall events were simulated under a variety of

snow conditions, plot slopes, and air temperatures. Observed runoff hydrographs analysis obtained from simulated rain-on-snow events was used to improve estimates of the initial abstraction term during such events. From the analyses of the hydrographs, a clear dependence of the initial abstraction ratio on the conditions of snow, the plot slope, and the average air temperature during the rain-on-snow event was found. These combined factors governed the magnitude of the snowmelt runoff volume, the rate of snow melting, as well as how fast runoff may starts during rain-on-snow events.

Using the SBUH method calibration, a new procedure for determining the initial abstraction term in the SCS-CN method during rain-on-snow events was proposed. The regression equation for calculating the initial abstraction during rain-on-snow events produces a more realistic estimate of the initial losses during such events and improves outflow hydrograph prediction for design of infiltration treatment BMPs in cold regions. However, while this procedure will result in more efficient BMPs in terms of performance, large size facility will be required.

3.8 ACKNOWLEDGEMENT

This project has been funded by the U.S. Federal Highway Administration (FHWA). The authors would like to acknowledge and thank Gary Held and Kurt Hutchinson from the machine shop at Washington State University for their help in the plumbing and Isak Andrews for his laboratory and field assistance.

3.9 REFERENCES

Battany, M.C. and Grismer, M.E. (2000). "Development of a Portable Field Rainfall Simulator for Use in Hillside Vineyard Runoff and Erosion Studies." *Hydrological Processes*, 14, 1119-1129.

Bedient, Ph.B., and Huber, W.C. (2002). "Hydrology and Floodplain Analysis." Prentice Hall, Upper Saddle River, NJ.

Booth, D.B. and Jackson, C.R. (1997). "Urbanization of Aquatic Systems–Degradation Thresholds, Stormwater Detention, and the Limits of Mitigation." *Journal of the American Water Resources Association*, 2 (5), 1077-1090.

Bubenzer, G.D. and Meyer, L.D. (1965). "Simulation of Rainfall and Soils for Laboratory Research." *Transactions ASCE*, 6, 73-75.

Carey, S.K. and Woo, M.K., (2001). "Slope Runoff Processes and Flow Generation in a Subarctic, Subalpine Catchment." *Journal of Hydrology*, 253, 110-129.

Gray, D.D., Katz, P.G., deMonsabert, S.M., and Cogo, N.P. (1982). "Antecedent Moisture Condition Probabilities." *Journal of Irrigation and Drainage Division*, Proceeding of the American Society of Civil Engineers, 108 (IR2), 107-114.

Frasier G., Weltz M., and Weltz L. (1998). "Technical Note: Rainfall Simulator Runoff Hdrograph Analysis." *Journal of Range Management*, 51(5), 531-535.

Hawkins, R.H. (1975). "The Importance of Accurate Curve Numbers in the Estimation of Storm Runoff." *Water Resources Bulletin*, 11 (5), 887-891.

Hawkins, R.H. (1978). "Runoff Curve Numbers with Varying Site Moisture." *Journal of Irrigation and Drainage Division*, Proceeding of the American Society of Civil Engineers. 104 (IR4), 389-398.

Hawkins, R.H. (1979). "Runoff Curve Numbers from Partial Area Watersheds." *Journal of Irrigation and Drainage Division*, Proceeding of the American Society of Civil Engineers, 105 (IR4), 375-389.

Hawkins, R.H. (1993). "Asymptotic Determination of Runoff Curve Numbers from Data." *Journal of Irrigation and Drainage Engineering*, 119 (2), 334-345.

Hawkins, R.H. (1998). "Local Sources for Runoff Curve Numbers." Presented at the 11th Annual Symposium of the Arizona Hydrological Society, Tucson, AZ.

Hawkins, R.H., Jiang, R., Woodward, D.E., Hjelmet Jr., A.T., and VanMullem, J.E. (2003). "Runoff Curve Number Method: Examination of the Initial Abstraction Ratio." World Water and Environmental Resources Congress, Philadelphia, PA.

Hawkins, R.H., Ward, T.J. Woodward, D.E., and VanMullem, J.E. (2005). "Progress Report: ASCE Task Committee on Curve Number Hydrology." Managing Watershed for Human and Natural Impacts, Engineering, Ecological, and Economic Challenges, Watershed 2005. Glenn E. Moglen-Editor, Williamsburg, VA.

Humphry J.B., Daniel T.C., Edwards D.R., and Sharpley A.N. (2002). "A Portable Rainfall Simulator for Plot-Scale Runoff Studies." *American Society of Engineers*, 18 (2), 199-204.

Linsley, R.K., Kohler, M.A. and Paulhus, J. L. H. (1975). "Hydrology for Engineers." 2nd edition, McGrawHill, New York, 265–266.

Massmann, J.W., and Allen, T. (2003). "A Design Manual for Sizing Infiltration Ponds." Final Research Report, Research Project Agreement No Y8265, Implementation of Infiltration Ponds Research.

Meyer L. D., and Harmon W. C. (1979). "Multiple-Intensity Rainfall Simulator for Erosion Research on Row Sideslopes." *Transactions of the ASAE*, 22(1), 100-103.

Miller W. P. (1987). "A Solenoid-Operated, Variable Intensity Rainfall Simulator." *Soil Science Society of America Journal*, 51, 832-834.

Mishra, S.K. and Singh, V.P. (1999). "Another Look at SCS-CN Method." *Journal of Hydrologic Engineering*, 4(3), 257-264.

Mishra, S.K. and Singh, V.P. (2003). "Soil Conservation Service Curve Number (SCS-CN) Methodology." Kluwer Academic Publishers, Dordrecht, The Netherlands, ISBN 1-4020-1132-6.

Mishra, S.K., Singh,V.P., and Sansalone, J.J. (2003). "A Modified SCS-CN method: Characterization and Testing." *Water Resources Management*, 17, 37-68.

Mishra, S.K., Sahu,R.K., Eldho, T.I., and Jain, M.K. (2006). "An Improved I_a-S Relation Incorporating Antecedent Moisture in SCS-CN Methodology." *Water Resources Management*, 20, 643-660.

Mockus, V. (1964). "Estimation of Direct Runoff from Storm Rainfall." National Engineering Handbook, Section 4, Chapter 10, U.S. Department of Agriculture Soil Conservation Service, Washington, D.C.

Natural Resources Defense Council, NRDC (1999). "Stormwater Strategies: Community Responses to Stormwater Pollution." www document, http://www.nrdc.org/water/pollution/storm/stoinx.asp

New York State Department of Environmental Conservation, NYSDEC (1992). "Reducing the Impacts of Stormwater Runoff from New Development." New York State

Department of Environmental Conservation, Division of Water, Bureau of Water Quality Management, Albany, NY.

Paige, G.B., Stone, J.J., Smith, J.R., and Kennedy, J.R. (2003). "The Walnut Gulch Rainfall Simulator: A computer- Controlled Variable Intensity Rainfall Simulator." *American Society of Agricultural Engineers*, 20(1), 25-31.

Perrone, J. and Madramootoo, C.A. (1998). "Improved Curve Number Selection for Runoff Prediction." *Canadian Journal of Civil Engineering*, 25, 728-734.

Plummer, A. and Woodward, D.E. (1998). "The Origin and Derivation of Ia/S in the Runoff Curve Number System." *Water Resources Engineering*, Proceeding of the American Society of Civil Engineers (ASCE), 1260-1265.

Ponce, V.M., and Hawkins, R.H. (1996). "Runoff Curve Number: Has it Reached Maturity?." *Journal of Hydrologic Engineering*, 1(1), 11-18.

Schneider L.E. and McCuen R.H. (2005). "Statistical Guidelines for Curve Number Generation." *Journal of Irrigation and Drainage Engineering*, 131 (3), 282-290.

South Florida Water Management District, SFWMD (1994) "Management and Storage of Surface Waters, Permit Information Manual.", Volume IV, Regulation Department, South Florida Water Management District, West Palm Beach, FL, USA.

Stubchaer, J.M. (1975). "The Santa Barbara Urban Hydrograph Method." National Symposium on Urban Hydrology and Sediment Control. University of Kentucky, Lexington, KY. 131-141.

Tsihrintzis, V.A. and Hamid, R. (1997). "Urban Stormwater Quantity/Quality Modeling Using the SCS Method and Empirical Equations." *Journal of American Water Resources Association*, 33(1), 163–176.

U.S. Army Corps of Engineering (USACE) (1998). "Engineering and Design- Runoff from Snowmelt." Manual No. 1110-2-1406, Washington, DC.

U.S. Department of Agriculture, Soil Conservation Service, USDA-SCS (1985). "National Engineering Handbook, Section 4, Hydrology." Soil Conservation Service, Washington, DC.

U.S. Department of Agriculture, USDA (2004). "National Engineering Handbook, Part 630, Hydrology, Chapter 11." Soil Conservation Service, Washington, DC.

U.S. Environmental Protection Agency, USEPA (1995). "Economic Benefits of Runoff Controls", EPA 841-S-95-002, Office of Wetlands, Oceans and Watersheds, Washington, DC.

U.S. Geological Survey, USGS (1995). "National Water Quality Assessment Program Report." Reston, VA.

Williams, J.D., Wilkins, D.E., McCool D.K., Baarstad L.L., Kleppe B.L., and Papendick R.I. (1998). "A New Rainfall Simulator for Use in Low-Energy Rainfall Areas." *American Society of Agricultural Engineers,* 14(3), 243-247.

Woodward, D.E., Hawkins, R.H., Hjelmfelt, A.T., Van Mullem, J.A, and Quan, D.Q. (2002). "Curve Number Method: Origins, Applications and Limitations." Second Federal Interagency Hydrologic Modeling Conference, Las Vegas, NV.

Washington State Department of Ecology, WDOE (2004). "Stormwater Management Manual for Eastern Washington." Publication Number 04-10-076, Olympia, WA.

Washington State Department of Transportation, WSDOT (2004). "Highway Runoff Manual." Olympia, WA.

CHAPTER 4

SUMMARY

Cold weather conditions negatively influence the performance of highway runoff treatment BMPs existing in cold regions. Therefore, to maintain the same level of treatment during cold conditions, it is necessary to modify the existing design parameters. This requires better understanding of the impacts of cold weather on the performance of BMPs and the influence of these conditions on the currently used design parameters. This study was carried out with a prime objective of investigating the impacts of two of the cold weather challenges that encountered the designer of runoff treatment BMPs in cold regions; frozen ground conditions and rain-on-snow events. Such conditions affect the parameters required for infiltration treatment facilities design in particular, the soil hydraulic conductivity and the initial abstractions during rain-on-snow events. The objective of this research was achieved though a number of experimental approaches. Summaries of the accomplished approaches, their objectives and the results are presented below.

4.1 FROZEN SOIL IMPACTS

The presence of frozen soil moisture negatively impacts the performance of infiltration treatment facilities by reducing the available pore spaces for infiltrating water, thus causing significant increases in runoff volumes. The objective of this research was to understand the impacts of frozen soils on hydraulic conductivity rates and to determine how the designers can better use infiltration treatment facilitates effectively in cold climates. This objective was accomplished by developing an air permeameter flow test

apparatus for hydraulic conductivity measurement of 16 frozen soil columns. The soil columns were constructed using two types of soils (loam and sandy loam) collected from two different infiltration facilities located in the cities of Spokane and Richland, Washington. The time allowed for soil-water redistribution was varied among the soil columns to investigate its significance on the reduction of hydraulic conductivity of frozen soils. The results showed the reduction in hydraulic conductivity of frozen soil depends greatly on the time allowed for soil-water redistribution prior to freezing. Using the data obtained from air permeameter flow tests, two regression equations were proposed to guide the selection of reduction factors for the hydraulic conductivity of loam and sandy loam soils. Incorporating the appropriate correction factor for hydraulic conductivity in infiltration treatment facility BMP designs in cold regions is important to provide for the reduction of infiltration rates during frozen ground conditions. The proposed modification should guarantee effective performance of these facilities during the cold season.

4.2 ESTMATING THE (I_a/S) PARAMTER DURING RAIN-ON-SNOW EVENTS

The initial abstraction storage ratio in the SCS-CN equation is traditionally set at 0.20. The prime objective of this study was to investigate the validity of the currently used initial abstraction ratio for runoff volume predictions in semi-arid cold climate regions where most runoffs are generated as a result of rain-on-snow events with frozen ground conditions. To accomplish this, a system to simulate rain-on snow events on a plot scale was developed. A plot scale was selected over a large scale in order to have a better control of the parameters of interest and therefore allow better understanding of the

hydrological responses during such events. A total of 19 rain-on-snow events were simulated under different snow conditions (snow density and snow depth), plot slopes and average air temperatures. By examining the observed runoff hydrographs, it was clear that the characteristics and shapes of the generated hydrographs reflected the integrated influences of snow cover condition, plot slope, and average air temperature during the simulated events. Therefore, model calibration was used to develop an alternative methodology to assign I_a/S ratios for use in semi-arid climates. The new methodology requires modification of the I_a/S parameter to make it a function of the snow conditions (snow depth and snow water equivalent) and average air temperature. A regression equation developed for the I_a/S ratio proposed by this study provides an easy way to obtain an appropriate estimate of the initial losses during rain-on-snow events and thus provides better predictions of runoff treatment volumes for infiltration treatment BMPs in cold regions.

4.3 CONCLUSION AND FUTURE NEEDS

This research enabled development of methodologies for modifying the existing design parameters, specifically the hydraulic conductivity and the I_a/S parameters, to account for cold weather conditions that negatively impact the performance of infiltration treatment facilities in cold regions. Adapting the proposed modification to the design process is expected to improve the performance of infiltration treatment facilities during cold season but ultimately this will require larger, more costly facilities.

APPENDIX A

BACKGROUND INFORMATION FOR CHAPTER 2

The movement of water through a porous medium is usually described by Darcy's Law which can be written in the following form (Freeze and Cherry, 1979):

$$Q = -KiA \qquad \text{(Equation A.1)}$$

where Q is the inflow rate [L^3/T], A is the cross sectional area of the medium [L^2], i is the hydraulic gradient [L/L], and K is the saturated hydraulic conductivity [L/T]. The hydraulic conductivity is a function of both the fluid and the medium. To describe the conductive properties of the medium independently from the fluid flowing through it, the term permeability is used. Permeability is related to hydraulic conductivity through the following relationship (Freeze and Cherry, 1979):

$$K = \frac{k\rho g}{\mu} \qquad \text{(Equation A.2)}$$

where k is known as the permeability [L^2], ρ is the fluid density [M/L^3], μ is the fluid viscosity [M/LT], and g is the gravitational acceleration [L/T^2].

Several approaches have been used to predict the hydraulic conductivity of porous materials including empirical relationships, statistical models, capillary models and hydraulic radius theories. Hazen (1911) developed the following formula for estimating the hydraulic conductivity of sandy sediments based on the grain size distribution (Fetter, 1994):

$$K = Cd_{10}{}^2 \qquad \text{(Equation A.3)}$$

where K is the hydraulic conductivity [L/T], d_{10} is grain diameter for which 10% of the soil is finer [L], and C is Hazen empirical coefficient [1/LT]. The Hazen formula is applicable only for uniform sand and therefore has limited applications for *in situ* soils (Carrier, 2003).

Chapuis (2004) proposed a new equation for predicting the saturated hydraulic conductivity of sand and gravel by extending the Hazen method to any soil porosity value. The new equation was obtained by using a best fit technique and was expressed as (Chapuis, 2004):

$$K = 2.4622\left(d_{10}^2 e^3 / (1+e)\right)^{0.7825} \qquad \text{(Equation A.4)}$$

where K is the hydraulic conductivity [cm/s], d_{10} is grain diameter [mm], and e is the void ratio defined as the ratio of the voids volume to the solids volume [L^3/ L^3].

Childs and Collis-George (1950) studied the permeability of porous materials and developed a statistical expression for permeability based upon the occurrence probability of a sequence of pairs of pores for all possible pore sizes and their contribution to the permeability term. However, in addition to the computational complexity, the statistical approach appeared to be very artificial since in its development, the existence of smallest pore in a sequence of many pores, and the effect of the different lengths of pores of different sizes are ignored (Childs and Collis-George, 1950).

Using a large set of saturated hydraulic conductivity measurements, Rawls and Brakensiek (1985) developed the following regression relationship that correlate the saturated hydraulic conductivity to the percentage of sand, percentage of clay, and porosity as:

$$K = 100[\exp(19.52348n - 8.96847 - 0.028212C + 0.0001807S^2 - 0.0094125C^2 - 8.395215n^2 + 0.077718Sn - 0.00298S^2n^2 - 0.019492C^2n^2 + 0.0000173S^2C + 0.02733C^2n + 0.001434S^2n - 0.000035C^2S)2.77 \times 10^{-6}] \quad \text{(Equation A.5)}$$

where K is the saturated hydraulic conductivity [cm/s], S and C are the sand and clay fractions, respectively, as obtained by the U.S. Department of Agriculture, and n is the porosity defined as:

$$n = \frac{V_v}{V_T} \quad \text{(Equation A.6)}$$

where V_v [L^3] is the volume of the voids and V_T [L^3] is the total sample volume.

The Rawls and Brakensiek regression equation was developed from soils that had clay and sand contents of 5 to 60 % and 5 to 70 %, respectively, which makes the accuracy of their proposed relationship for soils with higher sand contents unknown (Massmann et al., 2001).

Massmann et al. (2003) proposed another regression relationship by comparing hydraulic conductivity estimates from air permeability tests with grain size characteristics of soils typical of western Washington. The proposed relationship is used currently in the infiltration facility design in Eastern Washington and it takes the following form:

$$\log_{10}(K_{sat}) = -1.57 + 1.90D_{10} + 0.015D_{60} - 0.013D_{90} - 2.08f_{fines} \quad \text{(Equation A.7)}$$

where K_{sat} is the saturated hydraulic conductivity in cm/sec, D_{10}, D_{60}, D_{90} are the grain sizes in mm for which 10, 60 and 90 percent of the sample is finer and f_{fines} is the fraction of the soil by weight passing the number 200 sieve (Massmann et al., 2003).

Other expressions have been developed to link the hydraulic conductivity to porous medium properties by employing the hydraulic radius model in which the

permeability of the porous medium is linked to the hydraulic radius, porosity factor, and a dimensionless shape factor (Kozeny, 1927; Carman, 1937; Wyllie and Spangler, 1952). The most widely accepted relationship between hydraulic conductivity and porous medium properties is the Kozeny-Carman empirical relationship that is derived by treating the porous medium as a network of capillary tubes of equal lengths and then employing the concept of hydraulic radius *R*, defined as the ratio of the volume of the conduit filled with fluid to its wetted surface (Bear, 1990). The Kozeny-Carman relationship can be written as:

$$k = \frac{1}{5}\frac{n^3}{(1-n)^2}\frac{1}{S^2} \qquad \text{(Equation A.8)}$$

where k is the permeability [L^2], S is the specific surface of a porous material defined as the interstitial surface area of the pores to the total volume of the porous material [L^{-1}], and n is the porosity [L^3/L^3].

Carrier (2003) found that the specific surface area, *S*, can be estimated from the particle size distribution as:

$$S = \frac{6}{D_{eff}} \qquad \text{(Equation A.9)}$$

where D_{eff} is the effective diameter, and is defined as:

$$D_{eff} = 100\% \Big/ \sum \left(f_i / D_{averi} \right) \qquad \text{(Equation A.10)}$$

where f_i is the fraction of particles between two sieve sizes [%], and D_{averi} is the average particle size between two sieve sizes [L].

Walsh and Brace (1984) proposed a modified form for the Kozeny-Carman equation that included the tortuosity defined as the ratio of the actual length of the flow

path to a straight line distance between the ends of the flow path. The modified form is given by:

$$k = cT^2 \frac{n^3}{S^2} \qquad \text{(Equation A.11)}$$

where T is the tortuosity [L/L], S is the specific surface area parameter [L^{-1}], and c is a numerical coefficient constant.

Different attempts have been made in the literature to estimate the parameters in the different forms of Kozeny-Carman equation. Berryman and Blair (1987) used image processing technique to estimate the pore perimeter and area from thin sections, and used these estimated parameters for estimating permeability using the Kozeny-Carman equation, but no attempt have been done in their work to calculate magnitudes of parameters describing the connectivity and tortuosity in the soil.

Vervoort and Cattle (2003) employed an image analysis technique to identify the pore size distribution and the connectivity and tortuosity parameters of the soil measured in two dimensions, and used these parameters to predict the hydraulic conductivity of the soil using statistical hydraulic conductivity model developed by Kosugi (1999). By fitting the lognormal pore size distribution to measured hydraulic conductivities, Vervoort and Cattle (2003) were able to relate the hydraulic conductivity to porosity and pore genus which is a measure of connectivity in the horizontal direction. The tortuosity parameters in their work were related to mean pore size, with increasing mean pore size indicating decreasing tortuosity.

Al-Omari et al. (2002) used X-ray computed tomography and image analysis techniques to predict the permeability of hot mix asphalt by quantify the parameters in the modified form of Kozeny-Carman equation (Equation A.11). In their work, the total

porosity was estimated by calculating the average ratio of the air voids to the total area of each image along the asphalt sample. The specific surface area was quantified by calculating the ratio of the wetted area of the air voids to the specimen volume, and the tortuosity was calculated from the coordinates of the connected voids within the images.

Although there has been some debate about its applicability in clay soils, in general the Kozeny-Carman equation reasonably predicts the saturated hydraulic conductivity of many soils (Carrier, 2003; Chapuis and Aubertin, 2003). However, for frozen soils, the porosity and pore size distribution undergo changes due to ice formation during the freezing process thus limiting the utility of Equation A.8. The conductivity of the soil after freezing, the infiltration rate, and the available potential storage are controlled by the soil air-filled porosity. The water content and the time available for soil-water redistribution before the soil freezes are expected to have significant influence on the size, distribution and connectivity of the air-filled pores and hence they are likely predictors in determining the air-filled porosity in frozen soils. The higher content prior to freezing, the greater the amount of ice present in the frozen soil. Therefore, more reduction in infiltration rates and permeability will be expected compared to soils with low water contents prior to freezing.

REFERENCES

Al-Omari, A., Tashaman, L., Massad, E., Cooley, A., and Harman, T. (2002). "Proposed Methodology for Predicting HMA Permeability." *Journal of the Association of Asphalt pavement Technology*, 71.

Bear, J. (1990). "Dynamics of Fluids in Porous Media." New York; American Elsevier.

Berryman, J.G., and Blair, S.C. (1987). "Kozeny-Carman Relations and Image Processing Methods for Estimating Darcy's Constant." *Journal of Applied Physics,* 57, 2374-2384.

Carman, P.C. (1937). "Fluid Flow Through Granular Beds." *Transactions, Institution of Chemical Engineerings*, London, 15, 150-166.

Carman,P.C. (1956). "Flow of Gasses Through Porous Media." Academic Press, NY.

Carrier, W.D. (2003). "Goodbye, Hazen; Hello, Kozeny-Carman." *Journal of Geotechnical and Geoenvironmental Engineering ASCE.*129 (11), 1054-1056.

Chapuis, R., and Aubertin, M. (2003). "On the Use of Kozeny-Carman Equation to Predict the Hydraulic Conductivity of the Soils." *Canadian Geotechnical Journal*, 40, 616-628.

Chapuis, R. (2004). "Predicting the Unsaturated Hydraulic Conductivity of Sand and Gravel Using Effective Diameter and Void Ratio." *Canadian Geotechnical Journal*, 41, 787-795.

Childs, E., and Collis-George, N. (1950). "The Permeability of Porous Materials" *Proceedings of the Royal Society of London*. Series A, 201 (1066), 392-405.

Fetter, C.W. (1994). "Applied Hydrogeology." Macmillan College Publishing Company, NY.

Freeze, R., and Cherry, J. (1979). "Groundwater." Prentice-Hall, NJ.

Hazen, A. (1911). "Discussion: Dams on Sand Foundation." *Transactions, American Society of Civil Engineers*, 73, 199.

Kosugi, K. (1999). "General Model for Unsaturated Hydraulic Conductivity for Soils with Lognormal Pore-Size Distribution." *Soil Science Society American Journal,* 63, 270-277.

Kozeny, J. (1927). "Ueber Kapillare Leitung des Wassers im Boden,Wien." *Sitzungsberichte Wiener Akademie*, 136 (2a), 271-306.

Massmann, J.W., and Butchart, C.D., TRAC, Allen, T. (2001). "Infiltration Characteristics, Performance, and Design of Storm Water Facilities." Interim Report, Research Project Agreement No T1803, Task 12, Stormwater Facilities.

Rawls, W.J., Brakensiek, D.L., (1985)."Prediction of Soil Water Properties for Hydrologic Modeling." *Proceeding of Symposium on Watershed Management, ASCE*, 293-299.

Vervoort, R.W. and Cattle, S.R. (2003). "Linking Hydraulic Conductivity and Tortuosity Parameters to Pore Space Geometry and Pore-Size Distribution." *Journal of Hydrology.* 272, 36-49.

Walsh, J.B., and Bruce, W. F., (1984). "The Effect of Pressure on Porosity and the Transport Properties of Rocks." *Journal of Geophysical Resources,* 89, 9425-9431.

Wyllie, M.R., and Spangler, M.B., (1952). "Application of Electrical Resistivity Measurements to Problems of Fluid Flow in Porous Media." *Bulletin of American Association Petroleum Geol*., 36, 359-403.

APPENDIX B

Quantifying the Permeability of Frozen Soils Using X-ray Computed Tomography System and Image Analysis Techniques

To learn more about the impact of frozen soils on infiltration patterns, this research proposed using the WSU x-ray computed tomography (CT) system along with image analysis techniques for 3-D visualization and quantification of pore size distributions and connectivity parameters in frozen soils. After obtaining measured values for the conductivity of each soil column using an air permeameter flow test, the columns were scanned using the X-ray CT system to obtain 3D images of the frozen soil columns under different antecedent moisture contents. The X-ray images were then analyzed to obtain descriptive and quantitative information on hydraulic conductivity rates and porosity in frozen soils.

This appendix describes X-ray Computed tomography and image analysis techniques used in this study. It also presents a summary of the outcomes from this approach and gives recommendation for required improvements to obtain better results as the images collected in this endeavor turned out to be unsuitable for accurate analysis.

B.1 X-ray Computed Tomography (CT) Technique

Several investigators have demonstrated the use of X-ray computed tomography as an alternative for non-destructive measurements of soil properties including bulk density, porosity, water contents, solute concentration and macro pore size (Petrovic et al., 1982; Hopmans et al., 1994; Steude et al., 1994). In this study, the X-ray CT system

currently in use at the Washington Center for X-ray Tomography and Imaging Technology (WACXIT) has been applied to visualize, non-invasively, frozen soil columns (10 cm diameter and 45 cm depth), and to obtain three-dimensional characterization of their microstructures. The X-ray CT system has been applied previously by a number of investigators for characterization of air voids distribution in asphalt mixes (Romero and Masad, 2001; Masad et al., 2002; Al-Omari, 2002; Tashman et al., 2002).

The X-ray CT machine consists of a high energy x-ray source and detector with a specimen, e.g., a soil core, placed in between (Figure B.1).

Figure B.1. WACXIT X-Ray CT machine with a soil column section placed in it.

The scanning process for each soil column (45 cm in total height) was accomplished by scanning of three, 15-cm long sections separately using the X-ray CT machine. This column subdivision was necessary due to limitation of the X-ray CT machine in scanning objects more than this length. The scanning process involves transmitting the X-ray in a cone shape towards the soil column section while it is in rotation and measuring the intensity of the X-ray before and after it passes through the specimen. The x-ray source was located about 1646.5 mm from the center of the sample and about 1906.5 mm from the detector. The source current, and the voltage used during the scanning process are 2.8 mA and 270 kV, respectively. The scanning process is completed by collecting the intensity measurements for a full rotation of the soil column sections. Using the intensity values collected during the scanning process, a map of spatial distribution of the linear attenuation coefficient within the scanned soil column section is calculated. Based on the fact that differences in the attenuation coefficient at any point in the specimen depend directly on the density at that point, "gray scale" images that display differences in density at every point in 2-D slices throughout the soil column section were acquired. Intensity values were represented with 8-bit integers (Gray Scale 8). This scanning technique enables capturing the entire volume and directly generating 3-D data.

B.2 Image Analyses Technique

The X-ray images were rendered by image processing and analysis software (*Image-Pro Plus,* 1998) to distinguish between air voids, frozen water, and soil particles. The programming capabilities of *Image-Pro Plus*® made it possible to write image

analyses macros to facilitate the analysis process. The analysis process involved two steps. In the first step, each phase was separated from the other phases by thresholding all the X-ray images for each of the phases using a macro that has been originally developed by Tashman et al. (2002). The macro was modified to be applied in this study for frozen soil images.

Using the thresholding macro, the threshold value for the air phase is selected based on visual evaluation of the images, and to match the percent air voids calculated using the following equation:

$$n_a = n - 1.09\theta_w \qquad \text{(Equation B.1)}$$

where n_a and n are the air filled porosity and the total porosity respectively [L^3/L^3], 1.09 is the density of water relative to ice, and θ_w [L^3/L^3] is the soil water content before soil is frozen.

The threshold value for the ice phase is selected by matching the percent water content from the images to the measured water contents of the soil columns before freezing.

Based on the results of the threshold process, the same macro is used to quantify the parameters in the Kozeny-Carman equation including the total porosity and the specific surface. The total porosity is estimated in the macro by the following relation (Al-Omari et al., 2002):

$$n = \frac{\sum_{i=1}^{N} \frac{(A_v)_i}{A_T}}{N} \qquad \text{(Equation B.2)}$$

where A_v is the area of the voids [L^2], A_T is the total area of the image, and N is the number of images.

The specific surface area is quantified by calculating the ratio of the wetted area of air voids (measured by the perimeter of each air void multiplied by its thickness) to the specimen volume. However, since the thickness is constant for all the images (0.2 mm), the specific surface area (S) was expressed as (Al-Omari et al., 2002):

$$S = \frac{\sum_{i=1}^{N}\sum_{J=1}^{M} P_{ij}}{A_T \times N} \qquad \text{(Equation B.3)}$$

where P_{ij} is the perimeter of an air void, M is the number of air voids on an image (Al-Omari et al., 2002).

The total porosity value in the above equation considers all the void space whether pores are interconnected or not. Therefore, the second step in the analysis process was to determine the effective porosity defined as the percent of the interconnected void space. This has been achieved by using a connectivity macro developed by Al-Omari et al. (2002), which keeps track of those air voids that were connected from the top to the bottom of the soil column. The macro has been modified to be applied for frozen soil columns.

It is important to point out that in this work, the threshold value was chosen by assuming that all water in the pores was frozen, thus each frozen soil columns was considered to be a three phase system consisting of solid, ice, and air. This assumption has been tested based on an experiment that conducted as a preliminary step in this work.

In this experiment, three holes were drilled into a solid piece of rock as illustrated in Figure B.2. One of the holes was filled with water and the rock was frozen, after which water was poured in the second hole, and the third hole was left empty. The rock specimen was then scanned and an attempt was made to identify a threshold for gray

intensity for each phase by image processing based on the knowledge of the location of each phase in the image. The small differences in density values between the ice and water phases made it impossible to differentiate between the two water phases. Therefore, in our image analysis we assumed that all water in the pores was frozen, thus each frozen soil columns was considered to be a three phase system consisting of solid, ice, and air.

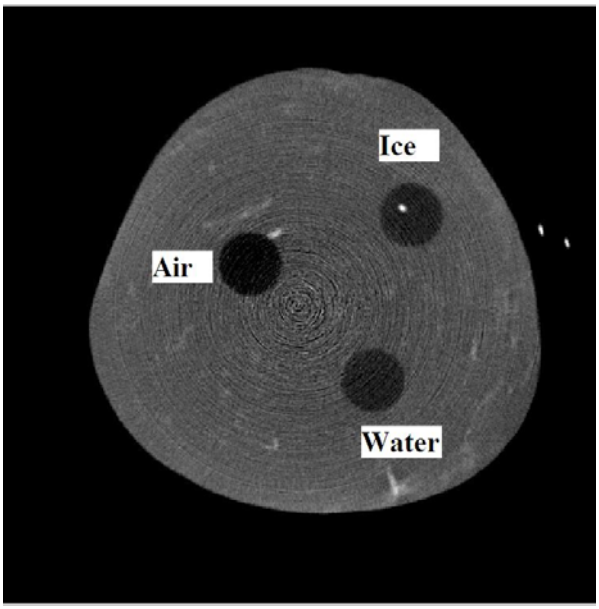

Figure B.2. X-ray CT image of rock with three drilled holes filled with ice, water and air

B.3 Results and Discussion

The scanning process resulted in a total of 762 images for each section of the frozen soil columns. The horizontal slices of 0.2 mm thick and a resolution of 0.2 mm/pixel were captured and saved in TIF format. Each image contains 256 levels of pseudo-gray each corresponds to a different density with white and light gray correspond to higher densities. Lower density regions correspond to the air voids appeared in the

images as dark gray and black. Example x-ray image of a frozen soil column is shown in Figure B.3.

a. XY plane b. XZ plane

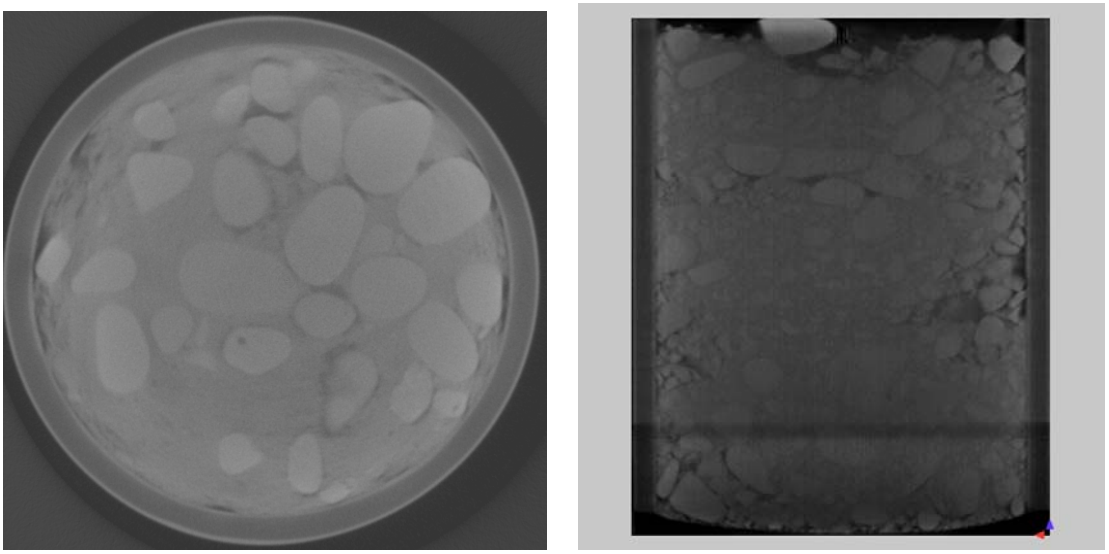

Figure B.3. Two-dimensional X-ray CT image of frozen soil column: a) XY plane, b) XZ plane.

Using *Image-Pro Plus*® software and image analyses macros mentioned earlier, the analysis process was performed to visualize the air void distribution in each soil column of different redistribution times based on a chosen gray intensity value. However, due to the low quality of the images obtained during the scanning process, it was impossible to capture the air voids and ice lenses within the image. The software produced estimates of soil porosity but the values did not seem to be consistent with typical porosity. As illustrated in Figure B.4, the vertical distribution of the air voids within the different section of a frozen soil column peaks at less than 3% far less than a typical void ratio. Furthermore, using different thresholds yielded almost the same

percentage air void and the specific surface area. Hence, it was impossible to identify an appropriate threshold value for use in the image analysis process.

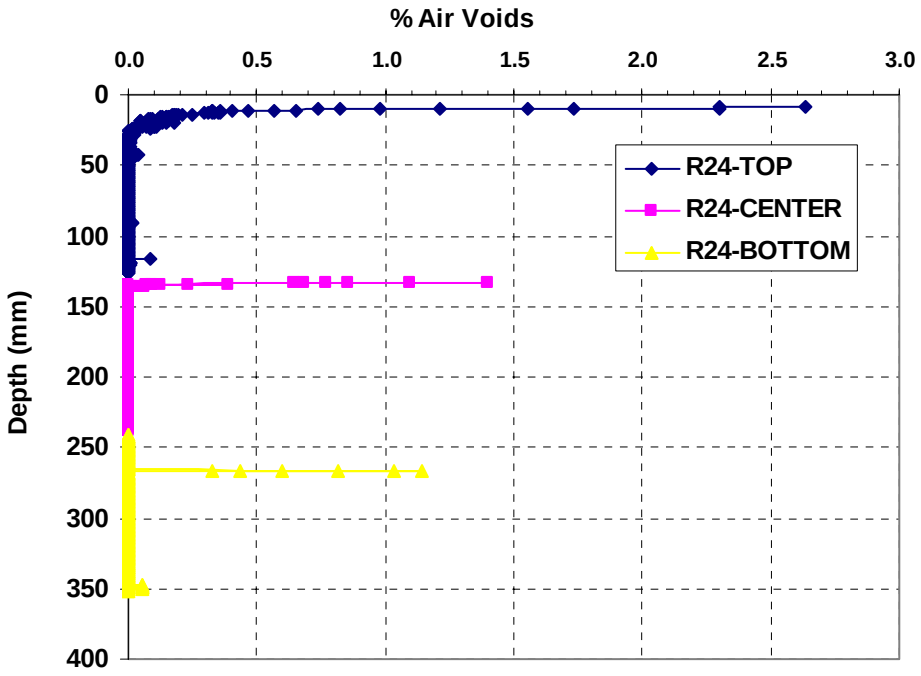

Figure B.4. Vertical air void distribution within the different section of a frozen soil column.

B.4 Conclusions

Laboratory experiments including x-ray computed tomography techniques and air permeameter flow tests were used in this research as a new tool for visualizing the pore size distribution and exploring the connectivity parameters in frozen soil cores. The research findings suggest the X-ray computed tomography technique can be a good tool for estimating the porosity and the hydraulic conductivity of frozen soils. However, the accuracy of using this method depends greatly on the quality of the images acquired by

the x-ray machine and used in the analysis process. Therefore, additional work is needed in this research area to evaluate different settings which might be used to improve the images quality to describe the pore size distribution properties of frozen soils.

B.5 REFRENCES

Al-Omari, A., Tashaman, L., Massad, E., Cooley, A., and Harman, T. (2002). "Proposed Methodology for Predicting HMA Permeability." *Journal of the Association of Asphalt pavement Technology*, 71.

Hopmans, J.W., Cislerova, M., and Vogel, T. (1994). "X-Ray Tomography of Soil Properties." *Tomography of Soil-Water-Root Processes. SSSA Special Publication*, (36), 17-28.

Masad, E., Jandhyala, V.K., Dasgupta, N., Somadevan, N., and Shashidhar, N. (2002). "Characterization of Air Void Distribution in Asphalt Mixes Using X-Ray Computed Tomography." *Journal of Materials in Civil Engineering,* 14(2), 122-129.

Petrovic, A.M., Siebert, J.E., and Riecke, P.E. (1982). "Soil Bulk Density Analysis in Three Dimensions by Computed Tomographic Scanning." *Soil Science Society of American Journa*l, 46, 445-450.

Romero, P. and Masad, E. (2001). "Relationship between the Representative Volume Element and Mechanical Properties of Asphalt Concrete." *Journal of Materials in Civil Engineering,* 13(1), 77-84.

Tashaman, L., Massad, E., Angelo, J., Bukowski, J., and Harman, T. (2002). "X-ray Tomography to characterize Air Void Distribution in Superpave Gyratory Compacted Specimens." *The International Journal of Pavement Engineering,* 3 (1), 19-28.

Steude, J.S., Hopkins, F., and Anders, J. E. (1994). "Industrial X-Ray Computed Tomography Applied to Soil Research." *Tomography of Soil-Water-Root Processes. SSSA Special Publication*, (36), 29- 41.

APPENDIX C

BACKGROUND INFORMATION FOR CHAPTER 3

The literature review for this chapter covers four distinct topics. First, a review of the SCS-CN method including some of the modifications that have been done on this method is presented. Second, detailed descriptions of the SBUH methodology, and the computation equations used in this method. Third, a detailed description of Eastern Washington long and short durations design storm events is provided. Fourth, rain-on-snow and snowmelt design considerations were summarized.

C.1 SCS-CN Method

The SCS-CN method was derived analytically in the late 1950's by the former Soil Conservation Service (USDA-SCS, 1985) (now the Natural Resources Conservation Service (NRCS)) using the following three assertions and definitions (Hawkins et al., 2005; McCuen, 1982). First, the water balance equation was written as:

$$F = P - I_a - Q \qquad \text{(Equation C.1)}$$

where F is the actual cumulative infiltration [in], P is the event rainfall depth [in], I_a is the initial abstraction that occurs before the start of runoff and is not limited to a single loss type but rather it includes evaporation, evapotranspiration, interception, surface depression, and initial infiltration losses [in], and Q is the direct runoff depth [in].

Second, the ratio of the actual direct runoff to the maximum potential runoff was set equal to the ratio of the amount of actual cumulative infiltration to the amount of the potential maximum storage:

$$\frac{Q}{P - I_a} = \frac{F}{S} \qquad \text{(Equation C.2)}$$

where S is the potential maximum storage [in] defined as the maximum possible difference between P and Q that can occur for the given storm and watershed conditions (Woodward et al., 2002). S values range from 0 to ∞.

Third, I_a was defined as the event rainfall required for the initiation of runoff and was assumed to be equal to some fraction of the maximum potential storage:

$$I_a = \lambda S \qquad \text{(Equation C.3)}$$

For convenience in practical application, the parameter S was mapped into a dimensionless parameter called the curve number (CN) which varies from 0 (no runoff) to 100 (all rainfall becomes runoff). The chosen relationship is:

$$S = \frac{1000}{CN} - 10 \qquad \text{(Equation C.4)}$$

The CN parameter was developed by recording the largest annual storm runoff and associated rainfall for a watershed having a known hydrological soil group, land use/cover class, and surface condition. The rainfall runoff data was then plotted with the rainfall in the abscissas and runoffs in the ordinates. A graph of CN array constructed at the same scale was laid over this plot and the median CN was selected, dividing the plotting into two equal numbers of points (Ponce and Hawkins, 1996).

Substituting Equation C.2 into Equation C.1, rearrange the terms, and setting the initial abstraction value equal to 20% of the storage, yields the well known form of the SCS-CN equation:

$$Q = \frac{(P - I_a)^2}{P - I_a + S} = \frac{(P - 0.2S)^2}{(P + 0.8S)} \quad \text{for P} \geq 0.2\text{S, Q=0 otherwise} \qquad \text{(Equation C.5)}$$

Numerous articles have been published concerning the SCS-CN method and several modifications have been proposed over the years on both the method and its parameters for more accurate computation of surface runoff volume. In the original development of the SCS-CN method, the curve numbers were found by analyzing measured rainfall and runoff data collected from watershed with different known soil and cover types. For each watershed, the maximum one day runoff volume in each year was plotted against the total rainfall in that day (Gray et al., 1982). The scatter observed in plots was interpreted as the measure of the natural variability in soil moisture in the associated rainfall-runoff relation and lead to the development of the antecedent moisture content (AMC) concept (Linsley et al., 1975). Three levels of antecedent moisture conditions are used by the Soil Conservation Service: AMC I (dry conditions), AMC II (average conditions) and AMC III (wet conditions) with each corresponding to a different curve number for the same watershed (Mockus, 1964; Hawkins 1978, 1979; Gray et al., 1982). Prepared tables and charts that guide the selection of the CN based on the soil type, soil cover, land use and the antecedent moisture content (AMC) were available in the National Engineering Handbook, Section 4, Hydrology (NEH-4) and in other agency publications (Hawkins, 1993; Hawkins et al., 2005). However, there was no clear guidance on how to vary antecedent condition, especially for lower curve numbers or lower rainfall amounts (Hawkins, 1975). The selection of an appropriate CN is left to the

professional judgment of the hydrologist (Hawkins, 1979). Therefore, over the years, several definitions for the moisture condition of the watershed before the start of the storm were developed to improve the definition of the AMC. Originally, the three AMC classes were defined using the concept of antecedent precipitation index (API) which was based on the amount of the 5-day antecedent rainfall (SCS, 1964). The AMC classes were defined for the dormant and growing seasons as shown in Table C.1.

Table C.1. Seasonal rainfall limits for the three antecedent soil moisture conditions (Woodward and Plummer, 2000)

AMC	Dormant Season	Growing Season
I	< 0.50 in	< 1.4 in
II	0.5 in to 1.1 in	1.4 in to 2.1 in
III	> 1.1 in	> 2.1 in

Gray et al. (1982) developed estimates of the antecedent moisture condition (AMC) probability for 17 locations in Kentucky, Tennessee, and Indiana, and used these estimates in two runoff models; the SCS-CN and the ILLUDAS models. Four levels of AMC were developed; bone dry, rather dry, rather wet, and saturated. Those levels were applicable to the locations studied and can be used for regions with similar rainfall patterns.

Van Mullem et al. (2002) stated that the relationship between the 5-day antecedent rainfall and the antecedent moisture condition (AMC) was developed for a local situation and was not intended to have nationwide application. The concept of antecedent moisture condition (AMC) was removed later by the NRCS and has been replaced by the antecedent runoff condition (ARC) (Woodward and Plummer, 2000).

Perrone and Madramootoo (1998) stated that the three antecedent moisture conditions used in the SCS-CN method are not appropriate for runoff volume prediction in humid regions such as Ottawa-St. Lawrence Lowland. Using rainfall and runoff data and Agricultural Non-Point Source Pollution (AGNPS) model simulation, Perrone and Madramootoo (1998) developed an antecedent precipitation index (API) for use as an alternative indicator to the soil moisture for selecting the appropriate curve number for the humid region. The developed relationship between the curve number and the antecedent precipitation index is:

$$CN = a\left(b - e^{cAPI}\right) \qquad \text{for } 0 \leq \text{API} \leq 100 \text{ mm} \qquad \text{(Equation C.6)}$$

where a, b, and c are constants having different values for each hydrologic soil group and land use.

Although the use of the antecedent precipitation index as a soil moisture indicator improved surface runoff simulation for the simulated events, it was observed that the AGNPS model performance was poor when complex storms or events occurring during cold climatic conditions were simulated (Perrone and Madramootoo, 1998). These short coming were attributed to the AGNPS model's inability to simulate snowmelt or frozen soils and its structure not allowing continuous updates of the input values as rainfall-runoff progress with time.

Hawkins (1975, 1993 and 1998) pointed out that there are two problems in estimating runoff using the SCS-CN method; first the difficulty in selecting an accurate CN from the available published tables, and second the sensitivity of the computed runoff volume from Equation B.5 or B.6 to the selected CN compared to the rainfall depth. Using event rainfall and runoff data, he determined runoff curve numbers for small

watersheds by applying an asymptotic method using the frequency matching technique that matches rank-ordered rainfall and runoffs, which preserves equal return periods (Hawkins, 1993, 1998). Hawkins (1993) observed three different responses for the curve number with storm rainfalls which he defined as standard, violent and complacent. In the standard case, which is the most common scenario, *CN* declines with increasing storm size until it approaches a constant value with increasingly larger storms. In the violent case, the *CN* rises suddenly and asymptotically approach an apparent constant value with increasing rainfall. However, for the complacent case, the *CN* declines steadily with increasing rainfall depth and shows no tendency to achieve a stable value.

By applying two techniques, Storm Event Analysis and Model Fitting on measured rainfall-runoff data collected at WS26030 located at Coshocton, OH, Hawkins et al. (2003) investigated the assumption of $I_a = 0.2S$ and found that $I_a = 0.05S$ provided a better fit to the data and would be more appropriate for use in runoff calculations.

Schneider and McCuen (2005) proposed the Log-Normal Frequency method as a new technique for estimating curve numbers and compared it to the Storm Event Analysis and Model Fitting methods developed by Hawkins et al. (2003). The Log-Normal Frequency method provided less bias estimates of runoff depths and was more accurate than the other two methods since taking the logarithms of the rainfall depths reduced the imbalance of weight given to the larger rainfall values.

Mishra and Singh (1999) proposed a modification of the SCS-CN method (Equation B.5) using the following empirical rainfall-runoff equation that developed by Mockus (1949):

$$Q = P\left[1 - 10^{-bP}\right] \qquad \text{(Equation C.7)}$$

where Q is the runoff depth [in], P is the rainfall depth excluding the initial abstraction [in], and b is a fitting coefficient that depends on antecedent moisture condition, vegetative cover, land use, time of year, storm duration, and soil type. Their modified SCS-CN equation is:

$$Q = \frac{(P - I_a)^2}{a(P - I_a) + S} \quad \text{(Equation C.8)}$$

where

$$a = \frac{1}{2} - \frac{S}{P} + \sqrt{\frac{1}{4} + \frac{S}{P}} \quad \text{(Equation C.9)}$$

The modified SCS-CN method (Equation C.7) and its parameters were investigated by Mishra et al. (2005) using a large set of rainfall-runoff events. The results showed consistently improved performance of the data with increasing rainfall amounts (> 38.1 mm). Mishra et al. (2005) demonstrated that when a = 0.50 and λ = a median value, the modified SCS-CN equation performed significantly better than the existing SCS-CN method on the data sets especially on rainfall data less than 2 inches.

Mishra et al. (2003) proposed another modification of the SCS-CN method by accounting for the statistic portions of infiltration and the antecedent moisture. The modified form of the SCS-CN equation takes the form:

$$Q = \frac{(P - I_a - F_c)(P - I_a - F_c + M)}{P - I_a - F_c + M + S} \text{ for } P \geq I_a + F_c;\ Q = 0 \text{ otherwise} \quad \text{(Equation C.10)}$$

where F_c is the static portion of infiltration [in], M is the antecedent moisture [in] and can be computed as:

$$M = 0.50[-1(1 + \lambda)S + \sqrt{(1 - \lambda)^2 S^2 + 4P_5 S}] \quad \text{(Equation C.11)}$$

where P_5 is the 5-days antecedent precipitation amount [in].

By applying the modified SCS-CN method on the same data sets used in the National Engineering Handbook, the modified method was found to perform well. The modified model was also applied to the Hemavati watershed in India and was found to yield satisfactory results in both calibration and validation (Mishra and Singh, 2004). However, this modified method requires a prior knowledge of the minimum infiltration rate which is often not available.

By investigating the performance of different I_a/S relationships incorporating antecedent moisture (M) as a function of antecedent precipitation (P_5) and using large datasets from 84 small watersheds in the USA, Mishra et al. (2006) developed an improved initial abstraction-potential maximum relation that incorporated the antecedent moisture and the 5-day antecedent precipitation term from the original SCS-CN equation. Their modified I_a/S relationship takes the form:

$$I_a = \frac{\lambda S^2}{S + M} \qquad \text{(Equation C.12)}$$

By incorporating Equation C.12 into Equation C.10, the modified Mishra-Singh (*MMS*) model takes the following forms:

$$Q = \frac{(P - \frac{\lambda S^2}{S+M})(P - \frac{\lambda S^2}{S+M} + M)}{P - \frac{\lambda S^2}{S+M} + M + S} \quad \text{for } F_c = 0 \qquad \text{(Equation C.13)}$$

Performance of the *MMS* model (Equation C.13) has been compared to the existing SCS-CN method and the Mockus method, and was found to be more accurate than both methods. However, as in the other existing models, the limitations of the *MMS* model are that it does not consider the effect of rainfall intensity or rainfall duration on the predicted runoff. In this work, we investigated the initial abstraction ratio (λ) taking into

consideration the characteristics of natural rainfall events encountered in semi-arid cold regions including the rainfall intensity and duration.

C.2 SBUH Methodology

In 1966, the Santa Barbara County Flood Control and Water Conservation District used the SCS-CN equation to develop the Santa Barbara Urban Hydrograph (SBUH) method to determine runoff hydrographs for urbanized areas directly without applying the SCS unit hydrograph method. Since its inception, the method has been widely applied in several single event models (Tsihrintzis and Sidan, 1998), and it is currently recommended by Washington State Department of Transportation (WSDOT) for calculating runoff treatment design volumes or flow rates of project sites in Eastern Washington. The SBUH method is more accurate for modeling drainage basins less than 100 acres (WDOE, 2004).

Inputs for the SBUH method include the pervious and impervious areas of the watershed, time of concentration, runoff curve numbers, soil characteristics, design storm precipitation and design storm hyetograph for a specific 24-hour event (Stubchaer, 1975; WSDOT, 2004). Detailed description of computation steps for the SBUH methods can be found in (Stubchaer, 1975; King County Surface Water Design Manual, 1998; WSDOT, 2004). The SBUH first determines the total runoff depth for each time increment by computing the runoff depth (R) for impervious and pervious portions of the watershed using the SCS-CN equations as follows (Stubchaer, 1975):

$$R_p = \frac{(P(t) - \lambda S_p)^2}{[P(t) + (1-\lambda)S_p]} \qquad \text{(Equation C.14)}$$

$$R_i = \frac{(P(t) - \lambda S_i)^2}{[P(t) + (1-\lambda)S_i]} \quad \text{(Equation C.15)}$$

$$\sum R(t) = R_i(t) + R_p(t) \quad \text{(Equation C.16)}$$

$$R(t) = \sum R(t) - \sum R(t - \Delta t) \quad \text{(Equation C.17)}$$

where the subscripts *i* and *p* stands for the impervious and pervious portions of the watershed.

Second, it converts the excess rainfall depth at each time period to an instantaneous hydrograph (flow) using the following relationship (Stubchaer, 1975):

$$I(t) = \frac{60.5R(t)A}{\Delta t} \quad \text{(Equation C.18)}$$

where *I(t)* is the instantaneous hydrograph [cfs], *R*(t) is the total runoff depth at each time increments [in], *A* is the area [acres] and *Δt* is time interval in [minutes].

Third, it computes the runoff hydrograph by routing the computed instantaneous hydrograph values through an imaginary reservoir with routing constants equal to the time of concentration using the following relationship (Stubchaer, 1975):

$$Q(t) = Q(t-1) + w\left[I(t-1) + I(t) - 2Q(t-1)\right] \quad \text{(Equation C.19)}$$

where the *t* and *t-1* stands for the present and previous time steps, *Q* and *I* are the routed and instantaneous runoff hydrographs [cfs] respectively, and *w* is the routing constant determined by (Stubchaer, 1975):

$$w = \frac{\Delta t}{(2T_c + \Delta t)} \quad \text{(Equation C.20)}$$

where T_c is the time of concentration [minutes] defined as the time it takes runoff to travel from the hydraulically most distant point of the watershed to the inlet of the BMP (WSDOT, 2004).

C.3 Eastern Washington Long and Short Durations Design Storm Events

In recognition of the climatic and topographic diversity in Eastern Washington, the area was divided into four climatic regions (1, 2, 3, 4) (WDOT, 2004). Each of the regions was similar in the spatial distribution of mean annual precipitation as well as the topographic characteristics, specifically the orientations of mountain ranges. Schafer et al., (2006) updated the region designations utilized previously and used two transition zones to provide for a smooth transition in the spatial mapping of precipitation at the boundary between adjacent climatic regions. The new region designations and the two transition zones are illustrated in Figure C.1. The regions are identified as:

- Zone 154 - Cascade Crest Transition Zone
- Region 14 (1): East Slopes Cascade Mountains.
- Zone 147: Cascade Foothills Transition Zone
- Region 77 (2): Central Basin.
- Region 7 (3): Okanogan, Spokane, Palouse.
- Region 13 (4): Northeastern Mountains and Blue Mountains.

The SCS originally developed four characteristic 24-hr dimensionless storm hyetographs for the entire country referred to as SCS 24-hr rainfall distributions (SCS, 1986). While all four hyetographs result in the same total precipitation, the temporal distributions are different with peak rainfall amounts occurring at different times. The Type II rainfall distribution hyetograph has been used in the SCS-CN method for conducting hydrologic analysis throughout much of the United States including Eastern Washington. However, based on recent analysis of historical rainfall records in Eastern

Washington, it has been concluded that the SCS Type II rainfall distribution does not match the historical record (WDOE, 2004). Instead, two types of design distributions were identified based on analysis of historical storms collected for 37-years of record since 1966 in Eastern Washington. These are: 1) the short duration storm and 2) the long duration storm (Schafer, 1993).

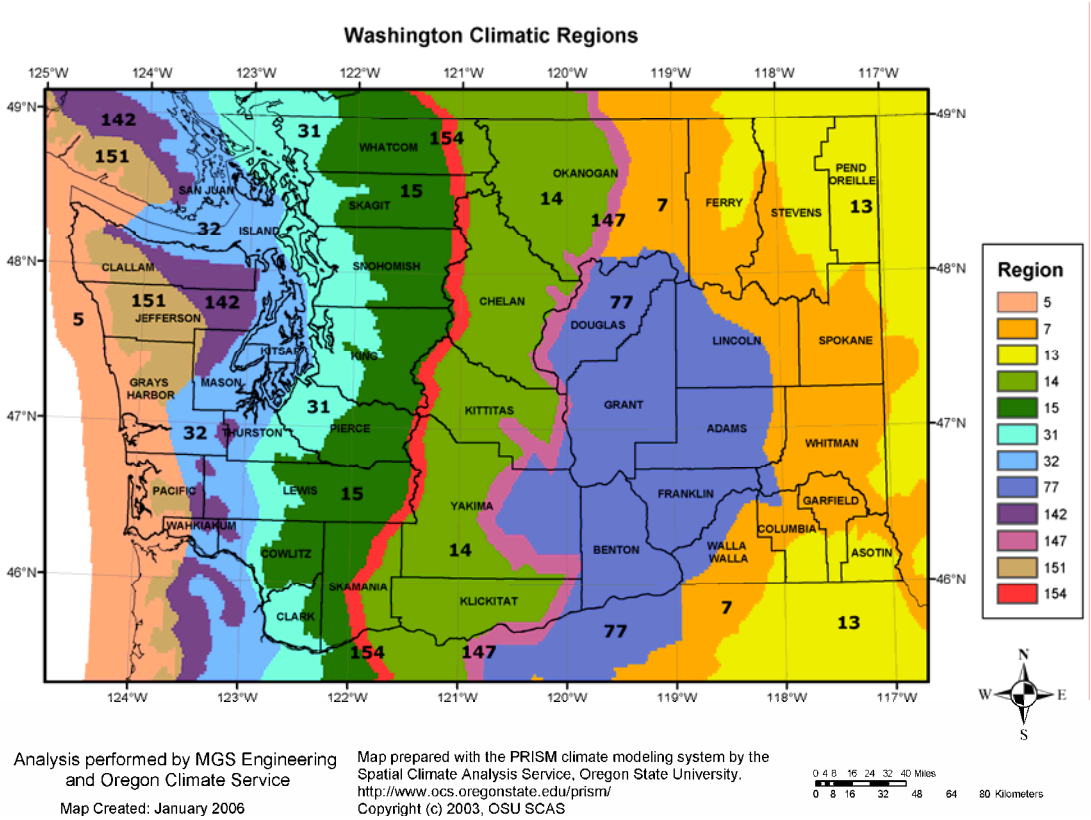

Figure C.1. Delineation of the climatic regions in Eastern Washington (From Schaefer et al., 2006).

The short duration storm occurs over a 3-hour duration for all climate regions in Eastern Washington (Figure C.2). The 3-hour short duration storm hyetograph appeared

to generate the greatest peak discharges for small urban watersheds and therefore it is more appropriate for flow based BMPs designs such as biofiltration swales (WDOE, 2004). The total 3-hour precipitation magnitude for a selected return period can be determined from the 2-hour duration, 2-year return period value using the following equation (WDOE, 2004):

$$P_{3hr,Xyear} = 1.06 \times C_{2hr,Xyear} \times P_{2hr,2year} \qquad \text{(Equation C.21)}$$

where $P_{3hr,Xyear}$ is the 3-hour total precipitation for a specified return period [in], 1.06 is the multiplier used for all climatic regions to convert *x-year*,2-hour precipitation to *x-year*,3-hour precipitation, $C_{2hr,Xyear}$ is the coefficient for converting the 2-year, 2-hour precipitation to x-year, 2-hour precipitation depth, and $P_{2hr,2year}$ is the 2-year, 2-hour precipitation [in].

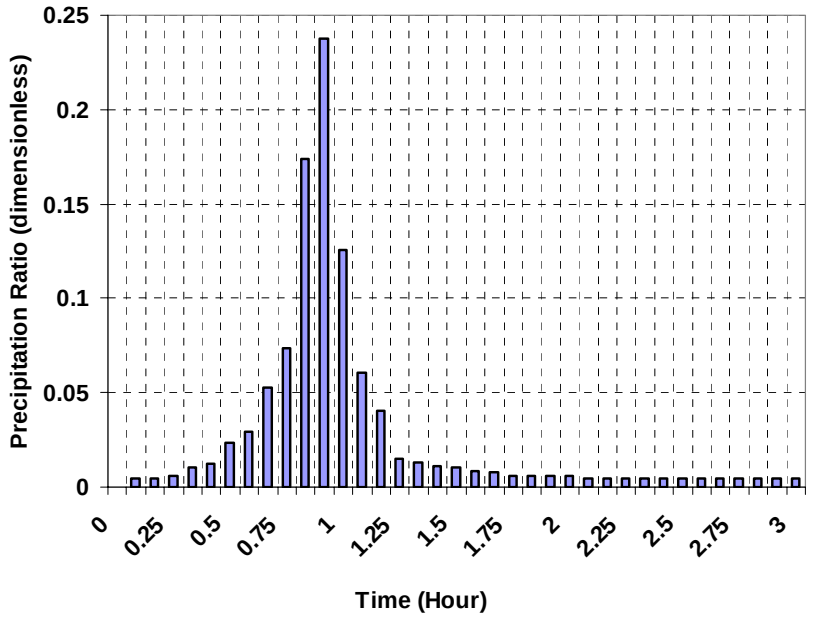

Figure C.2. Short duration storm hyetograph for regions 1, 2, 3 and 4 in Eastern Washington.

The long duration storm occurs over a period of 24 to 72 hours. However, it does not occur continuously, but rather it consists of a series of storm events with multiple peaks separated by a dry intervening period ranging from 12 to 18 hours, depending on the region (Figure C.3). The long duration storms appeared to generate the greatest runoff volumes, and is therefore used for designing volume based BMPs such as infiltration facilities and stormwater detention basins.

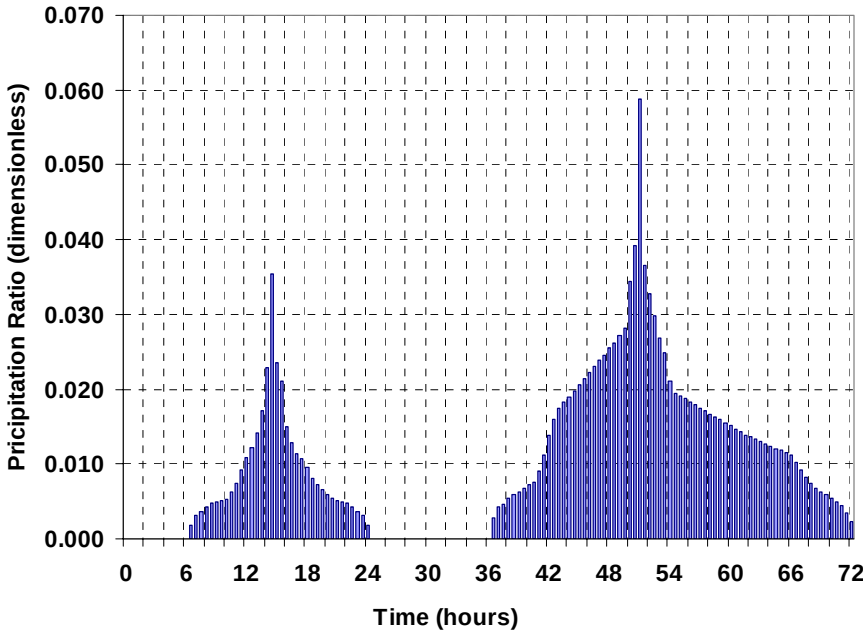

Figure C.3. Example 72-hour long duration storm hyetograph for region 7.

Two types of rainfall distribution can be used for long-duration design storms; 1) the 24-hour SCS Type 1A storm distribution for climatic regions 7 and 77, or 2) the regional long-duration storm for regions 7, 13, 14, and 77. The regional long-duration storm distributions were developed by Righellis (2003) as a modified Type IA storm distribution to more directly reflect the second portion of the long duration storm for each

region. If the regional long-duration hyetographs are used, the precipitation totals need to be adjusted as indicated in Table C.2.

Table C.2. Characteristics of the modified Type IA storm hyetographs used in each region.

Modified Type 1A Hyetograph	Region 14	Region 77	Region 7	Region 13
Duration (hour)	35	24	28	29
Duration as ratio of 24 hours	1.46	1.0	1.16	1.21
Conversion Factor	1.16	1.00	1.06	1.07

Schafer et al. (2006) updated the total depths of the 24-hour duration rainfall for the 6 months, 2, 5, 10, 25, 50 and 100-year recurrence intervals for the four different regions within Eastern Washington. These quantities are to be used with any one of the four distributions. The Modified Type IA rainfall distributions associated with a 24 hour 6-month return period design storm for four typical Eastern Washington cities are shown in Figure C.4 through Figure C.7 to illustrate the range of rainfall depths encountered in the area.

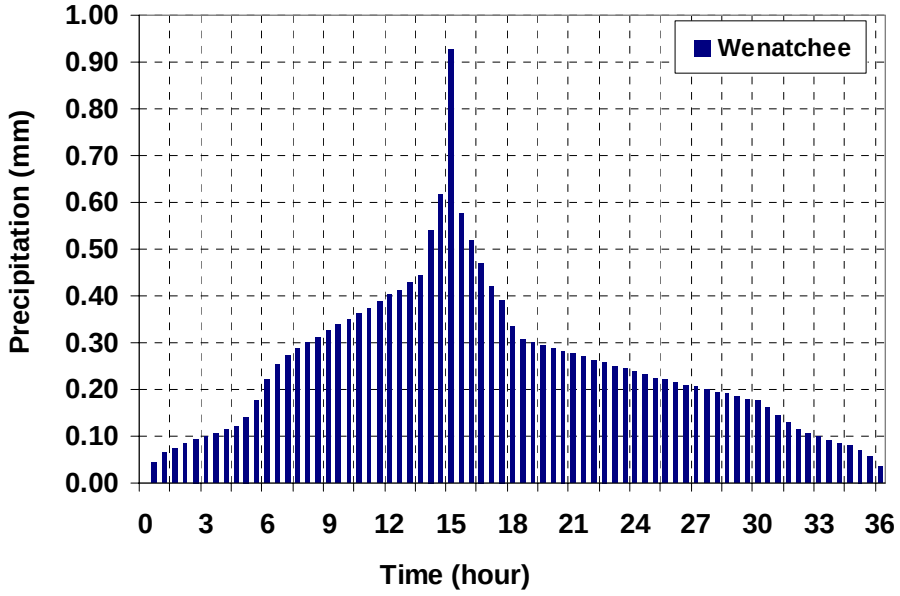

Figure C.4. Modified Type IA storm Applied to a 24 hour 6-month return period design storm for Wenatchee city, region 14.

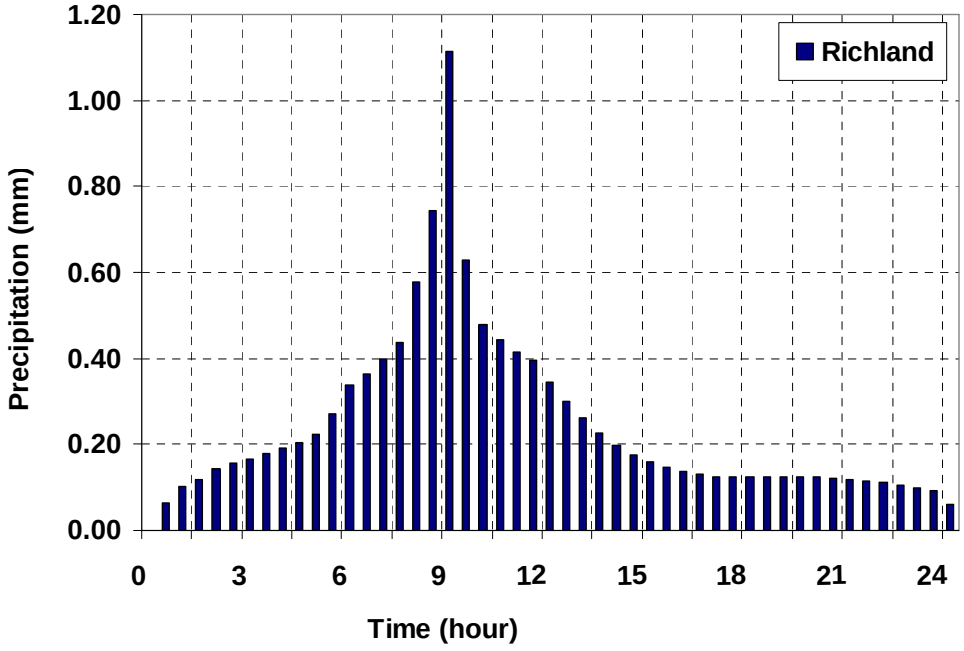

Figure C.5. Modified Type IA storm Applied to a 24-hour 6-month return period design storm for Richland city, region 77.

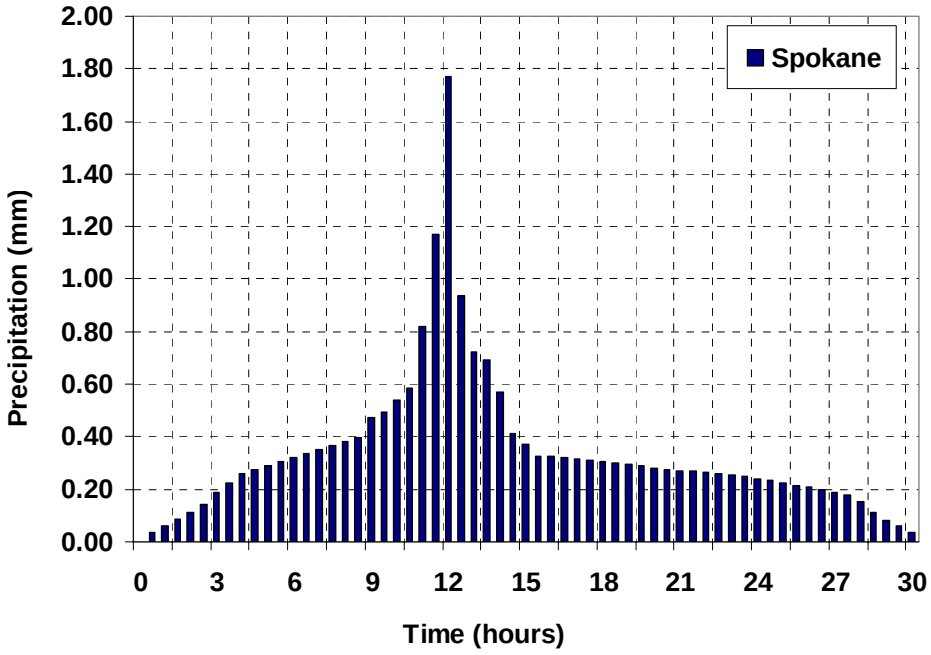

Figure C.6. Modified Type IA storm Applied to a 24-hour 6-month return period design storm for Spokane city, region 7.

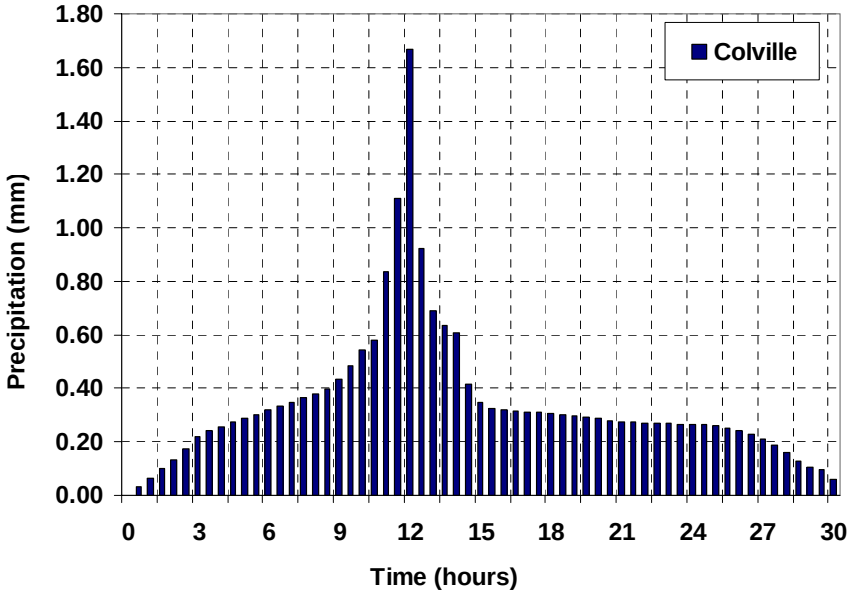

Figure C.7. Modified Type IA storm Applied to a 24-hour 6-month return period design storm for Colville city, region 13.

Although long duration storm hyetographs appear to be more appropriate to the storms likely to occur in Eastern Washington, there is a concern regarding using the SCS-CN method for modeling these types of multi-peak storms. Currently the initial abstraction in the SCS-CN method is computed by considering just the first portion of the hyetograph and does not take into account the occurrence of a dry period (and draining of soils) before the second portion of the hyetograph commences which would allow for additional abstractions. This results in greater peak flows and runoff volumes than what is encountered in real situations and thus causes over design of facilities. In addition, as can be seen in Figures C.4 through C.7, the storm totals in Eastern Washington are generally less than one inch which causes the predicted runoff to be extremely sensitive to the magnitude of initial abstraction and initial infiltration rate (Schafer, 2002). Thus an effort has been made in this work to assess the currently used initial abstraction storage ratio (I_a/S) in the SCS-CN equation and to develop I_a/S values that are more appropriate for use with long duration storms by model calibration tool.

C.4 Rain-on-Snow and Snowmelt Design Considerations

In many cold climate regions, a considerable amount of annual precipitation falls in the form of the snow. Snowfalls represents an important source of water in these regions since runoff generated from snow melting and rain-on-snow events plays a major role in recharging ground water and replenishing surface water storage (USACE, 1998). Snowfall from one or more events can accumulate over time on the contributing area, and if rainfall occurs, the snowmelt can be accelerated and generated runoff volumes may lead to flood (Sui and Koehler, 2001; Valeo and Ho, 2004). Rain-on-snow events, as well

as snowmelt can heavily influence the performance of the BMPs in cold regions. Increased runoff volumes due to snow melt can saturate or fill the BMP prior to the occurrence of the actual design event. This problem can be of critical important if the BMP's ground below the snow cover is frozen at the onset of rainfall or during the snow melt. The impacts of rain-on-snow events, as well as snowmelt should be considered while designing the runoff treatment BMPs and it may be more appropriate in some areas to use these events for design of stormwater storage facilities (NEH, 2004).

However modeling snow hydrology for cold regions is quite complicated and required too many input data that are not readily available in many cases (Walter et al., 2005). Despite this fact several methods have been used for estimating snowmelt runoff volumes and hydrographs (USACE, 1956; USDA, 2004). The US Army Corps of Engineers (USACE) developed an expression to calculate the snow melt in terms of the average daily rainfall rate and the free air temperature as follows (USACE, 1956):

$$M = 0.007P(T_a - 32) \qquad \text{(Equation C.22)}$$

where M is the daily snowmelt from rain [in], P is the daily precipitation [in], and T_a is the air temperature [^{o}F].

Urbonas and Stahre (1993) recommended the following minimum design value for snowmelt rates:

$$Snowmelt = impervious\ surface\ area \times 0.04\ cfs/acre + Pervious\ surface\ area \times 0.02\ cfs/acre \qquad \text{(Equation C.23)}$$

However, the Urbonas and Stahre (1993) method is not universally accepted. Instead the USACE (1956) proposed a temperature index approach for estimating daily snowmelt as follows:

$$M_s = C_m\left(T_{air} - T_{base}\right) \quad \text{(Equation C.24)}$$

where M_s is the daily snowmelt [inches/day], T_{air} is the average daily air temperature [^{o}F], T_{base} is the base temperature typically around 32 [^{o}F], and C_m is the melt rate coefficient that depends on site conditions [inch/(^{o}F /day)]. The range of melt rate is typically varies between 0.04 and 0.08 inch/(^{o}F /day).

In addition to the temperature index method, the USACE uses the most important parameters in the energy balance equation (such as temperature, wind, and radiation) to develop regression equations for estimating snowmelt for rainy and non-rainy periods. The equation for non-rainy period in partially forested area is (USACE, 1998):

$$M = C[0.002I_i(1-a) + (0.001v + 0.0145)(T_a - T_F) + 0.0039v(T_d - T_F)] \quad \text{(Equation C.25)}$$

For snowmelt during rainy periods, the equation is (USACE, 1998):

$$M = C[0.09 + (0.029 + 0.00504v + 0.007P)(T_a - T_F)] \quad \text{(Equation C.26)}$$

where M is the snow melt [in/day], I_i is the incident solar radiation on a horizontal surface [Langley/day], a is the albedo of the snow, v is the wind speed 50 feet above the snow surface [miles/hour], T_a is the air temperature [^{o}F], T_F is the freezing temperature [^{o}F], T_d is the dew point temperature [^{o}F], P is the rainfall [in/day], and C is the coefficient to account for variations.

In addition to the previous equations, there are numerous numbers of snowmelt computation models that were developed and used by Federal, State, and private institutions including PRMS (Leavesley et al., 1983), SRM (Martinec et al., 1983), HEC-1, HEC-1f (USACE, 1990), and SSARR (USACE, 1991). Moreover, efforts have been devoted recently to study and develop models that more precisely simulate the spatial distribution of snow accumulation and melt taking advantage of Geographic Information

System (GIS) and spatial data sets of elevation, vegetation, soils, and surface cover conditions (e.g. Models of Marks et al., 1999; Tarboton et al., 1995).

WDOE (2004) has indicated that the rain on snow condition can be neglected in many parts of Eastern Washington where the average daily snow depth from December to February is less than 1 inch. However, if the daily snow depth is greater than 1 in, the 24-hour design storm precipitation should be adjusted using the following steps:

1) Determine the snow water equivalent for the 24-hour storm by assuming 20% moisture content:

   $SWE = 0.20 \times average\ daily\ snow\ depth$

2) Determine the 24-hour to the 72-hour precipitation ratio based on climatic region.
3) Calculate the regional storm adjustment as the above ratio multiplied by the SWE computed in step 1.
4) Add the long duration adjustment factor calculated from step 3 to the 24-hour design precipitation storm.

The adjustment's factors vary among the regions and are based on the assumption that snow will melt completely during the 72-hour long duration storm. Table C.3 shows the adjustment factor value for selected cities in Eastern Washington.

Whether the snowmelt and rain on snow events or the additional contributions from them are more appropriate than the traditional design rainfall storms for stormwater runoff treatment facility design in areas of Eastern Washington are questions that were addressed by the work completed in this study.

Table C.3. Adjustment snow factor calculated for selected cities in Eastern Washington using the method proposed by WDOE (2004).

	Selected cities from Eastern Washington			
City Name	Wenatchee	Richland	Spokane	Colville
Region	14	77	7	13
Regional Long storm duration (hr)	36	24	30	30
Average daily snow depth (cm)	6.78	0.84	5.92	12.7
24-hr, 6-month design storm (cm)	1.57	1.19	1.96	1.96
Average rainfall intensity (mm/hr)	0.50	0.66	0.81	0.81
Snowmelt adjustment factor (cm)	2.89	N/A	2.26	4.52

C.5 REFRENCES

Gray, D.D., Katz, P.G., deMonsabert, S.M., and Cogo, N.P. (1982). "Antecedent Moisture Condition Probabilities." *Journal of Irrigation and Drainage Division*, Proceeding of the American Society of Civil Engineers, 108 (IR2), 107-114.

Hawkins, R.H. (1975). "The Importance of Accurate Curve Numbers in the Estimation of Storm Runoff." *Water Resources Bulletin*. 11 (5), 887-891.

Hawkins, R.H. (1978). "Runoff Curve Numbers with Varying Site Moisture." *Journal of Irrigation and Drainage Division*, Proceeding of the American Society of Civil Engineers. 104 (IR4), 389-398.

Hawkins, R.H. (1979). "Runoff Curve Numbers from Partial Area Watersheds." *Journal of Irrigation and Drainage Division*, Proceeding of the American Society of Civil Engineers. 105 (IR4), 375-389.

Hawkins, R.H. (1993). "Asymptotic Determination of Runoff Curve Numbers from Data." *Journal of Irrigation and Drainage Engineering*. 119 (2), 334-345

Hawkins, R.H. (1998). "Local Sources for Runoff Curve Numbers." Presented at the 11th Annual Symposium of the Arizona Hydrological Society, Tucson, AZ.

Hawkins, R.H., Jiang, R., Woodward, D.E., Hjelmet Jr., A.T., and VanMullem, J.E. (2003). "Runoff Curve Number Method: Examination of the initial abstraction ratio." World Water and Environmental Resources Congress. Philadelphia, PA.

Hawkins, R.H., Ward, T.J. Woodward, D.E., and VanMullem, J.E. (2005). "Progress Report: ASCE Task Committee on Curve Number Hydrology." Managing Watershed for Human and Natural Impacts, Engineering, Ecological, and

Economic Challenges, Watershed 2005. Glenn E. Moglen-Editor, Williamsburg, VA.

King County Surface Water Management Division (1999). *"King County Runoff Time series (KCRTS), Computer Software Reference Manual"*, Version 4.4.

Linsley, R.K., Kohler, M.A. and Paulhus, J. L. H. (1975). "Hydrology for Engineers." 2nd edition, McGrawHill, New York, 265–266.

Marks, D., J. Domingo, D. Susong, T. Link, and D.Garen. (1999). "A Spatially Distributed Energy Balance Snowmelt Model for Application in Mountain Basins". *Hydrological Processes*, 13, 1953-1959.

McCuen R.H. (1982). "A Guide to Hydrologic Analysis Using SCS Methods." Prentice Hall Inc, Englewood Cliffs, NJ.

Mishra, S.K. and Singh, V.P. (1999). "Another Look at SCS-CN Method." *Journal of Hydrologic Engineering*. 4(3), 257-264.

Mishra, S.K., Singh,V.P., and Sansalone, J.J.. (2003). "A Modified SCS-CN method: Characterization and Testing." *Water Resources Management*. 17, 37-68.

Mishra, S.K. and Singh,V.P. (2004). "Long-Term Hydrological Simulation Based on the Soil Conservation Service Curve Number." *Hydrological Processes*. 18, 1291-1313.

Mishra, S.K., Jain, M.K., Bhunya, P.K. and Singh,V.P. (2005). "Field Applicability of the SCS-CN Based Mishra-Singh General Model and its Variants." *Water Resources Management*. 19, 37-62.

Mockus,V. (1949). “Estimation of Total (Peak rate of) Surface Runoff for Individual Storms.” Exhibit A of Appendix B. Interim Survey Rep. Grand (Neosho) River Watershed. USDA. Washington ,D.C.

Mockus,V. (1964). “Estimation of Direct Runoff from Storm Rainfall.” National Engineering Handbook, Section 4, Chapter 10, U.S. Department of Agriculture Soil Conservation Service, Washington, DC.

Perrone, J. and Madramootoo, C.A. (1998). “Improved Curve Number Selection for Runoff Prediction.” Canadian Journal of Civil Engineering, 25, 728-734.

Ponce, V.M., and Hawkins, R.H. (1996). “Runoff Curve Number: Has it Reached Maturity?.” *Journal of Hydrologic Engineering*, 1(1), 11-18.

Righellis, A.O., (2003). “Modeling Methodology for Custom Design Storms in Eastern Washington.”, Technical Memorandum, Harper-Houf-Righellis, Inc.

Schaefer, M.G. (1993). “Dam Safety Guideline, Technical 3, Design Storm Construction.” Washington State Department of Ecology, Water Resources Program, Report 92-55G.

Schaefer, M.G. (2002). “Estimation of Runoff from Long-Duration Storms Using Event-Based Rainfall-Runoff Models.” For Technical Advisory Group, Eastern Washington Stormwater Manual Committee, MGS Engineering Consultants Incorporation.

Schaefer. M.G., Barker B.L., Taylor G.H., Wallis J.R. (2006). “Regional Precipitation-Frequency Analysis and Spatial Mapping of Precipitation for 24-hour and 2-hour Durations in Eastern Washington.” Prepared for Washington State Department of Transportation. MGS Engineering Consultants Incorporation.

Soil Conservation Service, SCS (1964). "National Engineering Handbook, Section 4 Hydrology." USDA, Washington, DC.

Soil Conservation Service, SCS (1971). "National Engineering Handbook, Section 4 Chapter 10." USDA, Washington, DC.

Soil Conservation Service, SCS (1986). "Technical Release 55: Urban Hydrology for Small Watersheds." USDA, Washington, DC.

Stubchaer, J.M. (1975). "The Santa Barbra Urban Hydrograph Method." National Symposium on Urban Hydrology and Sediment Control. University of Kentucky, Lexington, KY. 131-141.

Sui J. and Koehler G. (2001). "Rain-On-Snow Induced Flood Events In Southern Germany." *Journal of Hydrology*, 252, 205-220.

Tarboton D.G., Chowdhury T.G., and Jackson T.H. (1995). "A Spatially Distributed Energy Balance Snowmelt Model.", In Biogeochemistry of Seasonally Snow-Covered Catchments (Proceedings of Boulder symposium), International. Association of Hydrologic Science Publication, 228, 141-155.

Tsihrintzis, V. A. and Hamid, R. (1997). "Urban Stormwater Quantity/Quality Modeling Using the SCS Method and Empirical Equations", *Journal of American Water Resources Association*, 33(1), 163–176.

Tsihrintzis, V.A., and Sidan, C.B. (1998). "Modeling Urban Stormwater Runoff Processes Using Santa Barbara Method." *Water Resources Managemen*t, 12, 139-166.

Urbonas, B. R. and Stahre P. (1993). "Stormwater-Best Management Practices Including Detention." Prentice Hall, Englewood Cliffs, NJ.

U.S. Army Corps of Engineering, USACE (1956). "Summary Report of the Snow Investigation Snow Hydrology." North Pacific Division, Corps of Engineering. U.S. Army, Portland, OR.

U.S. Army Corps of Engineering (USACE) (1998). "Engineering And Design-Runoff From Snowmelt." Manual No. 1110-2-1406, Washington, DC.

U.S. Department of Agriculture, Soil Conservation Service, USDA-SCS (1985). "National Engineering Handbook, Section 4, Hydrology." Soil Conservation Service, Washington, DC.

U.S. Department of Agriculture, USDA (2004). "National Engineering Handbook, Part 630, Hydrology, Chapter 11." Soil Conservation Service, Washington, DC.

Valeo, C., Ho, C.L.I. (2004). "Modeling Urban Snowmelt Runoff." *Journal of Hydrology*, 299, 237-251.

Van Mullem, J.A., Woodward D.E., Hawkins, R.H., Hjelmfelt, A.T., and Quan, Q.D. (2002). "Runoff Curve Number Method: Beyond the Handbook." Second Federal Interagency Hydrologic Modeling Conference, Las Vegas, NV.

Walter, M.T., Brooks, E.S., McCool, D.K., King,L.G., Molnau, M., and Boll, J., (2005), "Process-Based Snowmelt Modeling: Does It Require More Input Data Than Temperature-Index Modeling?." *Journal of Hydrology*, 300, 65-75.

Washington State Department of Ecology, WDOE (2004). "Stormwater Management Manual For Eastern Washington." Publication Number 04-10-076, Olympia, WA.

Washington State Department of Transportation, WSDOT (2004). "Highway Runoff Manual." Olympia, WA.

Woodward, D.E. and Plummer, A. (2000). "Antecedent Moisture Conditions NRCS View Point." *Proceedings of Watershed Management and Operations Management (ASCE),* Marshall Flug, Donald Frevert, David W. Watkins, Jr.-Editors, Fort Collins, CO, USA.

Woodward, D.E., Hawkins, R.H., Hjelmfelt, A.T., Van Mullem, J.A, and Quan, D.Q. (2002). "Curve Number Method: Origins, Applications and Limitations." Second Federal Interagency Hydrologic Modeling Conference, Las Vegas, NV.

APPENDIX D

LONG DURATION HYETOGRAPH FOR CITY OF SPOKANE, WASHINGTON

The long duration storm hyetograph for Spokane city was computed using two components: (1) the dimensionless storm pattern for region 3 (Okanogan, Spokane, Palouse) presented in the second column, and (2) the 24 hr precipitation amount for a 6 month return period for Spokane city (P = 0.77 in). The 24 hr precipitation values times 1.06 was used to determine the long duration storm total precipitation amount (fourth column), where the 1.06 is the long duration scaling factor for region 3.

Time (Hr)	Incremental Rainfall Ratio	Cumulative Rainfall	Rainfall (in)	Rainfall Intensity (in^3/hr)	Rainfall Intensity (mm^3/hr)	Rainfall Intensity (ml/min)
0.0	0.0	0.0	0.0	0.0	0.0	0.0
0.5	0.0017	0.0017	0.001388	12.79	209550.71	3.49
1.0	0.0030	0.0047	0.002449	22.57	369795.36	6.16
1.5	0.0041	0.0088	0.003346	30.84	505387.00	8.42
2.0	0.0053	0.0141	0.004326	39.87	653305.14	10.89
2.5	0.0068	0.0209	0.00555	51.15	838202.82	13.97
3.0	0.0092	0.0301	0.007509	69.20	1134039.11	18.90
3.5	0.0108	0.0409	0.008815	81.24	1331263.31	22.19
4.0	0.0126	0.0535	0.010284	94.78	1553140.52	25.89
4.5	0.0132	0.0667	0.010774	99.29	1627099.60	27.12
5.0	0.0139	0.0806	0.011345	104.56	1713385.18	28.56
5.5	0.0147	0.0952	0.011998	110.57	1811997.28	30.20
6.0	0.0154	0.1106	0.012569	115.84	1898282.86	31.64
6.5	0.0162	0.1268	0.013222	121.86	1996894.96	33.28
7.0	0.0169	0.1437	0.013794	127.12	2083180.54	34.72
7.5	0.0177	0.1614	0.014447	133.14	2181792.64	36.36
8.0	0.0184	0.1798	0.015018	138.41	2268078.23	37.80
8.5	0.0192	0.199	0.015671	144.42	2366690.32	39.44
9.0	0.0228	0.2219	0.018609	171.50	2810444.76	46.84
9.5	0.0238	0.2457	0.019426	179.03	2933709.88	48.90
10.0	0.026	0.2717	0.021221	195.57	3204893.15	53.41
10.5	0.0282	0.2999	0.023017	212.12	3476076.41	57.93
11.0	0.0395	0.3394	0.03224	297.12	4868972.28	81.15
11.5	0.0564	0.3958	0.046034	424.25	6952152.82	115.87

12.0	0.0855	0.4813	0.069785	643.14	10539167.85	175.65
12.5	0.0451	0.5265	0.036811	339.25	5559256.96	92.65
13.0	0.0348	0.5612	0.028404	261.77	4289626.21	71.49
13.5	0.0335	0.5948	0.027343	251.99	4129381.55	68.82
14.0	0.0276	0.6223	0.022527	207.61	3402117.34	56.70
14.5	0.0199	0.6422	0.016242	149.69	2452975.91	40.88
15.0	0.0179	0.6601	0.01461	134.65	2206445.67	36.77
15.5	0.0158	0.6759	0.012896	118.85	1947588.91	32.46
16.0	0.0156	0.6915	0.012733	117.34	1922935.89	32.05
16.5	0.0154	0.7069	0.012569	115.84	1898282.86	31.64
17.0	0.0152	0.7221	0.012406	114.34	1873629.84	31.23
17.5	0.015	0.7372	0.012243	112.83	1848976.82	30.82
18.0	0.0148	0.7519	0.01208	111.33	1824323.79	30.41
18.5	0.0145	0.7664	0.011835	109.07	1787344.25	29.79
19.0	0.0142	0.7806	0.01159	106.81	1750364.72	29.17
19.5	0.0139	0.7945	0.011345	104.56	1713385.18	28.56
20.0	0.0136	0.8081	0.0111	102.30	1676405.65	27.94
20.5	0.0133	0.8215	0.010855	100.04	1639426.11	27.32
21.0	0.0131	0.8346	0.010692	98.54	1614773.09	26.91
21.5	0.013	0.8475	0.010611	97.79	1602446.57	26.71
22.0	0.0128	0.8603	0.010447	96.28	1577793.55	26.30
22.5	0.0126	0.8729	0.010284	94.78	1553140.52	25.89
23.0	0.0123	0.8852	0.010039	92.52	1516160.99	25.27
23.5	0.012	0.8972	0.009794	90.27	1479181.45	24.65
24.0	0.0116	0.9088	0.009468	87.26	1429875.40	23.83
24.5	0.0112	0.92	0.009141	84.25	1380569.36	23.01
25.0	0.0108	0.9308	0.008815	81.24	1331263.31	22.19
25.5	0.0104	0.9412	0.008488	78.23	1281957.26	21.37
26.0	0.01	0.9512	0.008162	75.22	1232651.21	20.54
26.5	0.0096	0.9607	0.007836	72.21	1183345.16	19.72
27.0	0.0092	0.9699	0.007509	69.20	1134039.11	18.90
27.5	0.0086	0.9785	0.007019	64.69	1060080.04	17.67
28.0	0.0074	0.9859	0.00604	55.66	912161.90	15.20
28.5	0.0054	0.9913	0.004407	40.62	665631.65	11.09
29.0	0.004	0.9953	0.003265	30.09	493060.48	8.22
29.5	0.003	0.9983	0.002449	22.57	369795.36	6.16
30.0	0.0017	1	0.001388	12.79	209550.71	0.00

APPENDIX E

FLOW METER AND CONTROLLER SCRIPT FILE

The script below presents the data format that defined the set point which corresponded to each of the rainfall intensities at the defined interval. The number of lines in this script file corresponds to the total number of times the flow meter will be polled, and thus the total number of lines of data it will produce. The letter A proceeding the value in each line is the flow meter unit address on the RS-232 line. The set point value for each time interval was calculated using the following formula:

$$Value = \frac{\text{Desired Set Point} \times 64000}{\text{Full Scale Flow Range}} \qquad \text{(Equation E.1)}$$

where, the full scale flow range for the flow meter device that used in this work is 200 CCM.

A0
A1306
A2305
A3150
A4073
A5225
A7069
A8299
A9682
A10143
A10681
A11296
A11833
A12448
A12986
A13601
A14139
A14753
A17520
A18288
A19979
A21669
A30352
A43338
A65699
A34655
A26741
A25742
A21208
A15291
A13754
A12141
A11987
A11833
A11680
A11526
A11372
A11142
A10911
A10681
A10450
A10220
A10066
A9989
A9836
A9682
A9451
A9221
A8914
A8606
A8299
A7991
A7684
A7377
A7069
A6608
A5686
A4149
A3074
A2305
A0

APPENDIX F

CALIBRATING THE SCS-CN FOR THE TEST PLOT

Based on the SCS-CN published tables, a CN of 98 was selected to describe the characteristics of the plot surface. However, the accuracy of using this value for calculating the runoff hydrograph under the different plot slopes used in this study (S = 1.56 %, 3.13%, and 4.69%) was examined by conducting three control runs. For each of the control runs, rainfall was applied on the test plot with no snow cover. The observed runoff hydrograph obtained from each of the control runs was plotted and compared to the calculated runoff hydrograph obtained by SBUH method. As can be see in Figures F.1 and F.2, for S =1.56 % and S = 3.13 %, the simulated runoff volume and discharge peak resulted from using a curve number of 98, overestimates the measured runoff volume, and the measured peak discharge. While for S = 4.69 % the simulated runoff volume and discharge peak resulted from using a curve number of 98, underestimates the measured runoff volume, and the measured peak discharge as shown in Figure F.3. To achieve a better agreement between the simulated and observed runoff hydrograph, the curve number parameter in SBUH method has been adjusted using a trial and error adjustment procedure until the difference between the SBUH outputs (runoff volume and peak discharge) and the measured hydrograph outputs (measured runoff volume and measured peak discharges) was minimum. The calibrated CN values for each of the test runs were then recorded to be used in calculating the runoff hydrograph for the simulated rain-on-snow events.

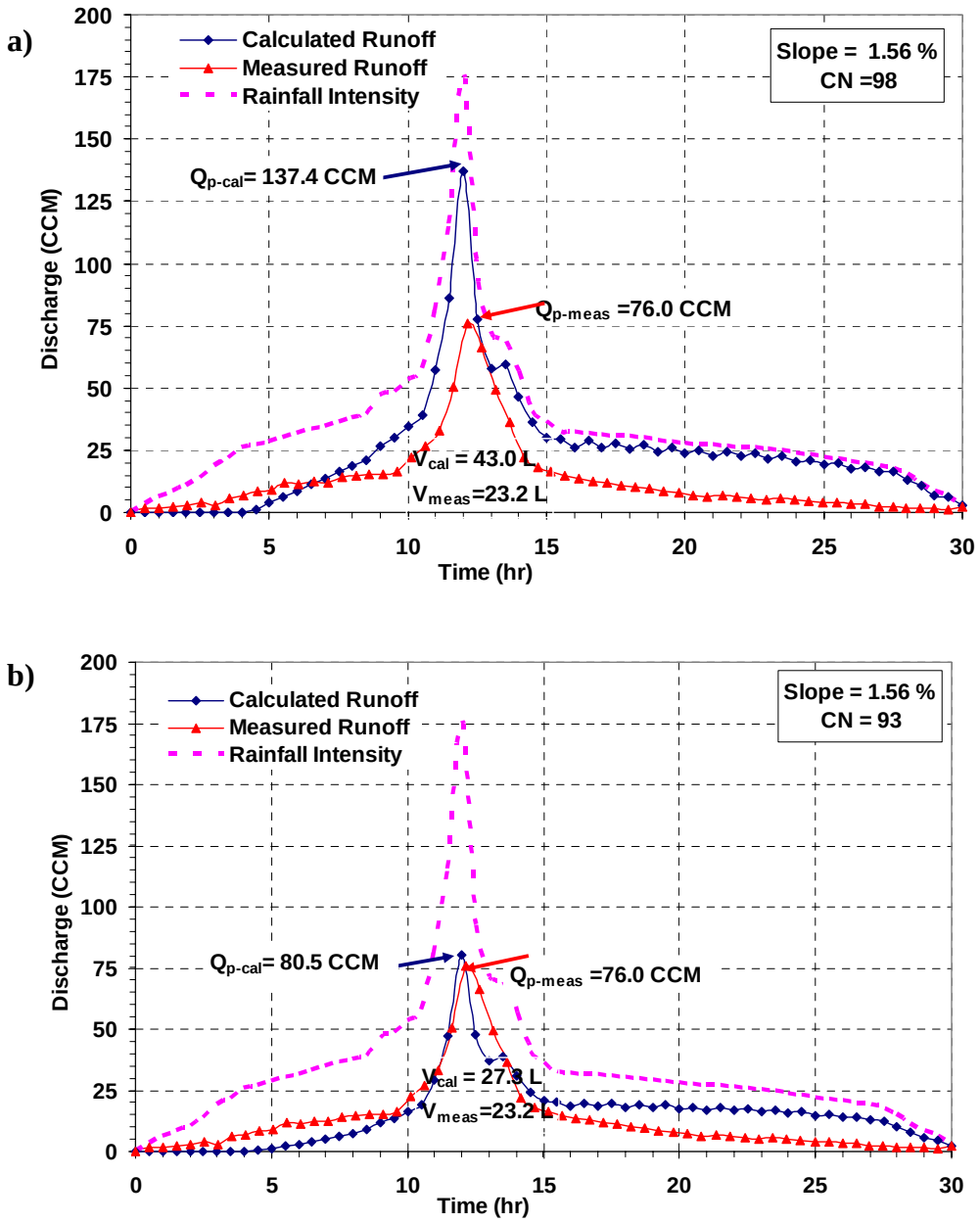

Figure F.1. Measured and calculated plot runoff for control run 1 (S =1.56 %) where a) before calibration CN = 98, b) after calibration CN = 93.

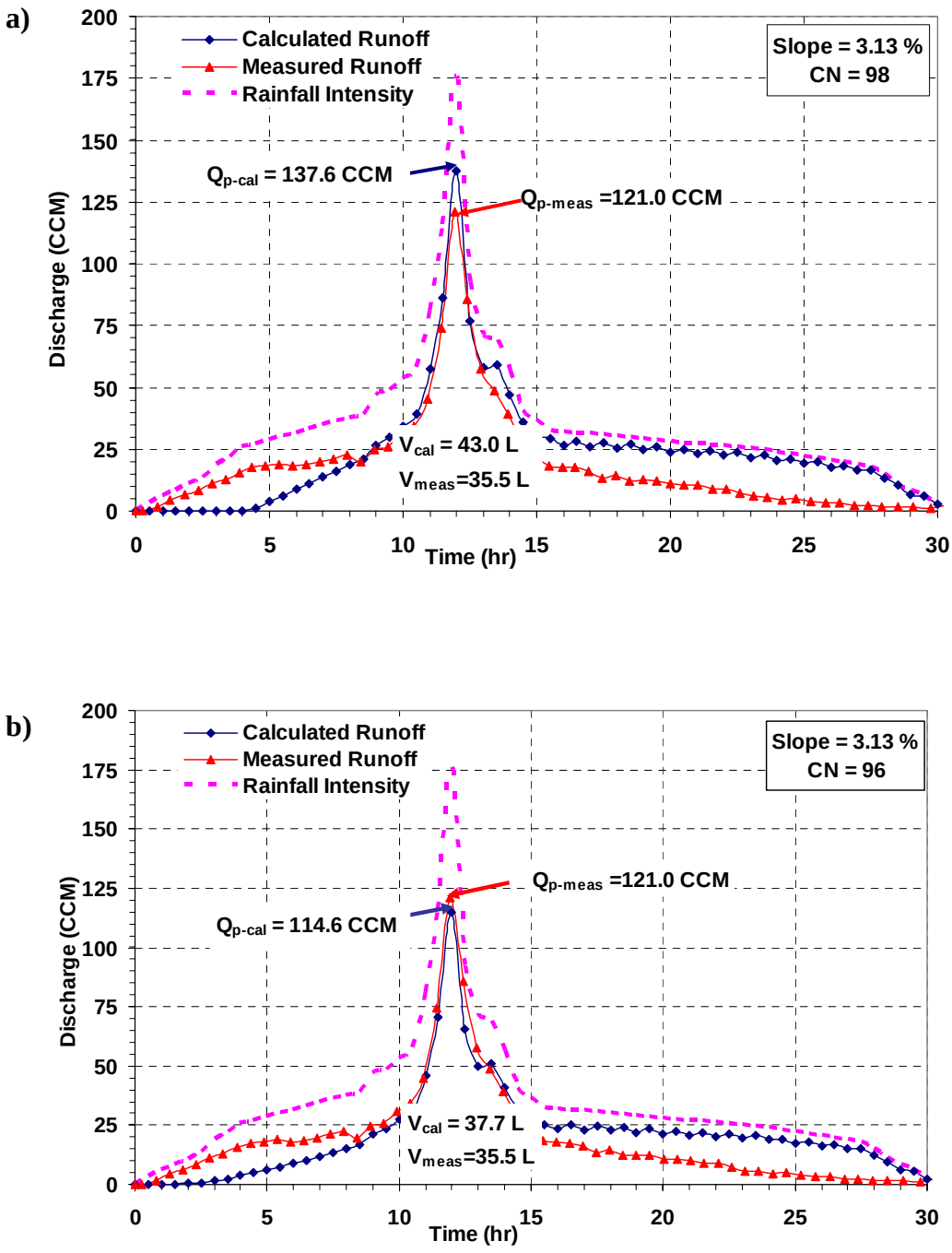

Figure F.2 Measured and calculated plot runoff for control run 2 (S =3.13%) where a) before calibration CN = 98, b) after calibration CN = 96.

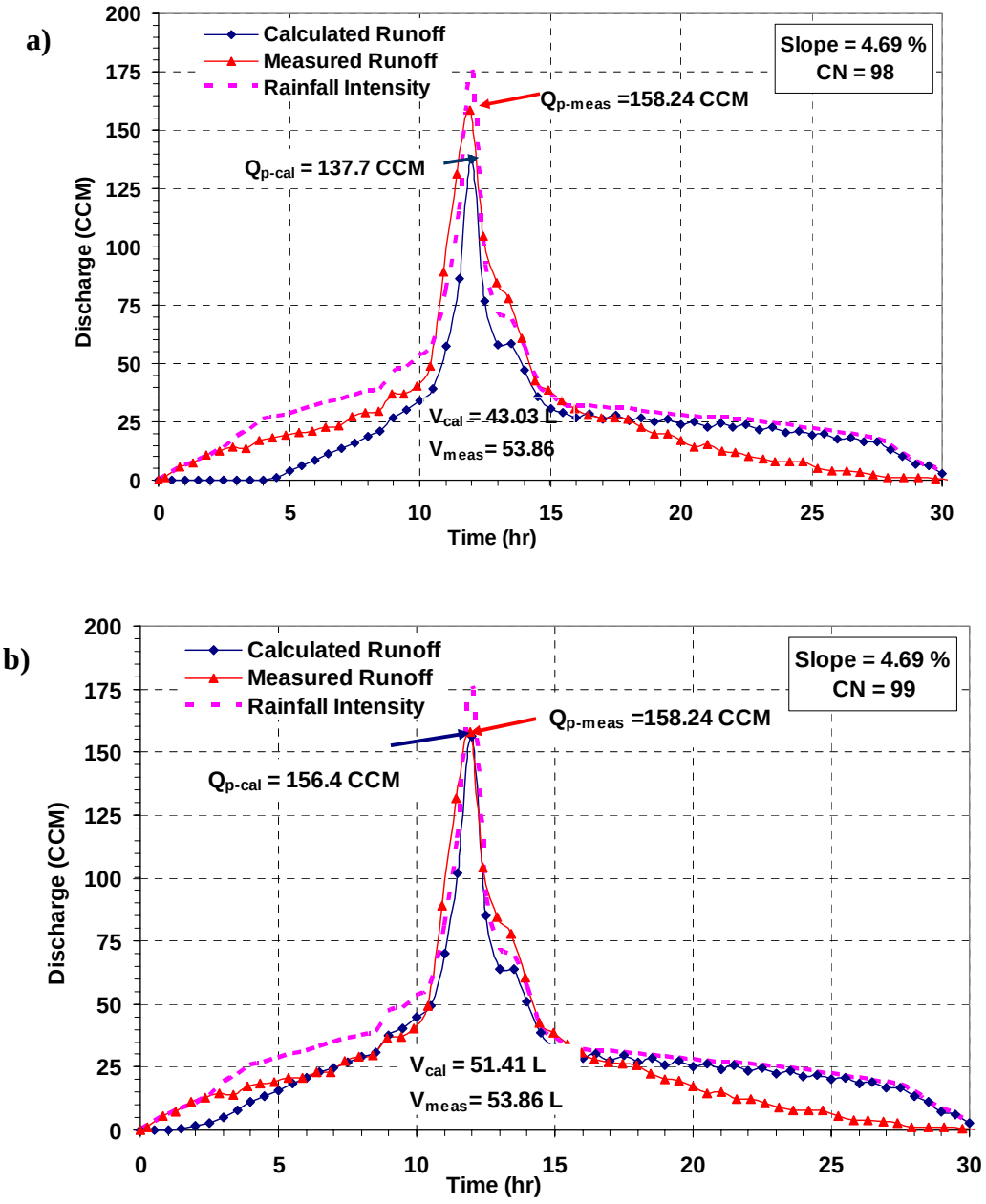

Figure F.3. Measured and calculated plot runoff for control run 3 (S = 4.69 %) where a) before calibration CN = 98, b) after calibration CN = 99.

APPENDIX G

CALCULATED RUNOFF HYDROGRAPHS USING THE CALIBRATED PARAMETER, λ

The following figures illustrate the results of the calibration task. The figures compared calculated runoff hydrograph using the calibrated initial abstraction storage ratio (λ) to the measured runoff hydrograph for each of the rain-on-snow events simulated in this study.

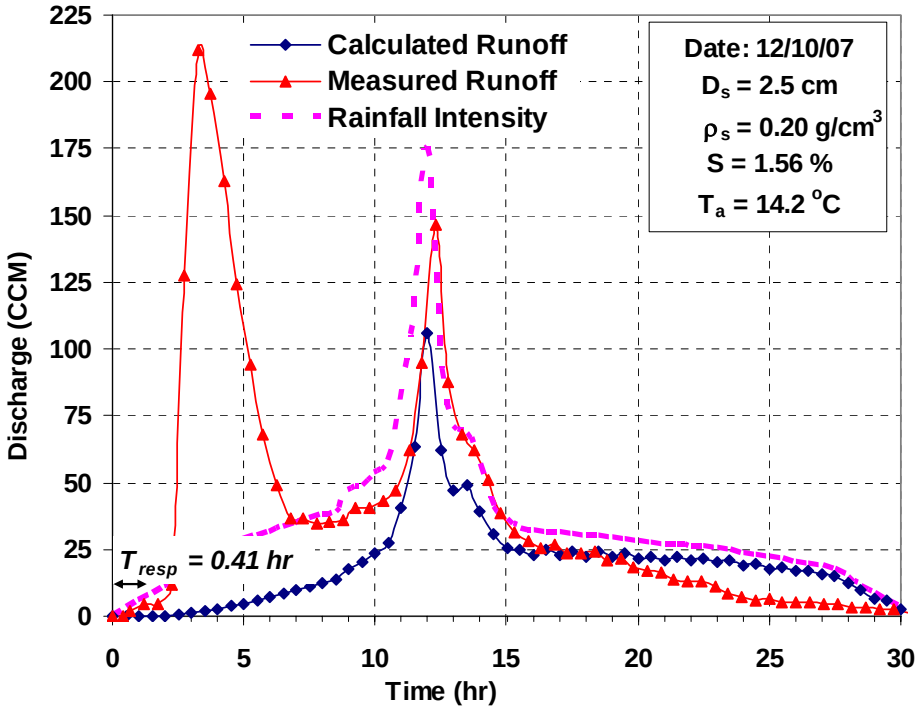

Figure G.1. Measured versus calculated runoff hydrographs using the calibrated λ value for event 1.

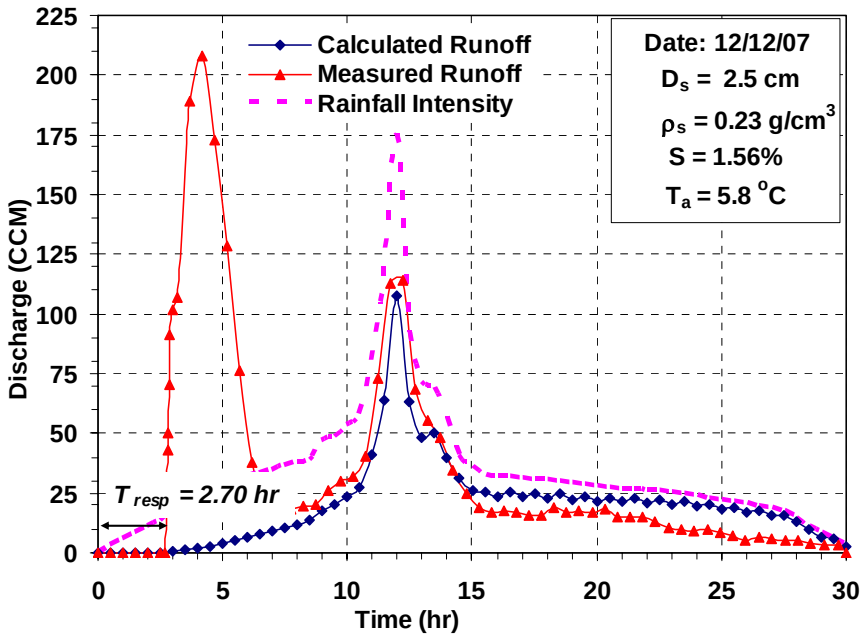

Figure G.2. Measured versus calculated runoff hydrographs using the calibrated λ value for event 2.

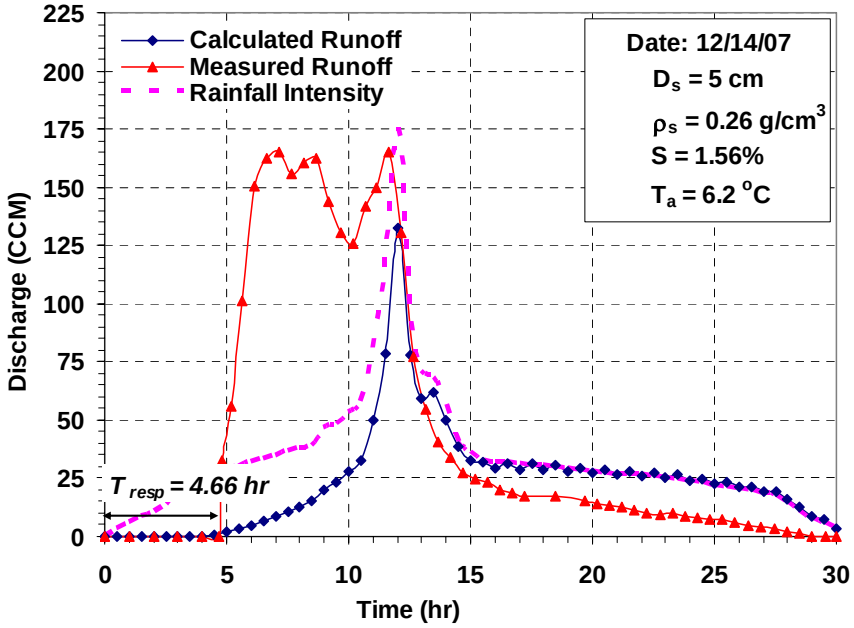

Figure G.3. Measured versus calculated runoff hydrographs using the calibrated λ value for event 3.

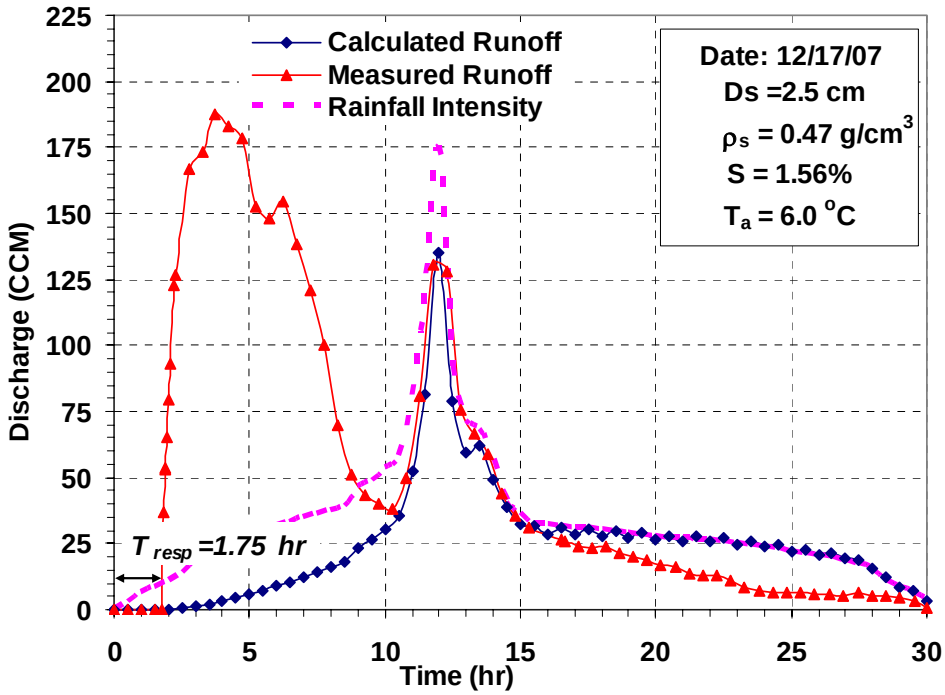

Figure G.4. Measured versus calculated runoff hydrographs using the calibrated λ value for event 4.

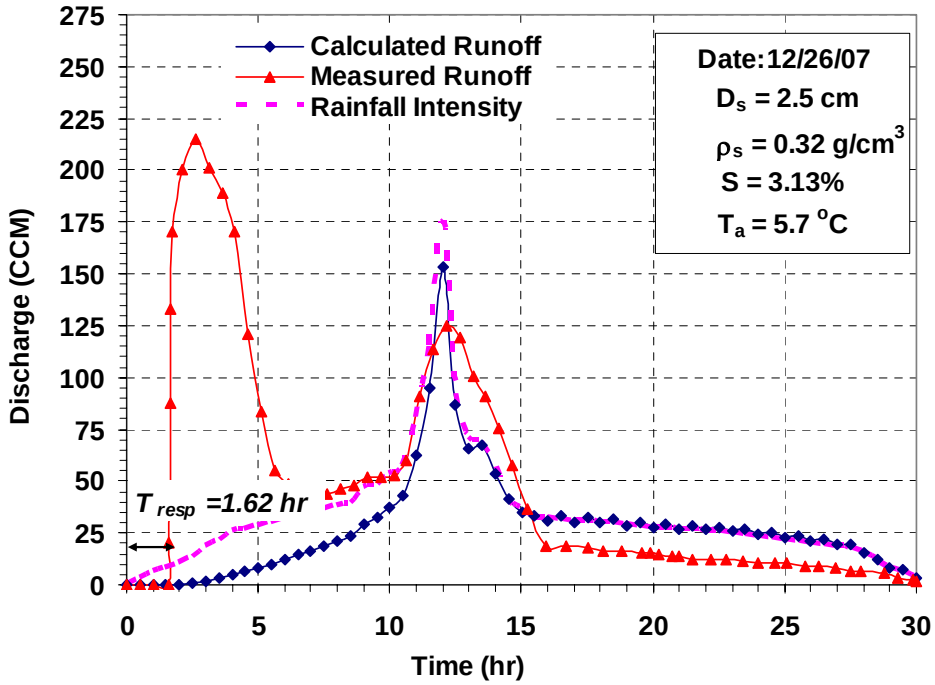

Figure G.5. Measured versus calculated runoff hydrographs using the calibrated λ value for event 5.

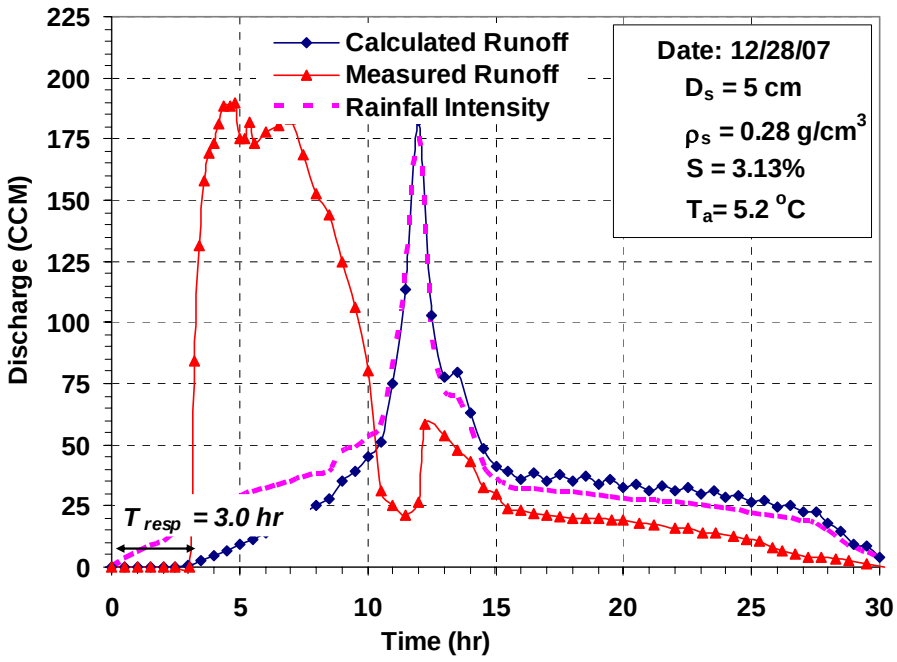

Figure G.6. Measured versus calculated runoff hydrographs using the calibrated λ value for event 6.

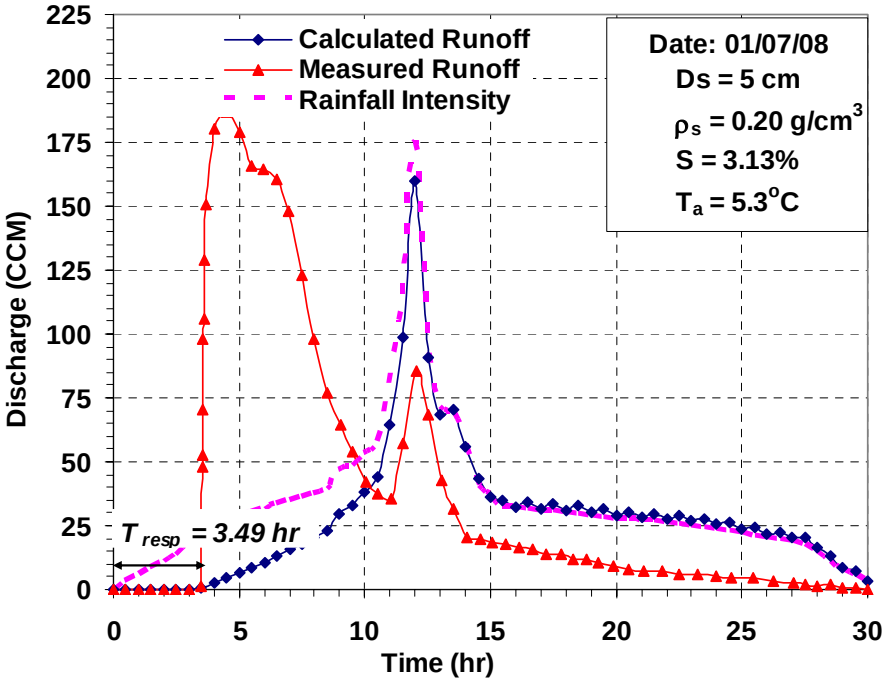

Figure G.7. Measured versus calculated runoff hydrographs using the calibrated λ value for event 7.

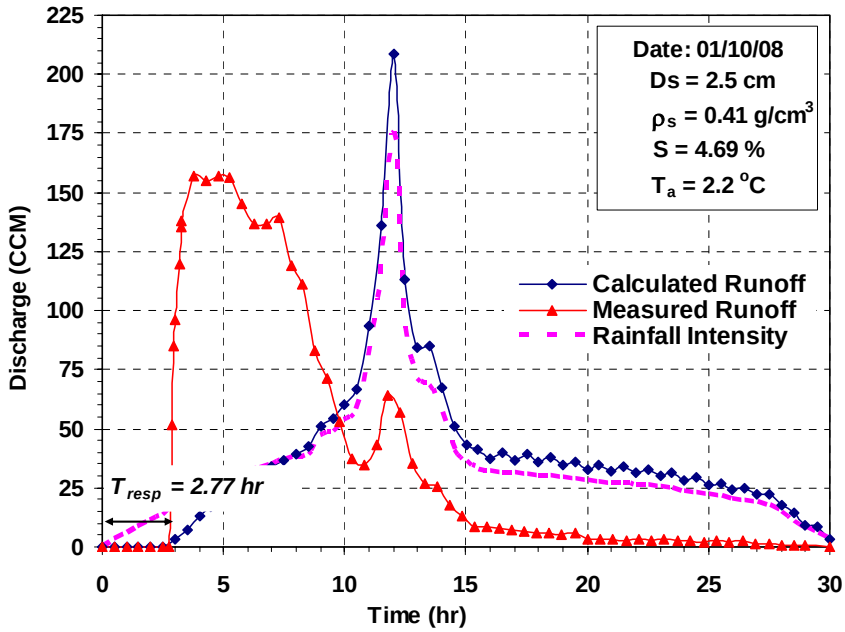

Figure G.8. Measured versus calculated runoff hydrographs using the calibrated λ value for event 8.

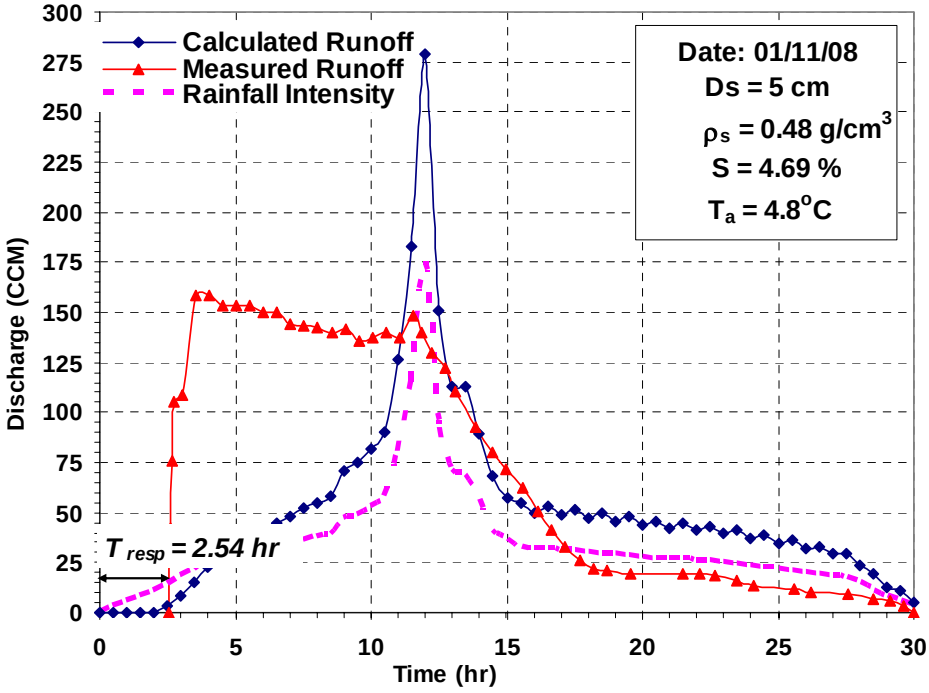

Figure G.9. Measured versus calculated runoff hydrographs using the calibrated λ value for event 9.

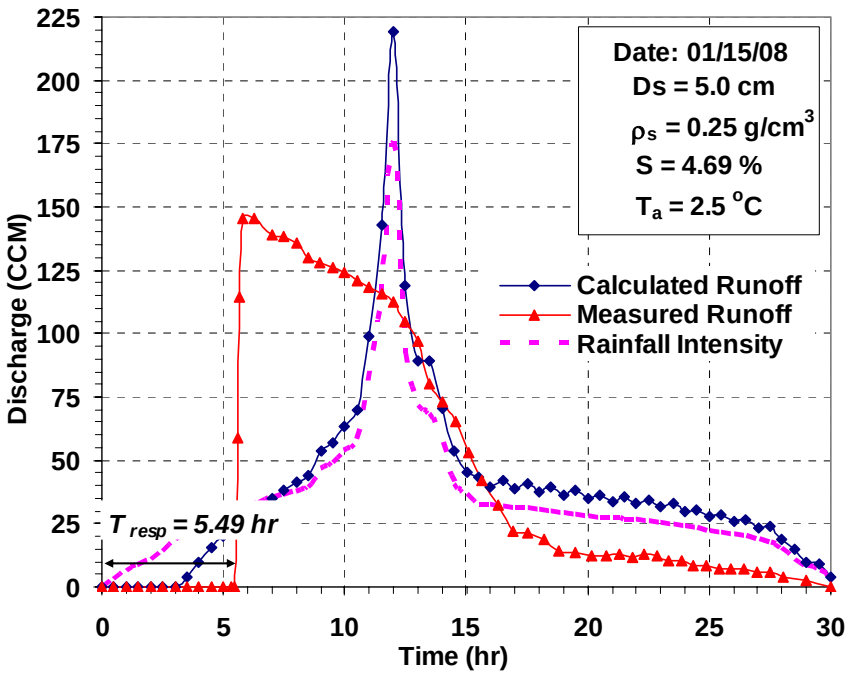

Figure G.10. Measured versus calculated runoff hydrographs using the calibrated λ value for event 10.

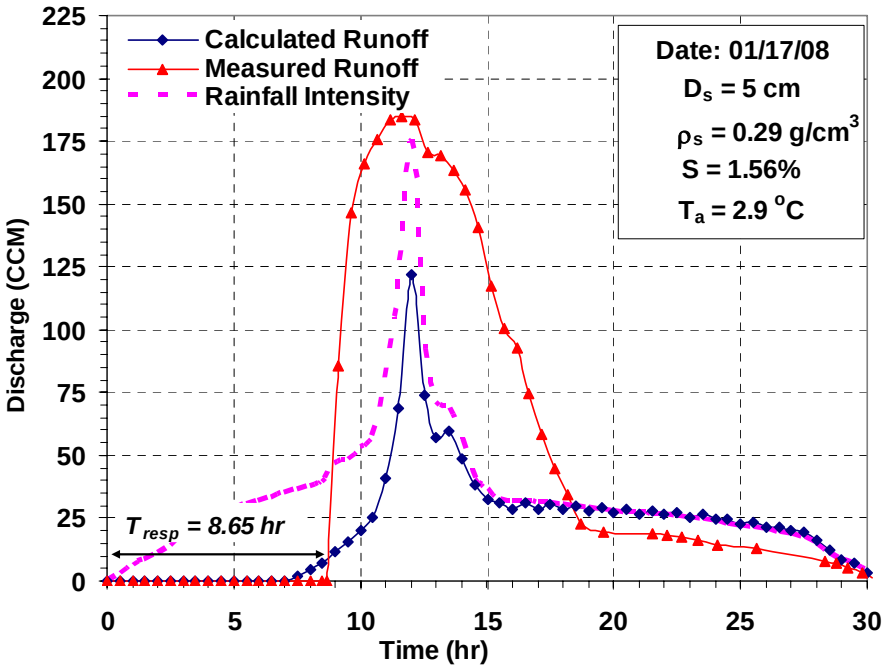

Figure G.11. Measured versus calculated runoff hydrographs using the calibrated λ value for event 11.

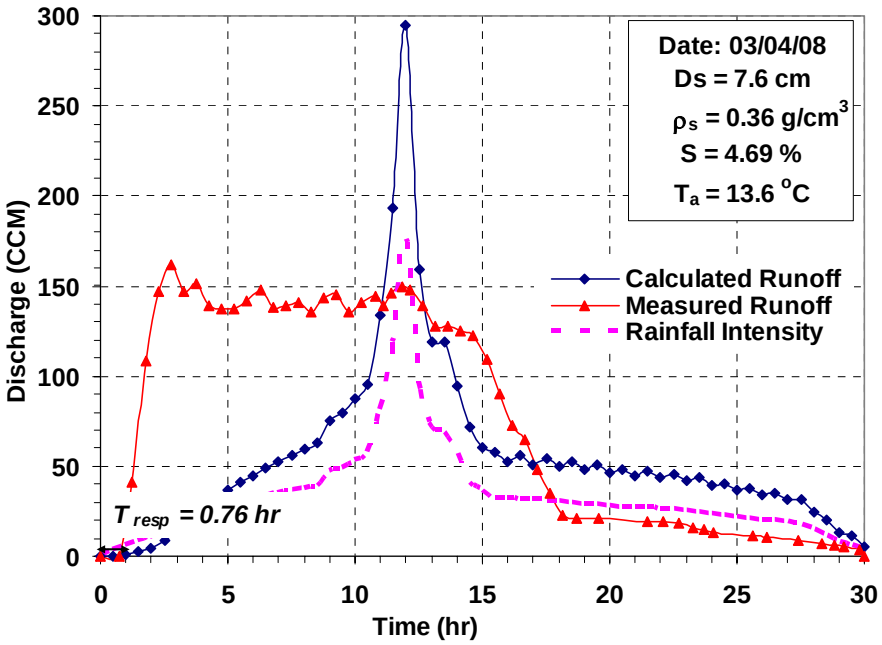

Figure G.12. Measured versus calculated runoff hydrographs using the calibrated λ value for event 12.

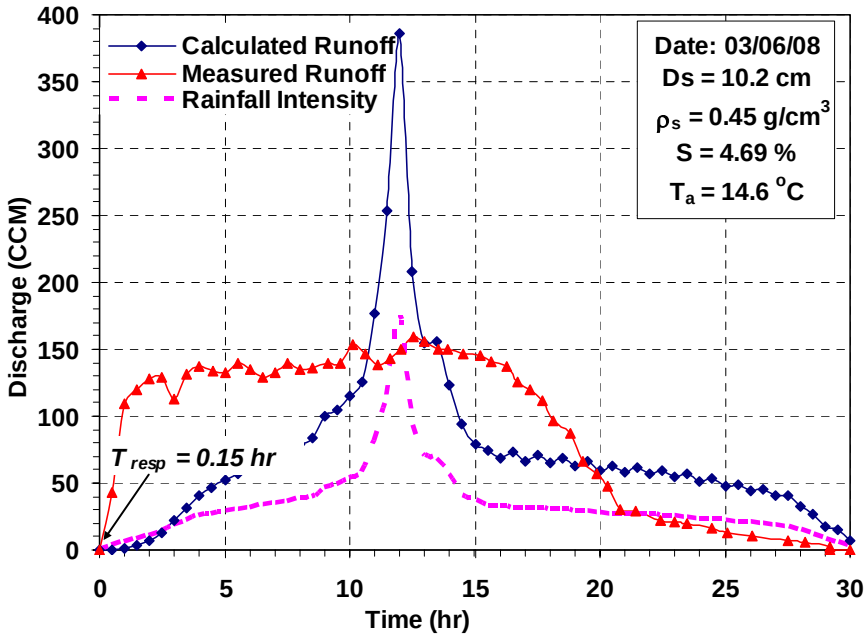

Figure G.13. Measured versus calculated runoff hydrographs using the calibrated λ value for event 13.

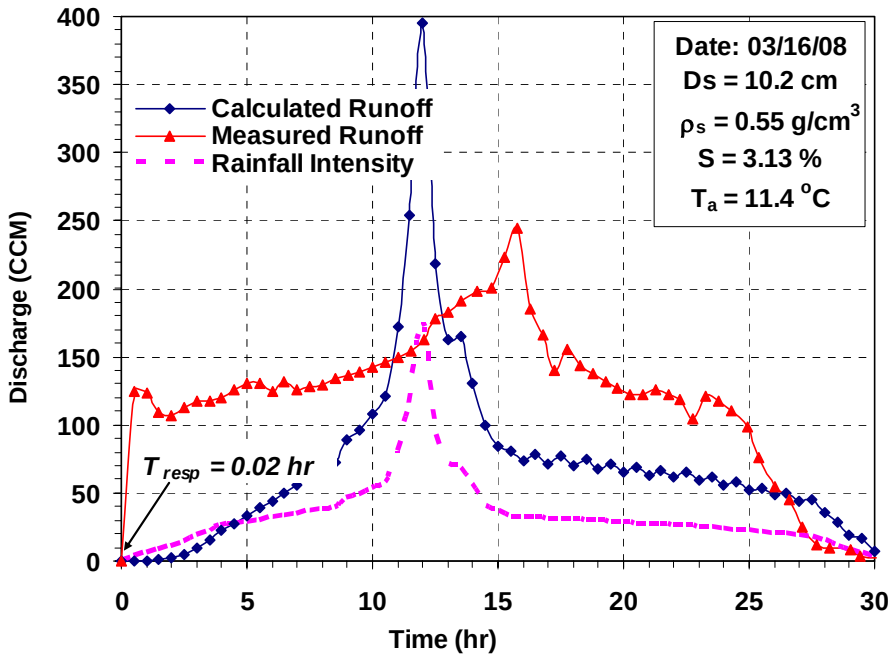

Figure G.14. Measured versus calculated runoff hydrographs using the calibrated λ value for event 14.

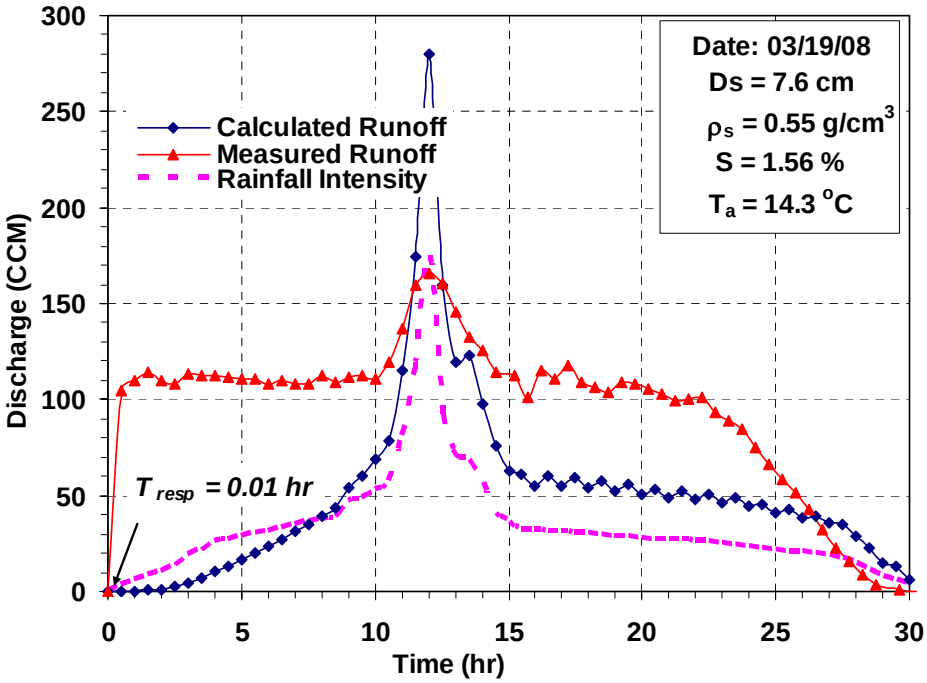

Figure G.15. Measured versus calculated runoff hydrographs using the calibrated λ value for event 15

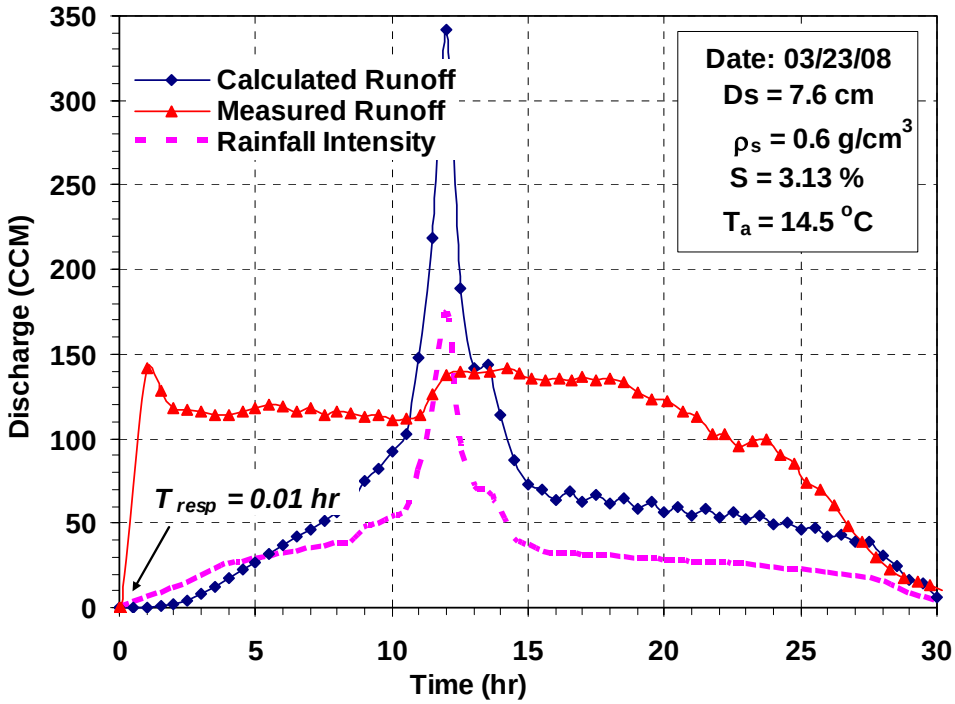

Figure G.16. Measured versus calculated runoff hydrographs using the calibrated λ value for event 16.

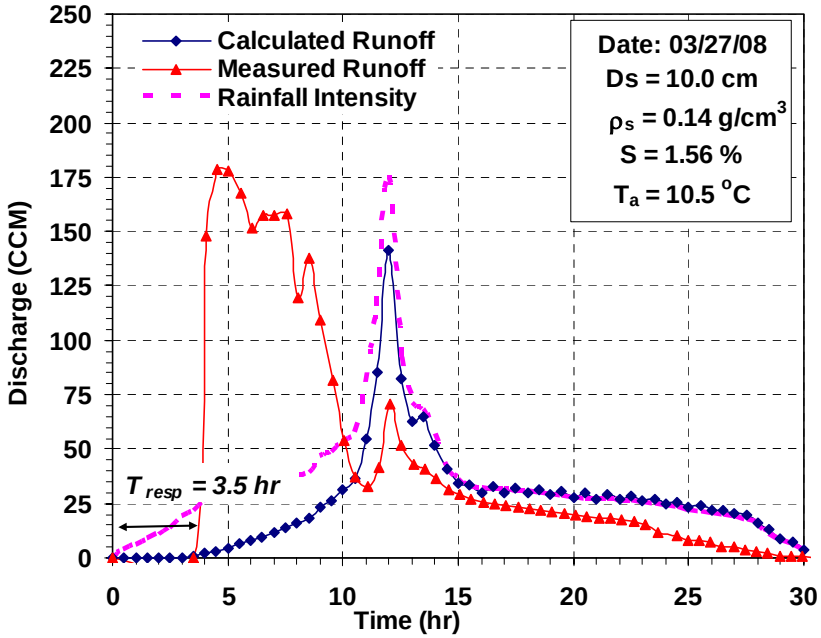

Figure G.17. Measured versus calculated runoff hydrographs using the calibrated λ value for event 17.

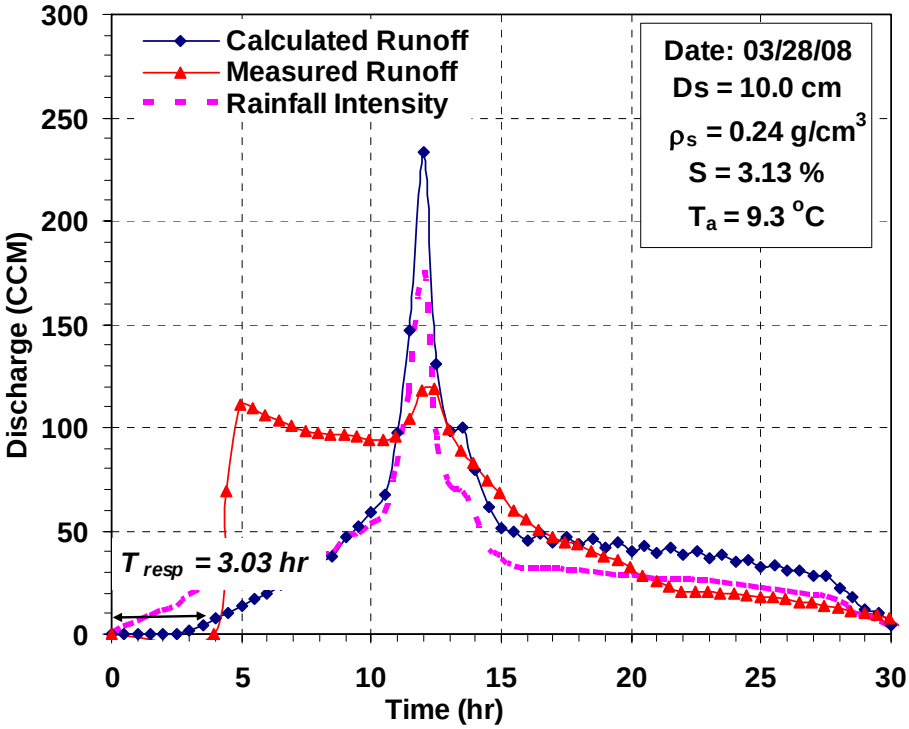

Figure G.18. Measured versus calculated runoff hydrographs using the calibrated λ value for event 18.

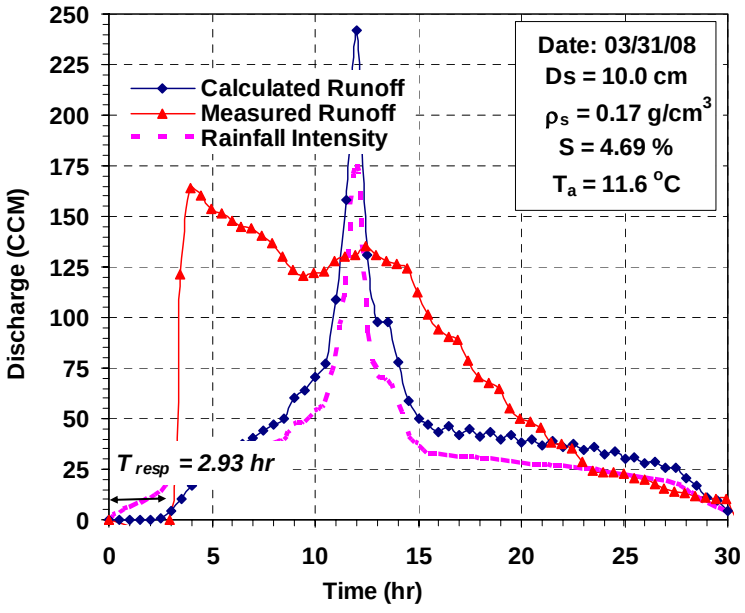

Figure G.19. Measured versus calculated runoff hydrographs using the calibrated λ value for event 19.

APPENDIX H

EXAMPLE APPLICATION OF THE PROPOSED MODIFICATIONS

The following example illustrates the necessary calculations to obtain the percentage change in the proposed design treatment volume for a site near Spokane.

Given:

Site Location	Spokane area
Drainage Basin Area, A	1.37 acre – Paved surfaces
Curve Number, CN	98
Design rainfall event, $P_{6\text{-month}, 24\text{-hour}}$	0.77 in
The 24-hour to regional storm precipitation depth conversion factor for Region 3 (from Table C.2)	1.06
Snowmelt adjustment factor (from Table C.3)	0.45 inch

The design runoff volume for this example can be obtained using the following steps:

1. Determine the total rainfall depth during the long duration regional storm

   The total rainfall during the regional storm = (1.06)*(0.77 in) = 0.82 in

2. Compute the maximum storage using the following equation

$$S = \frac{1000}{CN} - 10 \qquad \text{(Equation H.1)}$$

   Applying the assigned CN for the given drainage basin surface, (CN = 98) and solving for S yields:

$$S = 0.20 \quad inch$$

3. To account for the rain-on-snow, the total rainfall during the regional storm was adjusted using the snow melt adjustment factor as follows:

P = 0.82 inch +0.45 inch = 1.27 inch

4. The runoff depth from the given basin area is solved by the following form of the SCS-CN equation:

$$Q = \frac{(P - \lambda S)^2}{[P + (1 - \lambda)S]} \qquad \text{(Equation H.2)}$$

Setting the initial abstraction storage ratio λ to 0.20 in the above equation and solving for Q yields:

$$Q = \frac{(1.27 - 0.2 \times 0.2)^2}{[1.27 + (1 - 0.2)0.2]}$$

$$Q = 1.06 \quad inch$$

5. To convert this runoff depth to total runoff volume, we multiply this runoff depth by the drainage basin area:

Total runoff volume (ft^3) = Q (inch) * A (acre) * 3630 ft^3 /acre-in (Equation H.3)

Total runoff volume, V = 1.06 * 1.27 acre * 3630 ft^3 /acre-in

Total runoff volume, V = 4886.7 ft^3

6. Determine the % change in the required facility area if λ value other than 0.20 is used in the SCS-CN equation for runoff volume computations. The following computation was used to determine the percentage change in the required facility area:

$$T_{req} = \frac{V_{design}}{f_{design}} \qquad \text{(Equation H.4)}$$

Where, T_{req} [T] is the time required for runoff treatment, V [L^3] is the design runoff volume, and f [L/T] is the design infiltration rate.

The design infiltration rate is estimated by the following equation:

$$f = K \cdot i \cdot A \qquad \text{(Equation H.5)}$$

Where K [L/T] is the hydraulic conductivity, i [L/L] is the hydraulic gradient, and A [L^2] is the infiltration area.

Substituting Equation H.5 into Equation H.4 yields:

$$T_{req} = \frac{V_1}{f_1} = \frac{V_2}{f_2} \Rightarrow \frac{V_1}{V_2} = \frac{A_1}{A_2}$$

By computing the design runoff volume for different λ values, the % change in the required facility area can then be determined. The results are presented in Table H.1.

Table H.1. Percentage change in the required facility area for different assigned values of initial abstraction storage ratio, λ.

λ	Runoff Depth (in)	Runoff Volume (ft^3)	$Area_{\lambda=0.2}/Area_{\lambda=new}$	Increase in Required Facility Area (%)
0.01	0.609	3030.22	1.063	6.34
0.02	0.607	3020.70	1.060	6.0
0.04	0.604	3001.66	1.053	5.33
0.05	0.602	2992.15	1.050	5.00
0.06	0.600	2982.63	1.047	4.67
0.07	0.598	2973.12	1.043	4.33
0.08	0.596	2963.61	1.040	4.0
0.09	0.594	2954.10	1.037	3.67
0.10	0.592	2944.60	1.033	3.33
0.12	0.588	2925.59	1.027	2.67
0.13	0.586	2916.09	1.023	2.33
0.14	0.584	2906.59	1.020	2.0
0.16	0.581	2887.60	1.013	1.33
0.18	0.577	2868.62	1.007	0.67
0.20	0.573	2849.64	1.000	0